The Thesis Committee for Samuel Franz Hiebert
Certifies that this is the approved version of the following thesis

High-Resolution Correlation Framework of the Grayburg Formation-Shattuck Escarpment and Plowman Ridge: Testing Models of Shelf-to-Basin Frameworks

APPROVED BY
SUPERVISING COMMITTEE:

Supervisor:

Charles Kerans

Stephen C. Ruppel

William L. Fisher

High-Resolution Correlation Framework of the Grayburg Formation-Shattuck Escarpment and Plowman Ridge: Testing Models of Shelf-to-Basin Frameworks

by

Samuel Franz Hiebert, B.A.

Thesis

Presented to the Faculty of the Graduate School of

The University of Texas at Austin

in Partial Fulfillment

of the Requirements

for the Degree of

Master of Science in Geological Sciences

The University of Texas at Austin

August 2013

Dedication

To Julie, Franz, Simon, and Jake
To my family and friends, thanks for the support and good times

Acknowledgements

First and foremost I would like to thank my advisor, Charlie Kerans. Charlie has been a friend and mentor since I began studying carbonate rocks during my junior year of undergraduate studies in the Jackson School at The University of Texas at Austin. I am grateful to have had the opportunity to spend so much time studying in the field with my advisor.

I also gratefully acknowledge the incredible financial and scientific support I received from UT's Reservoir Characterization Research Laboratory. Charlie Kerans, Bob Loucks, Xavier Janson, Chris Zahm, Steve Ruppel, Harry Rowe, Stephaine Lane, and Jerry Lucia taught me much during the last few years.

Significant financial contributions to cover my living expenses and tuition during the last 2½ years were provided by the Jackson School. The Jackson School's ability to provide this kind of support results from the vision of the late John A. Jackson, who willed his fortune to support geological sciences at The University of Texas at Austin. I sincerely thank Dr. William L. Fisher for persuading him to do so.

July 29, 2013

Abstract

High-Resolution Correlation Framework of the Grayburg Formation-Shattuck Escarpment and Plowman Ridge: Testing Models of Shelf-to-Basin Frameworks

Samuel Franz Hiebert, M.S.GeoSci

The University of Texas at Austin, 2013

Supervisor: Charles Kerans

The San Andres and Grayburg Formations are important stratigraphic units for constructing correlation frameworks of the Guadalupe Mountains because these strata record the transition between the ramp profiles of the San Andres along the Algerita Escarpment and the reef-rimmed platforms of the Capitan Formation of the southern Guadalupe Mountains (Franseen et al. 1989). Sarg et al. (1999) and Kerans and Tinker (1999) have published significantly different models of shelf-to-basin correlations within this stratigraphic interval. Central to the debate is the correlation of mixed carbonate-siliciclastic strata exposed at Plowman Ridge in the Brokeoff Mountains to the better-constrained strata along the Shattuck Escarpment in the Guadalupe Mountains. This study applies high-resolution cyclostratigraphy, inorganic carbon isotope geochemistry, and sequence stratigraphic concepts to test the hypothesis that the strata exposed at Plowman Ridge are equivalent to Grayburg strata exposed at the Shattuck Escarpment in the southern Guadalupe Mountains (Kerans and Nance 1991, Kerans and Kempter 2002).

The shelf-to-basin cyclostratigraphic framework of the Grayburg Formation used in this study was established at the Shattuck Escarpment with data compiled from nine detailed measured sections, high-resolution photopans, and petrographic analysis. Based

on one- and two-dimensional cycle stacking analysis, the Grayburg Formation was divided into three high-frequency sequences (HFSs). The high-frequency sequences contain transgressive systems tracts separated by maximum flooding surfaces from the highstand systems tracts. The Grayburg high-frequency sequences are composed of between 6 and 20 high-frequency cycles (HFCs), which were identified and classified into vertical facies successions.

The Grayburg succession at Shattuck section 7 (32.09°, -104.81°) was selected as the reference section from the Guadalupe Mountains for comparison with Plowman section PR1 (32.03°, -104.89°) in the Brokeoff Mountains. Correlation between sections is documented at the 3rd-order composite sequence, high-frequency sequence, and when feasible, high-frequency cycle scale. Three high-frequency sequences recognized at Plowman Ridge section PR1 are equivalent to the G10, G11, and G12 Grayburg sequences described at Shattuck section 7. Correlation of the Grayburg G10-G12 high-frequency sequences with the three sequences at Plowman Ridge is based on comparison of overall thicknesses, facies proportions, cycle number, vertical facies succession, stratigraphic position of diagnostic units, and excursions within the inorganic carbon isotope profiles taken from both sections. Establishing the links between Grayburg strata on the Shattuck wall with strata on Plowman Ridge corroborates the framework/correlation scheme of Kerans and Tinker (1999) in lieu of other published correlation frameworks.

Table of Contents

List of Tables

List of Figures

List of Facies Plates

INTRODUCTION

The goal of this thesis is to resolve discrepancies of shelf-to-basin correlation frameworks within the San Andres-Grayburg stratigraphic interval published by Sarg et al. (1999) and Kerans and Tinker (1999). These discrepancies hinge on the correlation of the mixed carbonate-siliciclastic cycles exposed at the Plowman Ridge in the Brokeoff Mountains to those of the strike-offset Shattuck Escarpment in the Guadalupe Mountains (Figure 1). Sarg et al (1997) correlated these strata as the transgressive and highstand systems tracts of the San Andres Formation GP2 3rd-order depositional sequence. Kerans and Tinker (1999) correlated these same strata as their G10-G12 high-frequency sequences of the Grayburg Formation.

No previous study has definitively correlated the main Grayburg exposures found in the Guadalupe Mountains to the Grayburg exposures in the Brokeoff Mountains. In this thesis, new, high-resolution cyclostratigraphic data and $\delta^{13}C_{(inorganic)}$ isotope data were used to demonstrate the correlation of Grayburg strata between the Shattuck Escarpment in the Guadalupe Mountains and Plowman Ridge in the Brokeoff Mountains.

Correlation of Grayburg strata between these oblique-dip outcrop profiles separated by 10 km along strike can be used to resolve discrepancies in shelf-to-basin correlation frameworks within the San Andres-Grayburg interval. Resolution of the shelf-to-basin framework within the San Andres-Grayburg interval will help guide the application of San Andres and Grayburg reservoir analogue outcrop studies from the Guadalupe Mountains. These studies have contributed sequence stratigraphic models that serve as a reference for formation thickness, sequence divisions, facies tract dimensions, and reservoir facies distribution (Sonnenfeld 1991; Kerans and Nance 1991, Lindsay 1992, Fitchen 1993, Kerans and Fitchen 1994, Barnaby and Ward 2007). The sequence stratigraphic models are relevant because San Andres and Grayburg reservoirs have produced more than 7 billion barrels of oil at approximately 30% recovery efficiency (Bebout and Harris 1986, 1990). Reservoirs targeting Grayburg Formation mixed carbonate-siliciclastic strata have produced more than 670 million barrels of oil (Dutton

et al. 2005). San Andres and Grayburg fields remain active, having ongoing development by infill drilling programs, selective completions, and enhanced oil recovery techniques.

The $\delta^{13}C_{(inorganic)}$ isotope profiles provided in this thesis provide a tool for linking the Grayburg sequence stratigraphic framework developed at the Shattuck Escarpment in the Guadalupe Mountains to Grayburg sequence stratigraphic models developed using subsurface data (Ruppel and Rowe, 2013). High-resolution cyclostratigraphic data used to confirm the shelf-to-basin model depiction by Kerans and Tinker (1999) may be applied to detailed reservoir characterization of Grayburg units on the northwest shelf of the Delaware Basin (Figure 2). The Grayburg cross-section developed in this study can be used to guide prediction of the occurrence, thickness, and abundance of reservoir facies in this area.

.

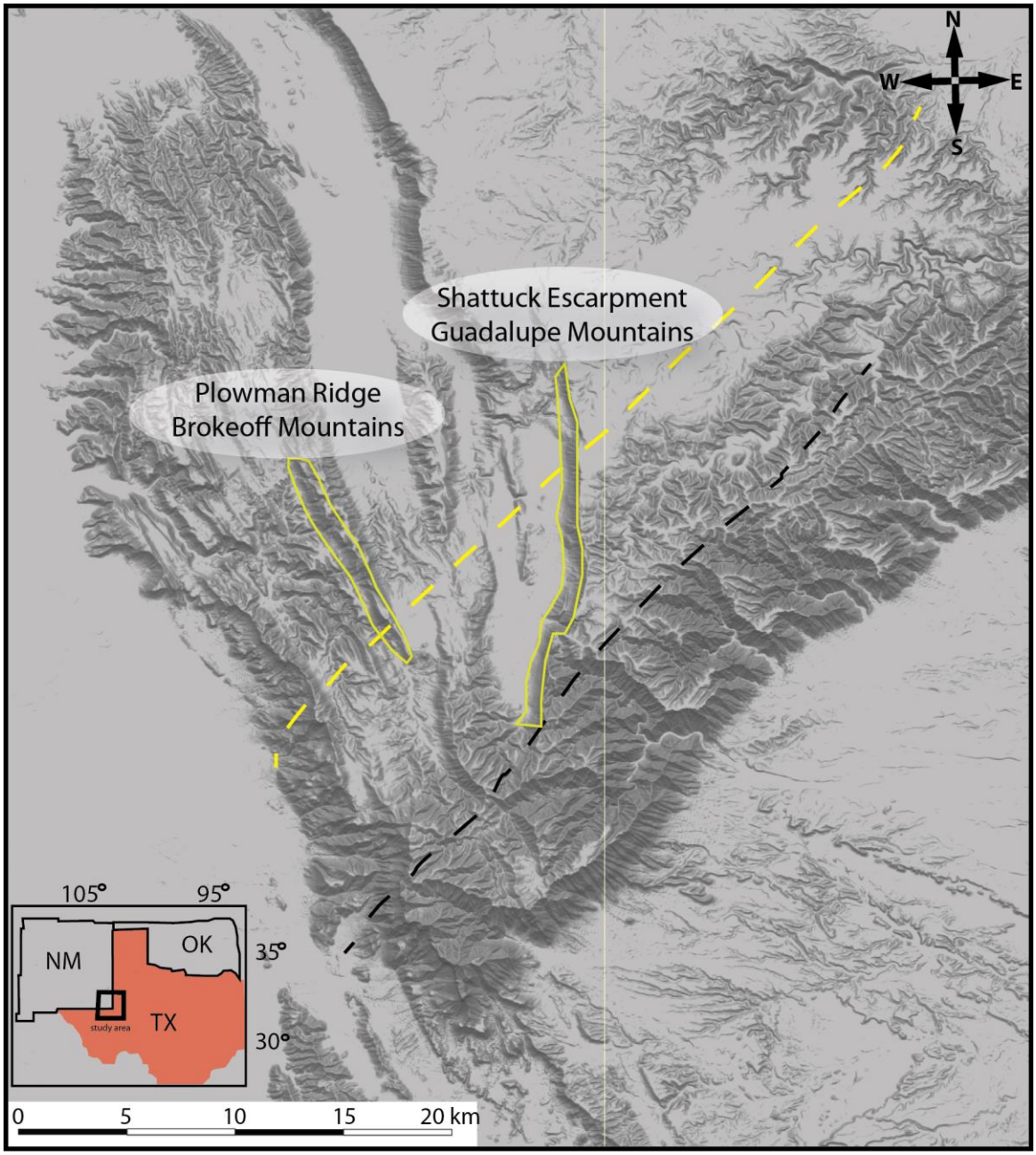

Figure 1: Map of Southern Guadalupe Mountains and Brokeoff Mountains: The position of the terminal San Andres shelf margin is dashed in yellow, the Grayburg shelf margin in dashed in black. Correlation of Grayburg strata is between the Plowman Ridge (outlined in yellow in the Brokeoff Mountains), and the Shattuck Escarpment (outlined in yellow in the Guadalupe Mountains).

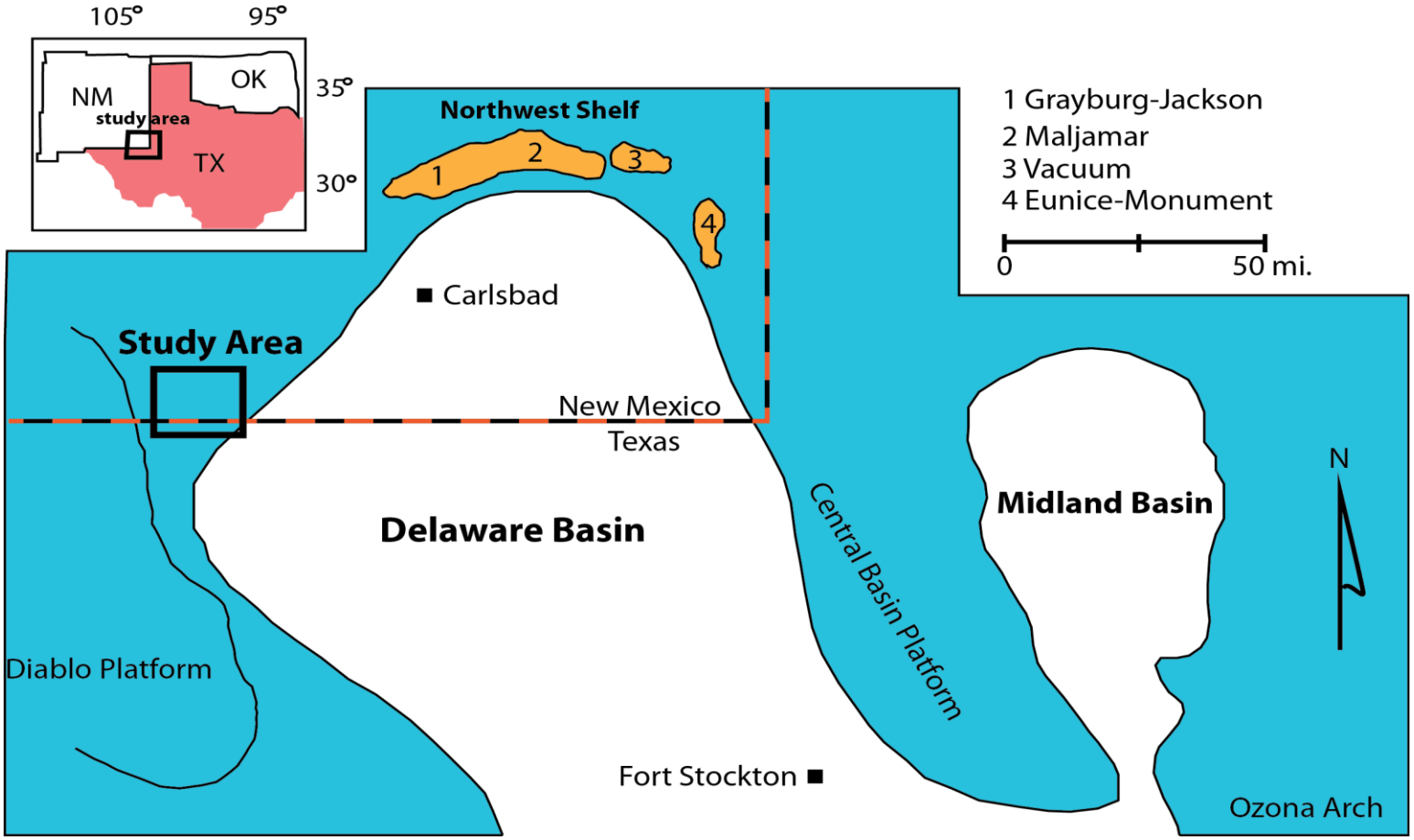

Figure 2: Paleogeography of Permian Basin during Guadalupian Time. Grayburg strata deposited on the shallow platforms rimming the deep-water basins are shaded in blue. Grayburg oil fields on the Northwest Shelf that have produced >10MMbbl are outlined in orange. The approximate location of the study area is outlined in black. Figure modified from Kerans (1995).

GEOLOGIC SETTING

The Grayburg Formation (Late Permian, Guadalupian) is a shallow-marine mixed carbonate-siliciclastic succession deposited along the margins of the Permian foreland basin of West Texas and southeast New Mexico (Kerans and Nance 1991, Ruppel and Bebout 2001, Barnaby and Ward 2007) (Figure 2, Figure 3). The Permian Basin developed in late Mississippian through earliest Permian time, when Gondwana collided with Laurentia during the formation of the supercontinent Pangaea (Yang and Dorobek 1992). The Grayburg Formation is within the Guadalupian stage of the upper Permian (Figure 3). Grayburg strata are exposed in the Guadalupe Mountains of West Texas and southeastern New Mexico. Exhumation of the Guadalupe Mountains occurred during Cenozoic time (King 1948). The mountain belt is bounded to the west by large, high-angle normal faults having displacement of several thousands of feet (King 1948). The towering cliffs of the western Guadalupe Mountains diminish to the northeast; and eventually dip into the subsurface south of Carlsbad, New Mexico.

Paleogeographic reconstructions of the Permian Basin during Guadalupian time place it on the Pangean supercontinent between 0 and 5° N (Scotese and McKerrow 1990; Lottes and Rowley 1990; Coffin et al. 1992). Extensive evaporites and eolianites documented in the northern part of the Midland and Delaware Basins indicate the Guadalupian-age strata were deposited in an arid climate (Silver and Todd 1969, Meissner 1972, Fischer and Sarnthein 1988). Sea-level cyclicity during the Guadalupian was transitional from the high-amplitude glacial-eustatic fluctuations of the icehouse Pennsylvanian, to the low-amplitude eustatic fluctuations of the greenhouse Triassic (Lehrmann and Goldhammer 1999). Permian Basin platform carbonate units are autochthonous, and the sandstone units are allochthonous. The sandstones were sourced from the Anadarko Basin in Oklahoma (Kocurek and Kirkland 1998) and from the Pedernal Trend in northwestern New Mexico (Kerans and Fitchen 1995). The dominant transport mechanism of sand to the Permian Basin was by aeolian processes (Fischer and Sarnthein 1988, Kerans and Fitchen 1995, Kocurek and Kirkland 1998).

PREVIOUS WORK

Since the early study of the Permian stratigraphy in the Guadalupe Mountains geologists from state surveys, the USGS, universities, and oil companies and their colleagues and students have used the area as a laboratory to develop and test models in the fields of sedimentology, stratigraphy, paleontology, diagenesis, tectonics and structure (Sarg et al 1997). The term Grayburg was first applied by Dickey (1940), who designated the Cecil H. Lockhart Root well in Eddy County, New Mexico, as the subsurface type locality and suggested that the unit should be described in the Guadalupe Mountains. Moran (1940) described the type section on the outcrop in the Sitting Bull Falls area.

Prior to use of the term Grayburg, equivalent units described in the northern Guadalupe Mountains were called the Dog Canyon Limestone (Lang 1937). King (1948) referred to equivalent strata on the Manzanita Ridge in the southern Guadalupe Mountains as the Goat Seep Limestone (Boyd 1958, Hayes 1964). Boyd (1958) used the term Grayburg-Queen Sequence to describe a 360-m succession of "massive dolomite" that separated the Cherry Canyon sandstone tongue from the Capitanian shelf deposits in the Brokeoff Mountains. Hayes (1964) mapped the Grayburg Formation at the Shattuck Escarpment as being between 120 and 180 m thick. He defined the contact between the underlying Upper San Andres Formation at a sharp transition in lithology from the "almost sandstone free yellowish-gray to light olive gray-weathering dolomite in the upper part of the San Andres and the alternating beds of grayish-orange-weathering sandstone and dolomite in the lower part of the Grayburg" (Hayes 1964. p 29) . Hayes (1964) described the contact between the San Andres and Grayburg as conformable throughout the area.

More recent workers have applied sequence stratigraphic concepts to refine the Grayburg stratigraphy both in the Guadalupe Mountains and in the Brokeoff Mountains (Kerans and Nance 1991, Sarg et al. 1997, Kerans and Kempter 2002, Barnaby and Ward 2007). The Grayburg Formation is mapped as the GP3 3rd-order depositional sequence of Sarg et al. (1999) (Figure 4). The Grayburg and Queen Formations are combined in the

CS11 3rd-order composite sequence of Kerans and Tinker (1999) (Figure 5). Composite sequence 11 is divided into five high frequency sequences (HFSs). The Grayburg comprises G10-G12 HFSs, and the Queen Formation is the G13-14 HFSs (Kerans and Tinker 1999, Kerans and Kempter 2002) (Figure 5). Sequence stratigraphic studies conducted in the Brokeoff Mountains at Plowman Ridge and West Dog Canyon divide the Grayburg into four high-frequency sequences (Barnaby and Ward 2007).Reports about the subsurface of West Texas divide the Grayburg into four high-frequency sequences (Ruppel and Bebout 2001).

The original depositional model of the Grayburg Formation was a carbonate ramp. The depositional environments described include: inner ramp dominated by low-energy siliciclastics and mud-dominated carbonates, inner ramp crest with the fenestral-tepee facies indicative of supratidal/island settings, outer ramp crest dominated by oolitic facies, and the outer ramp with fusulinid-dominated facies indicative of water depths of as much as 30 m (Kerans and Nance 1991). More recent depositional models have been developed at the 4th-order high frequency sequence scale (Kerans and Kempter 2002, Kerans et al. in press). The Grayburg G10 HFS was deposited on a narrow <7-km-wide ramp profile (Figure 6).The G10 inner ramp was a sabhka environment with localized tepee complexes that transitioned downdip to the middle ramp depositional environment which was dominated by deposition of low-energy shallow subtidal packstones (Kerans et al. in press). The low-energy mud-dominated packstones grade seaward into high-energy ooid grainstones deposited within the ramp-crest depositional environment. The G10 ramp-crest ooid grainstones transition seaward to 5-35^{o} -dipping outer ramp/slope fusulinid packstones (Kerans et al. in press) The G11 HFS was deposited on a >7-km-wide rimmed-shelf area (Figure 6). The G11 inner shelf was a salina dominated by evaporites. The G11 inner shelf evaporites transition seaward to fenestral laminites and mud-dominated packstones deposited within the middle-shelf depositional environment. The muddy packstones and laminites of the middle-shelf grade seaward into ooid grainstones deposited within the shelf-crest environment (Kerans et al. in press). The shelf-crest ooid grainstones transition seaward to fusulinid-dominated outer shelf and

slope clinoforms that grade basinward into Cherry Canyon siliciclastic turbidites (Kerans et al. in press). The G12 HFS was deposited on a >7-km-wide rimmed-shelf similar in profile to the G11 HFS (Kerans et al. in press) (Figure 6). The G12 shelf margin is a steep, 80-100-m-wide collapse scarp mapped at Bush Mountain on the Western Escarpment (Franseen and Fekete 1989).

Significant discrepancies exist between published models of the shelf-to-basin stratigraphic framework within the San Andres-Grayburg-Queen interval. Sarg et al. (1999) show two prograding carbonate units within the San Andres GP2 depositional sequence (Figure 4). Kerans and Tinker (1999) show a single prograding carbonate unit within the CS10 (San Andres G8 HFS and G9 HFS) (Figure 5). Sarg et al (1999) show the stratigraphic relationship of the Goat Seep Formation overlying the San Andres Formation at the Bush Mountain collapse scarp on the Western Escarpment (Figure 4). Kerans and Tinker (1999) show the stratigraphic relationship of the Goat Seep Formation overlying the Grayburg Formation at the Bush Mountain collapse scarp (Figure 5). The stratigraphic relationship shown by Kerans and Tinker (1999) corroborates work by Franseen and Fekete (1989), which showed the Goat Seep Formation overlying the Grayburg Formation at the Bush Mountain collapse scarp on the Western Escarpment (Figure 7).

Inorganic $\delta^{13}C$ profiles have been used for both global and regional correlation of strata. Phelps et al. (2013) used $\delta^{13}C_{(inorganic)}$ profiles in conjunction with sedimentologic, wireline, seismic, and paleontological data to correlate Cretaceous carbonate strata of the Comanche Platform, in south-central Texas to globally recognized ocean anoxic events (OAEs) (Phelps et al. 2013) (Figure 8). Corsetti et al. (2000) used $\delta^{13}C_{(inorganic)}$ profiles in conjunction with biostratigraphy and sequence stratigraphic approaches to correlate Neoproterozoic strata within the southern Great Basin, southern California (Corsetti et al. 2000) (Figure 9). The $^{13}C/^{12}C$ ratios in the world's oceans have varied through time as the result of the partitioning of organic carbon and carbonate (Shackleton and Hall, 1984, Kump and Arthur, 1999, Sundquist and Visser, 2004). The main process that caused partitioning is photosynthesis, in which organic matter is depleted in the heavy isotope

^{13}C (Saltzman and Thomas 2012). The $\delta^{13}C_{(inorganic)}$ curves generated from samples deposited in shallow-water settings show greater variability and spatial heterogeneity relative to curves generated from sediments deposited in deep water as a result of primary processes, diagenetic processes, and differences in paleoenvironments (Saltzman and Thomas 2012, Oehlert et al. 2012). Primary marine $\delta^{13}C_{(inorganic)}$ values for the Permian of West Texas and New Mexico are estimated to be between +1.0 ‰ and +6.0‰ (Given and Lohmann, 1985) (Figure 10). Broad scatter of $\delta^{13}C_{(inorganic)}$ values observed in the Paleozoic portion of the global carbon isotope curve has been attributed to disruptions in marine circulation patterns caused by sea-level change (Panchuk 2006). Possible effects of diagenesis on original $\delta^{13}C_{(inorganic)}$ signature include depletion of $\delta^{13}C_{(inorganic)}$ as a result of oxidation during soil zone diagenesis. Enrichment or depletion of $\delta^{13}C_{(inorganic)}$ may also occur at depth during hydrocarbon generation and bacterial reduction (Allan and Wiggins, 1993). The carbon isotopic composition of dolomitized rocks reflects the ratio of inorganic carbon derived from pre-existing limestone to organic carbon derived from the microbial and thermal breakdown of organic material (Allan and Wiggins, 1993). Dolomitization does not usually produce significant $\delta^{13}C_{(inorganic)}$ shifts because the dolomitizing fluids do not typically contain carbon.

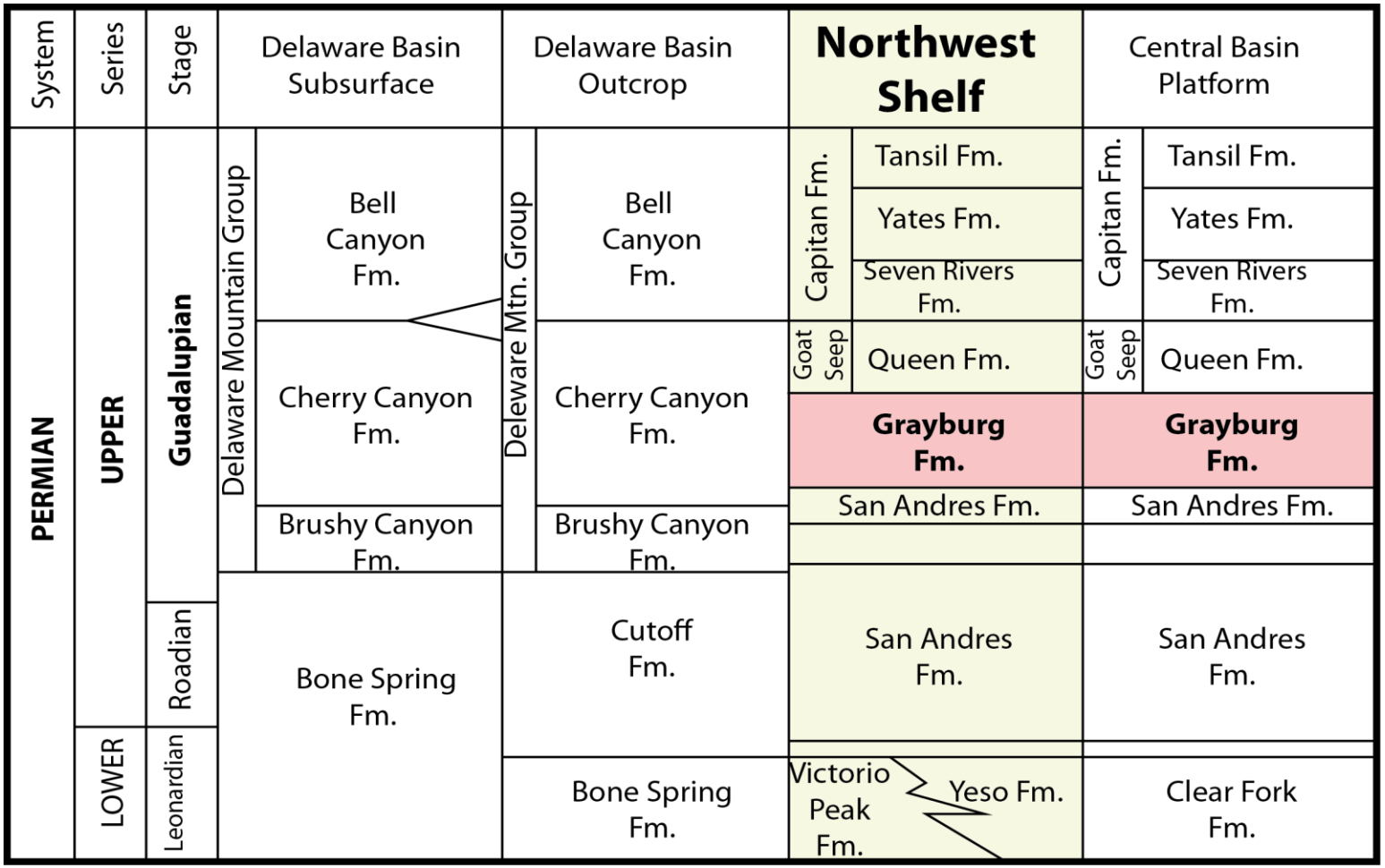

Figure 3: Stratigraphic Terminology of the Guadalupian Section of the Permian Basin. Northwest Shelf terminology is highlighted in yellow and the Grayburg interval is highlighted in red. Stratigraphic chart modified from Kerans and Fitchen (1995)

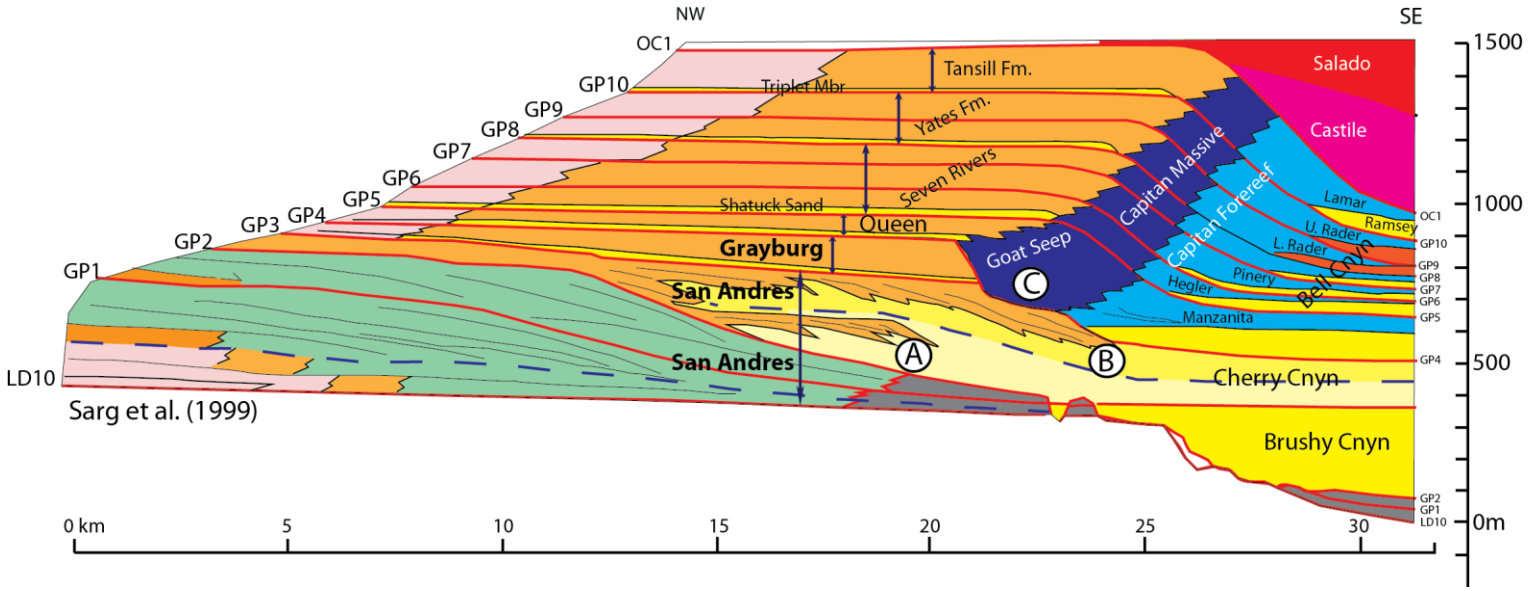

Figure 4: Shelf-to-Basin Correlation Framework of Sarg et al. (1999): The Grayburg Formation is the GP3 third-order depositional sequence. In this scheme there are two prograding carbonate units within the San Andres GP2 depositional sequence (A and B). In this model the Goat Seep Fm was interpreted to overly the distal toe of the upper prograding unit within the San Andres GP2 at the Western Escarpment (C).

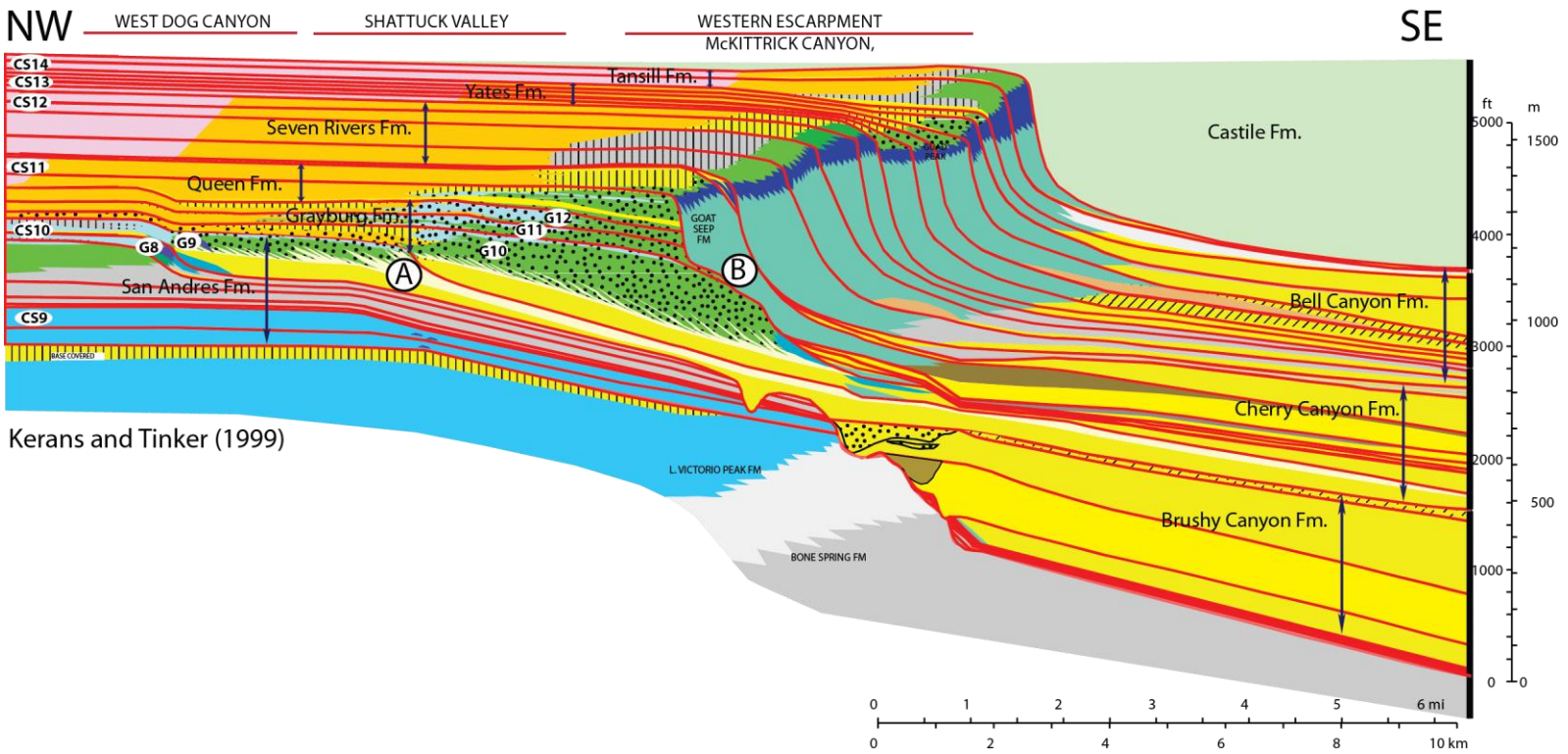

Figure 5: Shelf-to-Basin Correlation Framework of Kerans and Tinker (1999): The Grayburg is the G10-G12 high-frequency sequences within the CS10 third-order composite sequence of Kerans and Tinker (1999). In this interpretation there is a single prograding carbonate unit within the San Andres CS10 composite sequence (A). The Goat Seep Fm is shown overlying the distal toe of the Grayburg G10 HFS and part of the G11 HFS at the Bush Mountain collapse scarp along the Western Escarpment (B).

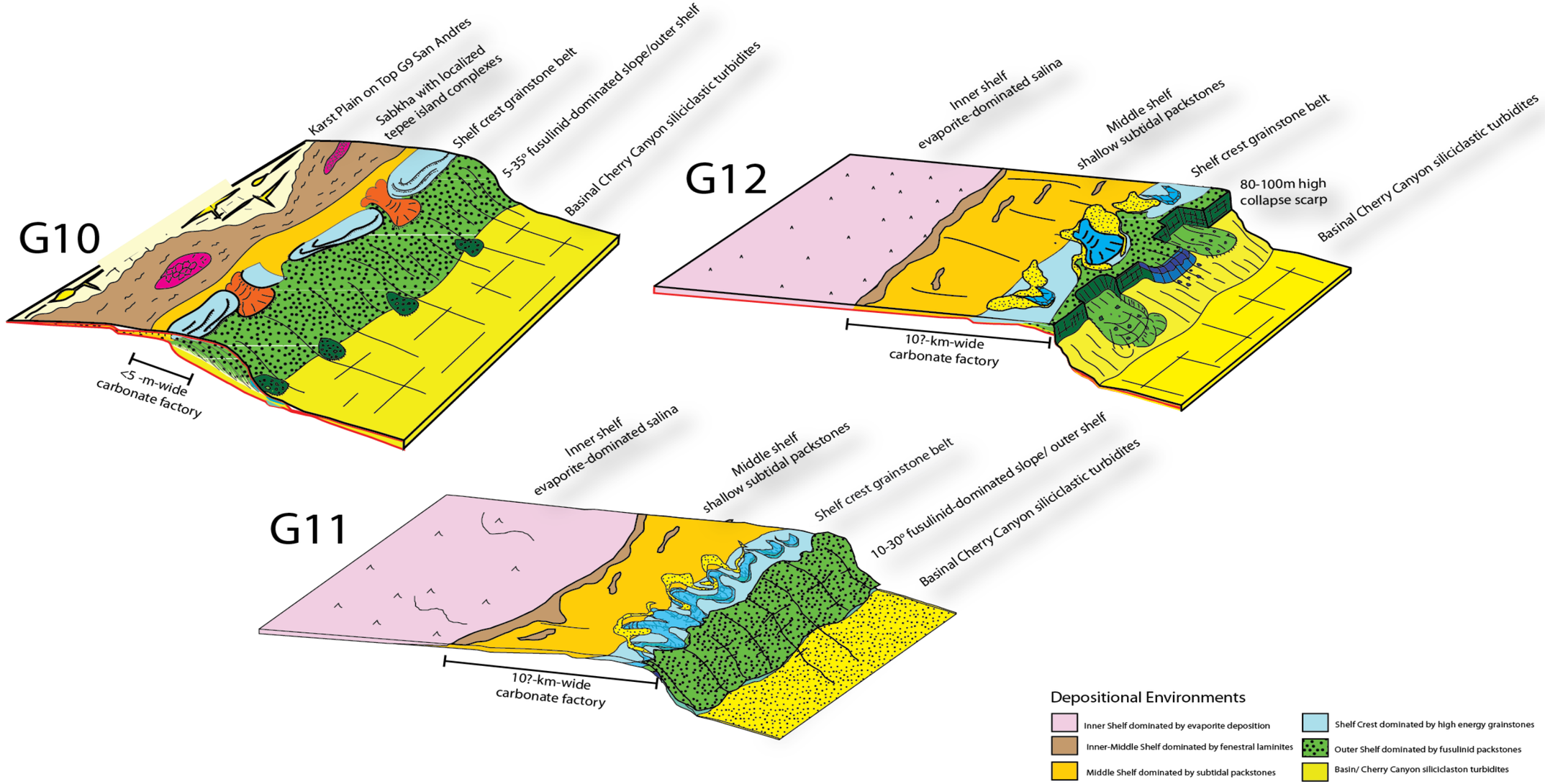

Figure 6: Grayburg High-Frequency Sequence Depositional Models. The G10 HFS was deposited on a <7km wide carbonate ramp profile while the G11 and G12 HFSs were deposited on >7km wide rimmed-shelf depositional profiles. Fundamental to the differentiation between the G10 ramp versus the G11 and G12 rimmed-shelf profiles is the overall width of the carbonate factories, development of extensive tide-dominated shelf crest grainstone belts within the G11 and G12, and the steep collapse scarp at the G12 shelf margin. Figures modified from Kerans et al. (in press).

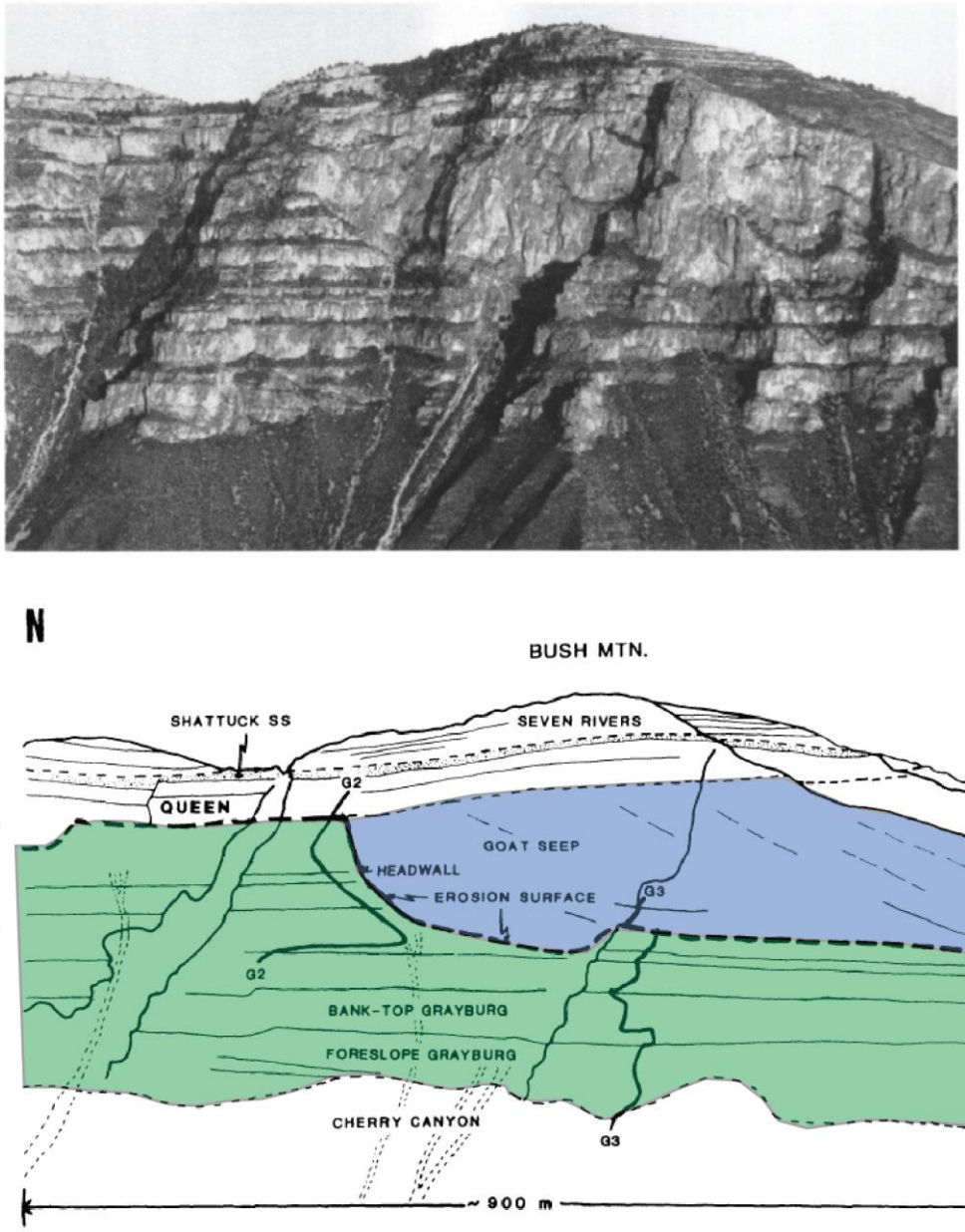

Figure 7: Bush Mountain Stratigraphic Relationship: Franseen and Fekete (1989) show Goat Seep Fm overlying Grayburg Fm at the Bush Mountain collapse scarp at the Western Escarpment. Figure from Franseen and Fekete (1989)

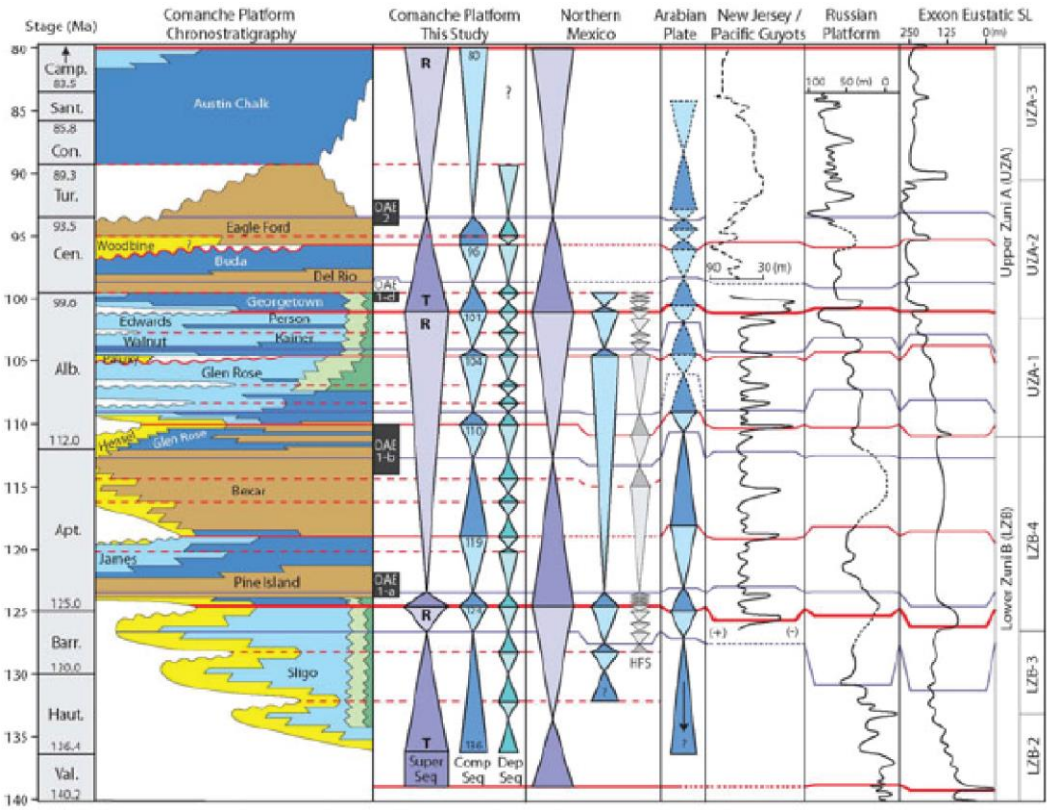

Figure 8: Global Correlation of Strata Using Inorganic $\delta^{13}C$ Profiles Phelps et al. (2013) used $\delta^{13}C_{(inorganic)}$ profiles in conjunction with sedimentologic, wireline, seismic, and paleontological data to correlate Cretaceous-age strata of the Comanche platform, south-central Texas, United States to globally recognized OAE events. Figure from Phelps et al. (2013)

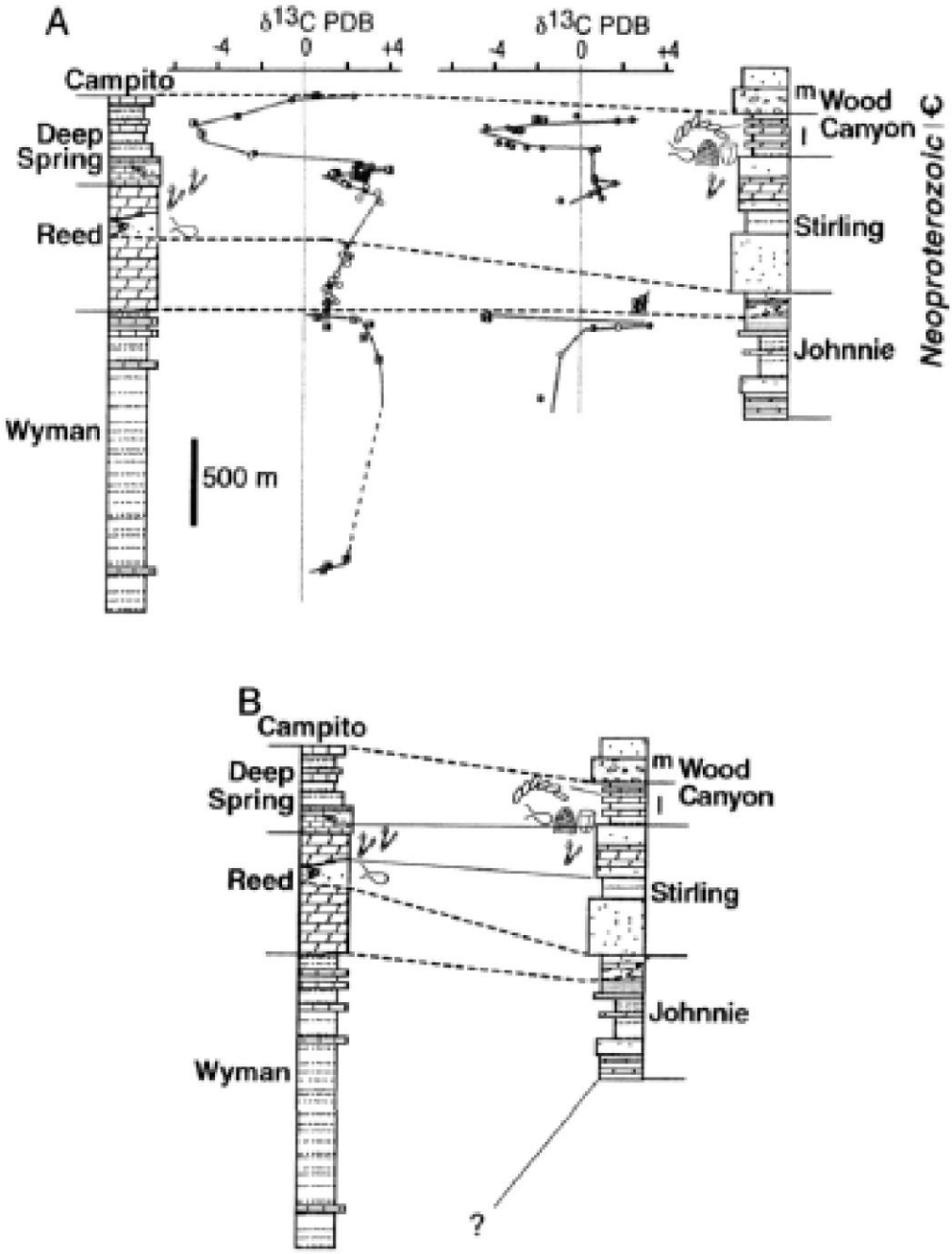

Figure 9: Regional Correlation of Strata Using Inorganic δ13C Profiles: Corsetti et al. (2000) used δ13C (inorganic) profiles in conjunction with biostratigraphy and sequence stratigraphic approaches to correlate Neoproterozoic strata within the southern Great Basin, southern California, United States. Figure from Corsetti et al. (2000)

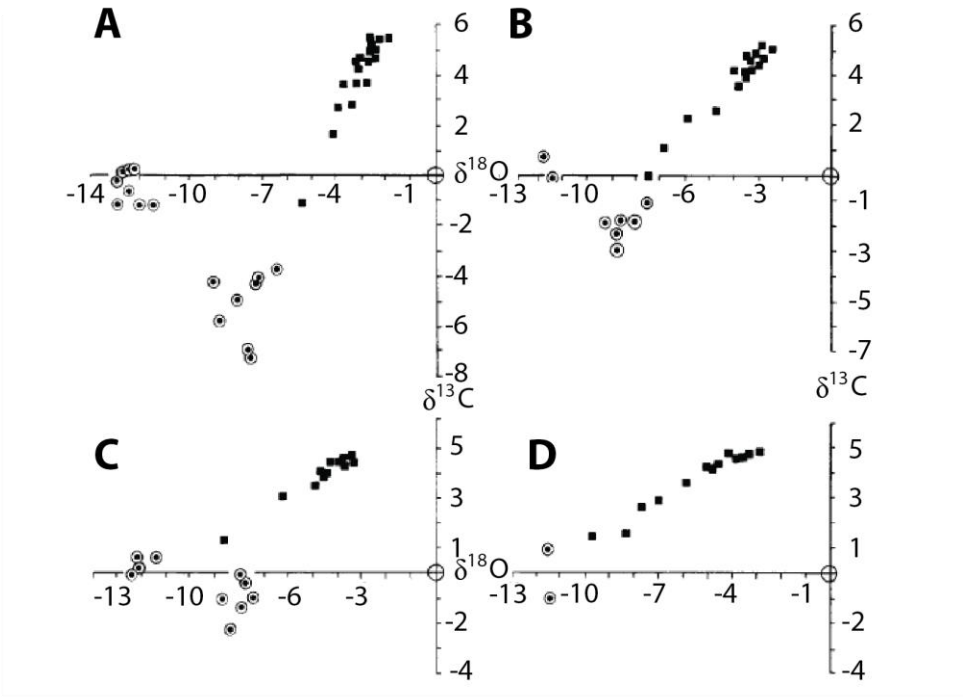

Figure 10: Estimated Original Marine $\delta^{13}C_{(inorganic)}$ Values for the Permian of West Texas and New Mexico: The filled squares indicate $\delta^{13}C_{(inorganic}$ values for unaltered Permian age marine cement. The open circles with a small dot in the middle indicate $\delta^{13}C_{(inorganic)}$ values for diagenetically altered Permian age calcite cements. Sample sites (A, B, C, and D) span the transition from reef massive to foreslope within the Capitan system of the Guadalupe Mountains. Figure from Given and Lohmann (1985).

METHODS

The shelf-to-basin correlation framework model by Sarg et al (1999) differs from the model by Kerans and Tinker (1999). The shelf-to-basin correlation discrepancies within the San Andres-Grayburg interval between Sarg et al. (1999) and Kerans and Tinker (1999) hinge on the correlation of the mixed carbonate-siliciclastic cycles exposed on Plowman Ridge in the Brokeoff Mountains to strata exposed in the Guadalupe Mountains. The correlation of these strata is tested by comparing the cyclostratigraphic architecture developed at Plowman Ridge section PR1 in the Brokeoff Mountains against the cyclostratigraphic architecture developed at Shattuck section S7 in the Guadalupe Mountains (Figure 11). Section S7 is measured through a known Grayburg interval along the Shattuck Escarpment in the Guadalupe Mountains (Hayes 1964, Kerans and Nance 1991). Section S7, the most complete Grayburg section along the Shattuck Escarpment, was deposited at a similar position to section PR1 along strike (Figure 11). Correlation of strata between the Guadalupe Mountains and the Brokeoff Mountains was done within the broader regional stratigraphic framework documented in the southern Guadalupe Mountains by Hayes (1964), Kerans and Nance (1991) and in the Brokeoff Mountains by Boyd (1957) and Barnaby and Ward (2007). The high-resolution cyclostratigraphic correlation between sections evolved within a detailed sequence-stratigraphic framework developed at the Shattuck Escarpment during this study.

The Grayburg Formation sequence-stratigraphic framework used in this study was developed at the Shattuck Escarpment in the southern Guadalupe Mountains. Nine detailed measured sections were collected along the length of the outcrop, and hand samples were collected for petrographic analysis. The measured sections were used to document vertical facies succession, high-frequency cycle number, cycle thickness, facies proportion, and diagnostic units. Petrographic analysis was used to confirm field-based facies identification, identify key allochems, qualitatively assess porosity type and percentage, and document dolomite crystal size variability. Continuous bench-forming units were either walked or traced between measured sections on high-resolution aerial photopans covering the length of the outcrop. High-frequency sequence boundaries and

maximum flooding surfaces were picked within the Grayburg Formation using the methods outlined by Kerans (1995) for construction of sequence stratigraphic frameworks using one- and two-dimensional cycle analysis.

Inorganic δ13C profiles were compiled at Shattuck section S7 and Plowman section PR1. Eighty-nine bulk rock samples were collected for analysis within a 130m interval at section PR1 and 79 bulk rock samples were collected within a 180m interval at section S7. The δ13C sample analysis was done at the University of Texas-Dallas in Dr. Harry Rowe's lab. Powdered whole-rock samples were digested in anhydrous phosphoric acid according to the method of McCrea (1950). After cryogenic purification, CO2 yields from the acid digest were measured using a manometer to determine wt. % CaCO3. Inorganic carbon analysis was performed on a dual inlet gas isotope ratio mass spectrometer. Isotopic results are reported in per mil (‰) relative to V-PDB for $\delta^{13}C$. The $\delta^{13}C_{\text{(inorganic)}}$ profiles were used to corroborate the high-resolution cyclostratigraphic comparison of strata between sections. The cyclostratigraphic correlation of strata between section PR1 and section S7 is focused on the comparison of cycle number, cycle thickness, vertical facies succession, and facies proportion.

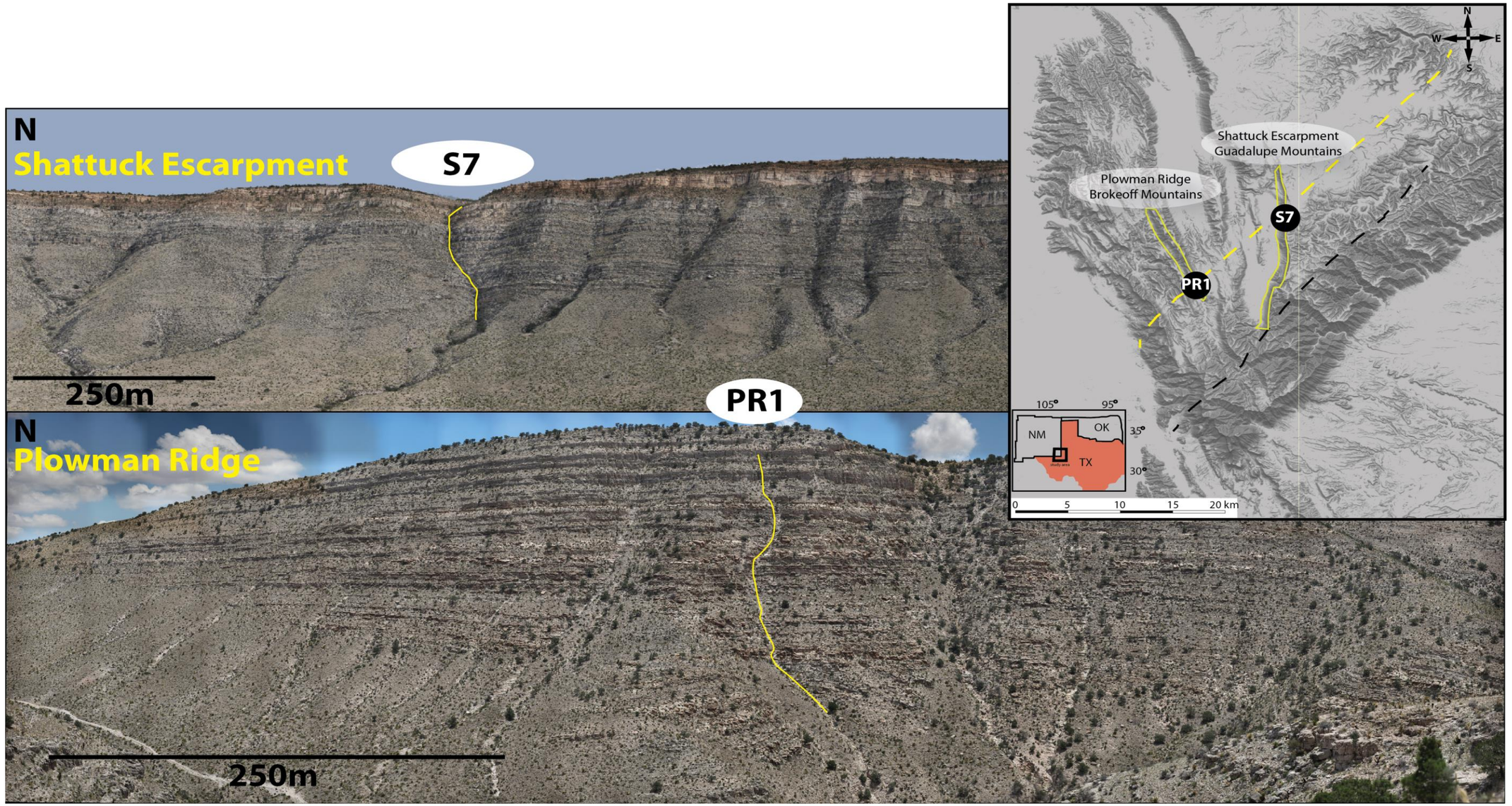

Figure 11: Location Map for Shattuck Section S7 and Plowman Section PR1: Section S7 is separated from section PR1 by 10Km along strike and 1.8Km along dip. Plowman section PR1 is 132m thick and was deposited directly above the terminal San Andres shelf margin (dashed in yellow). Shattuck section S7 is 172m thick and was deposited 1.8km seaward of the San Andres terminal margin. The Grayburg Fm shelf margin trend is dashed in black.

LITHOFACIES

Carbonate rocks described in this study are autochthonous, Primary fabric development was dictated by water depth, water temperature, water chemistry, and current/storm/wave energy. Most of the carbonate deposition on the shelf occurred during periods of sea-level highstand and transgression (Kerans 1995). The sandstones and siltstones described in this thesis were transported onto the carbonate shelf via aeolian processes (Fischer and Sarnthein 1988). Most of the sands were mobilized and delivered to the shelf at times of sea-level fall and during periods of sea-level lowstand (Sonnenfeld 1993, Kerans 1995, Kerans and Fitchen 1995, Sarg et. 1997) (Figure 12). During times of sea-level rise and during periods of sea-level highstand the sands were marine re-worked and the carbonate factory was re-established (Kerans 1995). Lithofacies of the Grayburg Formation recognized in this study are: (1) fenestral/ algal laminite, (2) peloid wackestone to mud-dominated packstone, (3) ooid-peloid grain-dominated packstone, (4) ooid grainstone, (5) fusulinid-peloid packstone, (6) skeletal-peloid mud-dominated packstone, and (7) coarse siltstone to very fine grained quartz sandstone. All carbonate facies are dolomitized unless otherwise noted. Basic attributes included sedimentary structures, allochems, and weathering profile; interpreted aspects were water depth range and depositional environment (Table 1).

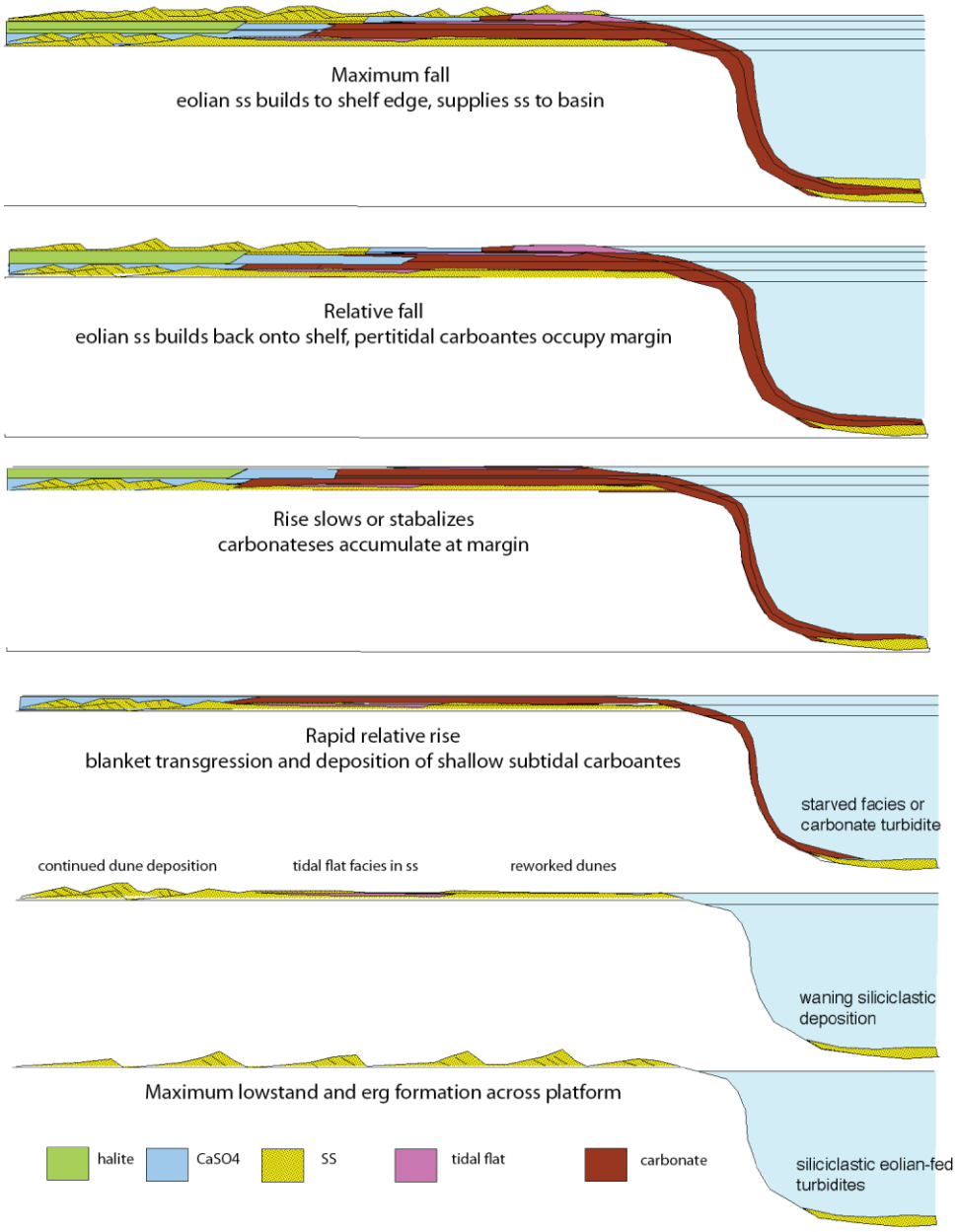

Figure 12: Sandstone Delivery Model: The majority of sandstones and siltstones were transported to the shelf during sea-level lowstand. The siliciclastics were marine re-worked during sea-level rise and periods of sea-level highstand. Figure from Kerans (1995)

Fenestral/algal laminite (Facies plate 1)

The chalky white to light-gray-fenestral laminite facies is either thin bedded and recessive or massive resistant bench former. Sedimentary structures include fenestrae, smooth to crinkly algal laminations, and rare tepee structures and sheet cracks. Fenestral type porosity of as much as 5% is often preserved within this facies. Rare skeletal allochems include fusulinid foraminifers and echinoid debris. Non-skeletal allochems include peloids, ooids, small rip-up clasts, rare sand grains, and moderately abundant pisoids. The dolomite crystal size is fine (<20μm). Contact between the fenestral/algal laminite facies and the underlying facies is generally gradational. Contact with the overlying facies is generally sharp. The fenestral laminite facies was deposited in an intertidal-to-supratidal setting in water depths of 0 to +1m (Kerans and Nance 1991, Sonnenfeld 1993, Ruppel and Bebout 2001, Barnaby and Ward 2007).

Peloid wackestone (wkst) to mud-dominated packstone (Facies plate 2)

The light-gray fine peloid wackestone to mud-dominated packstone facies is recessive. The peloid wackestone to mud-dominated packstone facies occurs as thin (5-10-cm) beds. Non-skeletal allochems include fine- sand-sized peloids and as much as 5% fine quartz sand grains. Undifferentiated skeletal fragments are locally common in this facies. The dolomite crystal size is fine-grained (<20μm). There is no apparent porosity preserved. The upper and lower contacts are generally sharp. This facies was deposited in a low-energy subtidal setting in water depths of 1 to 30 m (Kerans and Nance 1991, Sonnenfeld 1993, Ruppel and Bebout 2001, Barnaby and Ward 2007).

Ooid-peloid grain-dominated packstone (Facies plate 3)

The light-gray ooid-peloid grain-dominated packstone facies is moderately resistant, and it typically has a smooth texture after surface weathering. Sedimentary structures include centimeter-scale vertical burrows, rare polychaete worm tubes, low-angle current stratification, and 5-20 cm bedding. Non-skeletal allochems include fine-sand-sized peloids, fine-sand-sized ooids, and as much as 20% fine quartz sand. This

moderately well-sorted facies has as much as 10% moldic porosity and 5-10% interparticle porosity. The dominant dolomite crystal size is fine (<20μm), but medium crystalline dolomite (20-100 μm) is occasionally developed. The lower contact is gradational and the upper contact is typically sharp. The ooid-peloid grain-dominated packstone was deposited in a moderate-energy, shallow subtidal setting in water depths of 1 to 30 m (Kerans and Nance 1991, Sonnenfeld 1993, Ruppel and Bebout 2001, Barnaby and Ward 2007).

Ooid grainstone (Facies plate 4)

The medium-gray ooid grainstone facies is a resistant bench former. This facies is well-sorted and has an interparticle porosity of as much as 15%. Moldic porosity of 5% is less common. The dolomite crystal size is medium (20-100 μm). Sedimentary structures include: faint, low-angle current stratification, low-to-high angle tabular- planar cross stratification with 0.2 to 1.5 m bed set heights, 1.0 m trough cross stratification, sheet stratification, and vertical burrows. Non-skeletal allochems include fine-to-lower medium sand sized ooids and a maximum of 40% fine quartz sand. The upper and lower contacts are typically sharp, but are locally gradational. The ooid grainstone facies was deposited in a high-energy shallow subtidal setting within fair-weather wave base (0-10 m) (Kerans and Nance 1991, Ruppel and Bebout 2001, Barnaby and Ward 2007).

Fusulinid-peloid packstone (Facies plate 5)

The dark-gray fusulinid-peloid packstone facies is a resistant bench former. Sedimentary structures include low-angle current stratification and massive bedding. Skeletal allochems include abundant fusulinid foraminifers that are identified on the outcrop both as molds and are as preserved whole specimens. Non-skeletal allochems include fine-sand-sized peloids, rare ooids, and as much as 40% fine quartz sand. The dolomite crystal size developed in the peloid dominated matrix is fine (<20μm). Medium crystalline dolomite crystals partially occlude the molds after fusulinid dissolution. The lower contact is typically gradational and the upper contact is sharp. The fusulinid-peloid

packstone facies was deposited in a low-energy subtidal setting in water depths of 10 to >30 m (Kerans and Nance 1991, Sonnenfeld 1993, Ruppel and Bebout 2001).

Skeletal-peloid mud-dominated packstone (Facies plate 6)

The medium-gray skeletal-peloid mud-dominated packstone facies is moderately resistant and has a jagged surface texture after surface weathering. The skeletal-peloid mud-dominated packstone facies is massive. Skeletal allochems include mollusks and brachiopods. Non- skeletal allochems include abundant fine-sand-sized peloids, rare polychaete worm tubes, and rare algal laminations. The contacts are gradational. The mud-rich character and presence of deeper water fauna such as gastropods and brachiopods indicate that this facies was deposited in low-energy subtidal settings. Presence of rare polychaete worm tubes and algal laminations also supports deposition within very shallow subtidal settings. This facies was deposited across the depositional profile in water depths from 1 to 30 m (Kerans and Nance 1991).

Coarse siltstone to very fine grained sandstone (Facies plate 7)

The light/ medium gray-to-tan-brown quartz siltstone/sandstone is a recessive slope-former on the outcrop. Sedimentary structures include low- to high-angle planar cross stratification, ripple lamination, low-angle current stratification, and massive bedding. Where not occluded by dolomitic cement (fine crystalline <20μm), there is as much as 20% interparticle porosity in this well-sorted, fine grained facies. Fusulinid foraminifers are common in the massive units, and rare ooids are observed in the cross-bedded units. The lower contact with carbonate units is sharp. The upper contact with carbonate units is typically gradational. Cross-bedded quartz sandstone units were deposited in high-energy shallow subtidal settings in water depths of 1 to8 m (Kerans and Nance 1991). The massive fusulinid bearing sandstone units were deposited in a low-to-moderate-energy subtidal setting in water depths of 1 to 30 m (Kerans and Nance 1991).

Facies	Weathering profile	Sedimentary structures	Allochems	Environment	Water depth range (m)
Fenestal/algal laminite	Resistant, chalky white to light grey color	fenestrae, smooth to crinkly algal laminations, rare tepee structures, thin "platy" bedded, rare sheet cracks	pisoids, rip-up clasts, peloids, ooids, fusulinids, echinoid fragments	inner middle shelf	0-1m (intertidal)
Peloid wackestone to mud-dominated packstone	Recessive, light grey color	massive to 5-10cm bedded	peloids with rare sand grains and undifferentiated skeletal fragments	middle shelf to outer shelf	1-30m (low energy shallow sub-tidal to deep water)
Ooid-peloid grain-dominated packstone	Moderatly resistant, smooth weathered surface, light grey color	massive, 5-20cm bedded, low angle current stratified	peloids, ooids, sand grains, and rare undifferentiated skeletal fragments	middle shelf to shelf crest	1-30m (low to moderate energy shallow sub-tidal to deep water)
Ooid grainstone	resistant bench former, medium grey color	low to high angle planar cross stratified, trough cross stratified, planar sheet stratified, vertical tube burrows	ooids	shelf crest	1-10m (high energy shallow sub-tidal)
Fusulinid-peloid packstone	Resistant bench former, dark grey color, vuggy weathered surface	massive to low angle current stratified	fusulinids, peloids, quartz sand, and rare ooids	outer shelf	10-30m (low to moderate energy sub-tidal)
Skeletal-peloid mud-dominated packstone	Moderatly resistant, brecciated, medium grey color	massive	peloids, molluscs, brachiopods	middle shelf, outer shelf	1-30m (low to moderate energy sub-tidal)
Quartz sandstone	Resessive slope former, tan to brown color	massive, low to high angle planar cross stratified, ripple laminated	fusulinids	inner middle shelf, middle shelf, shelf crest, outer shelf	0-30m (supratidal, intertidal, low to high energy sub-tidal)

Table 1: Facies Characteristics: Table modified from Kerans and Nance (1991).

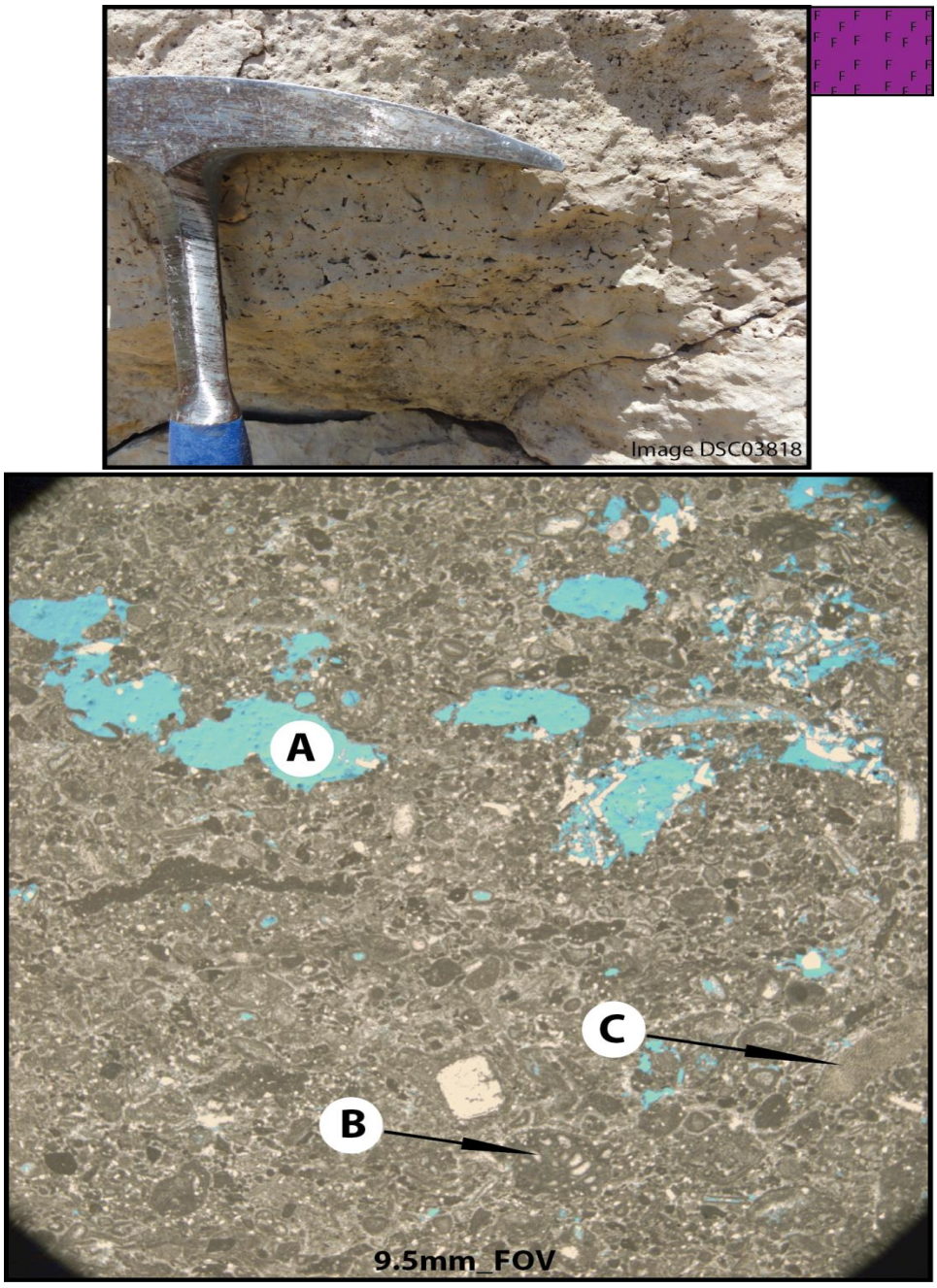

Facies Plate 1: Fenestral/algal laminite: The facies photo above shows linearly aligned fenestral pores commonly developed within an intertidal setting. The photomicrograph shows nicely preserved fenestral pores (A). Fusulinid foram fragments (B) and echinoid debris (C) were transported to the intertidal zone during storm events. Fabric preserving microcrystalline dolomite is common in this facies.

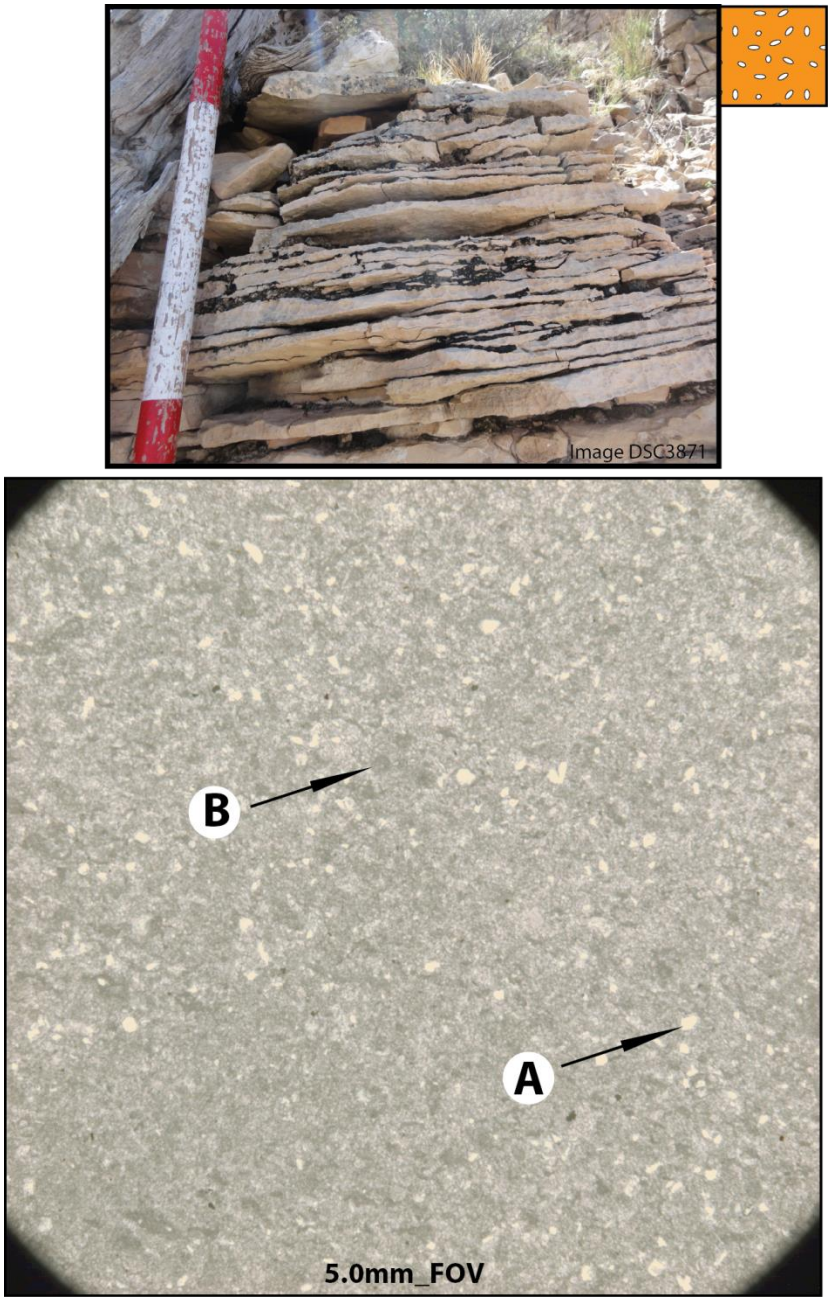

Facies Plate 2: Peloid wackestone to mud-dominated packstone: The thin 5-10cm bedding shown in the facies photo above is indicative of a low energy shallow subtidal depositional setting. Silt size quartz grains (B) and fine peloids (B) are found within the fine crystalline dolomite matrix in the photomicrograph above.

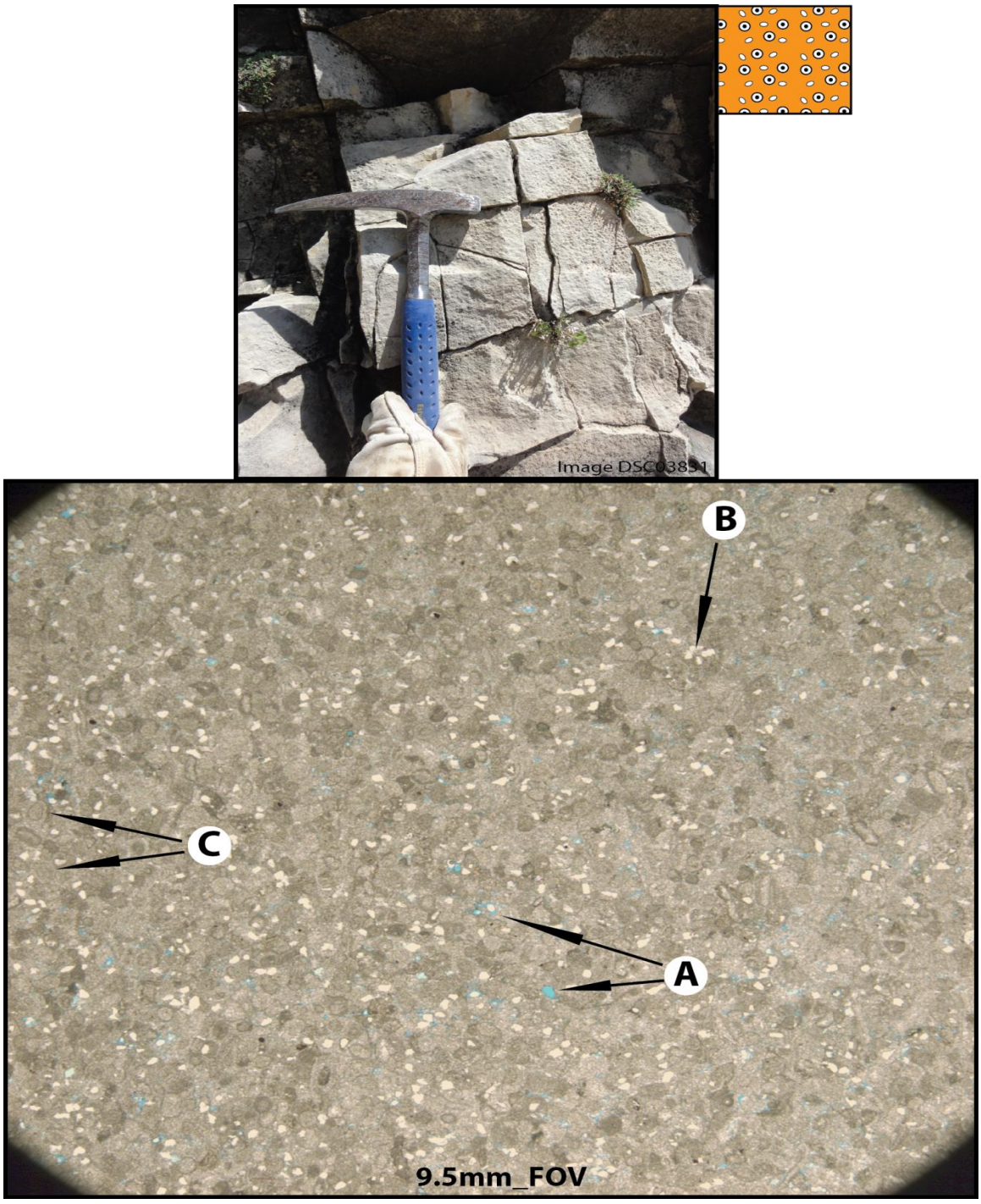

Facies Plate 3: Ooid-peloid grain-dominated packstone: There is small amounts of interparticle porosity (A) preserved within this facies. Silt size quartz grains are common within a matrix of moderately abundant ooids (C) and abundant fine peloids.

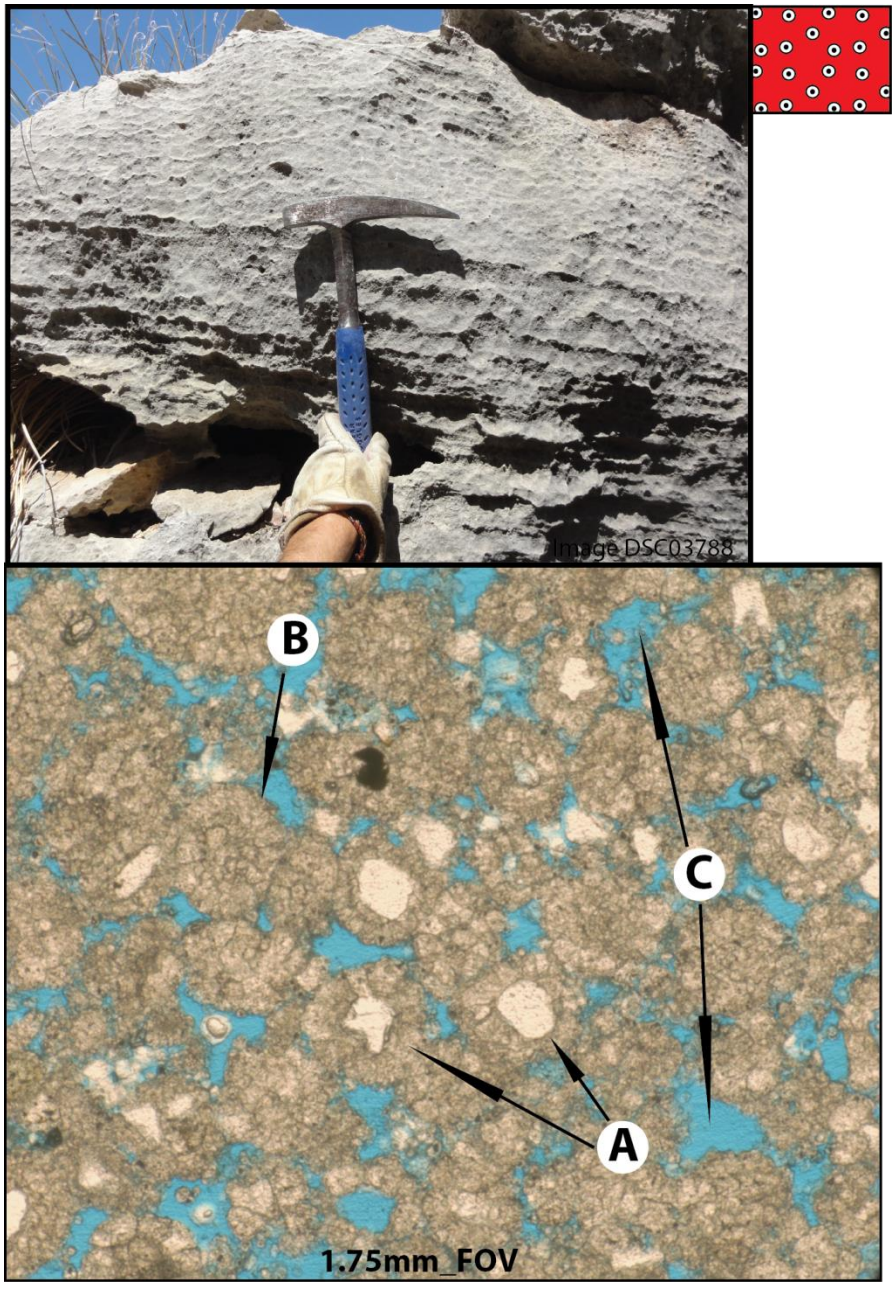

Facies Plate 4: Ooid grainstone: The ooid grainstone facies is typically cross bedded as shown in the facies photo above. Concentric cortices are observed around quartz cored (A) and non-quartz cored (B) ooids. The internal structure of the ooids is difficult to discern due to the fabric destructive medium crystalline dolomite. There is up to 15% interparticle/intercrystalline porosity (C).

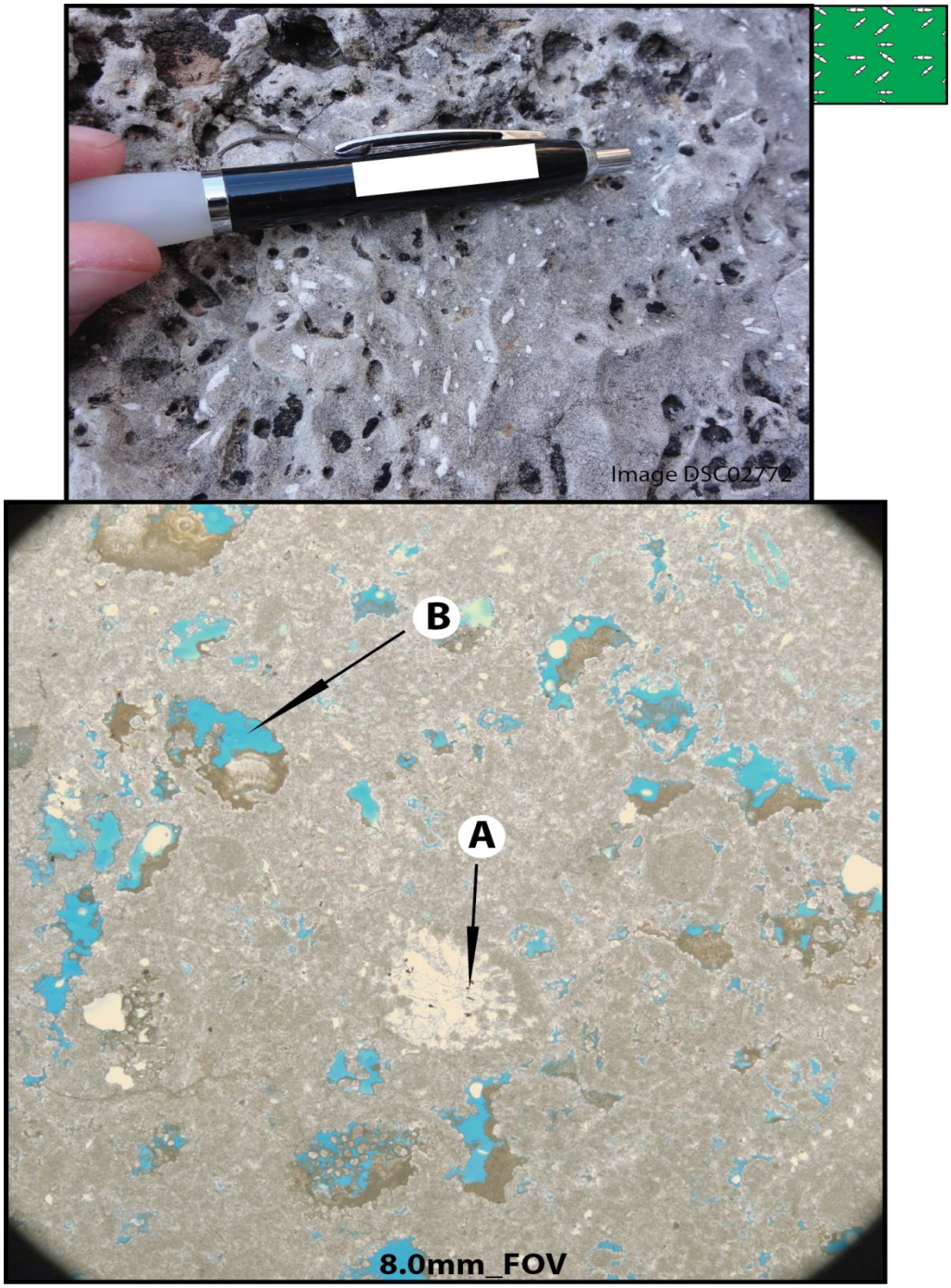

Facies Plate 5: Fusulinid-peloid packstone: The abundant oblong white shapes in the facies photo above are silicified fusulinid forams. The fusulinids are occasionally observed in thin section (A), more common are the molds after leaching partially filled with mottled tan carbonate tufa (B).

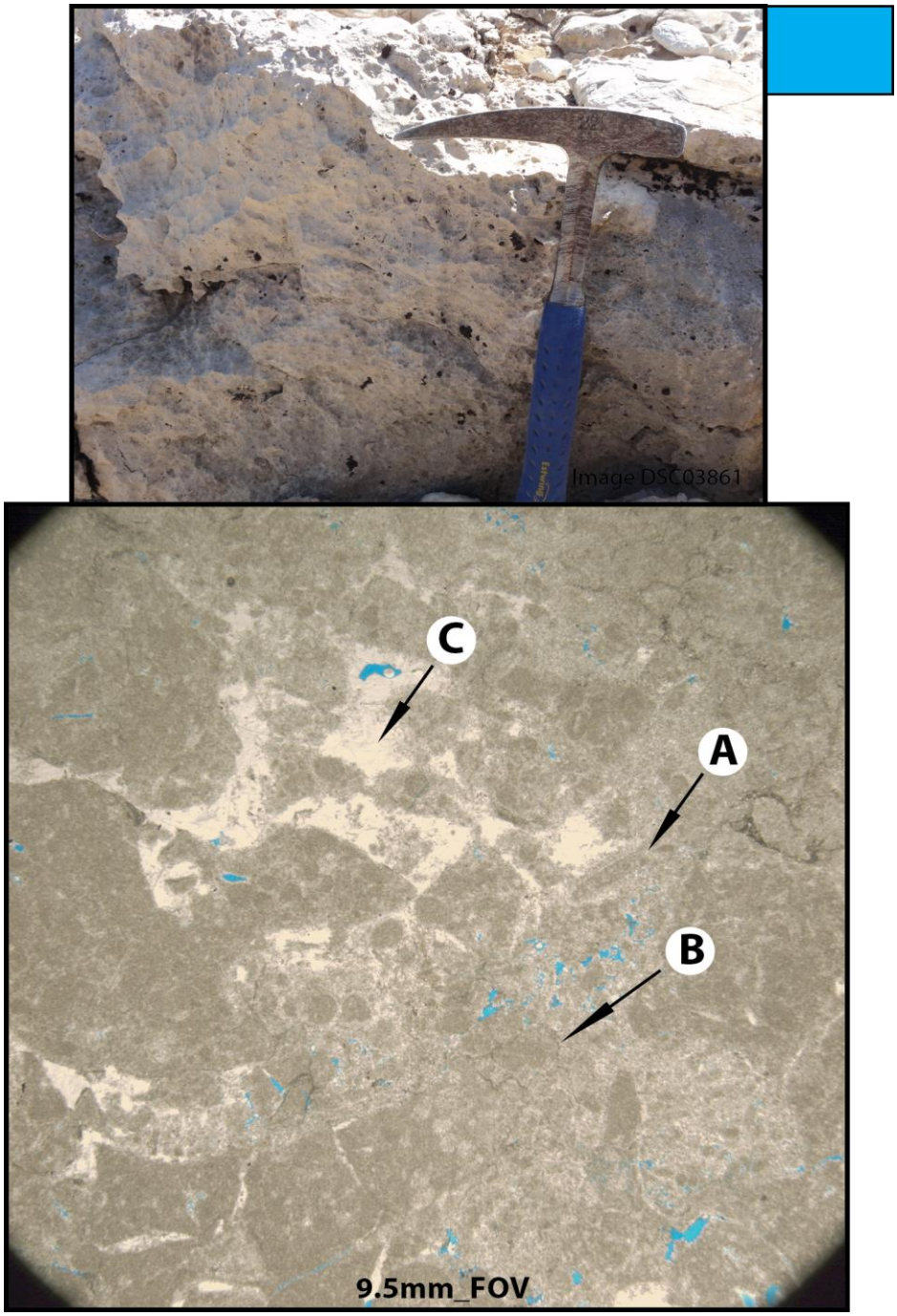

Facies Plate 6: Skeletal-peloid mud-dominated packstone: The facies photo above documents the jagged surface texture of the skeletal-peloid packstone facies. The brecciated fabric includes undifferentiated skeletal fragments (A), peloids (B), and calcite cement (C).

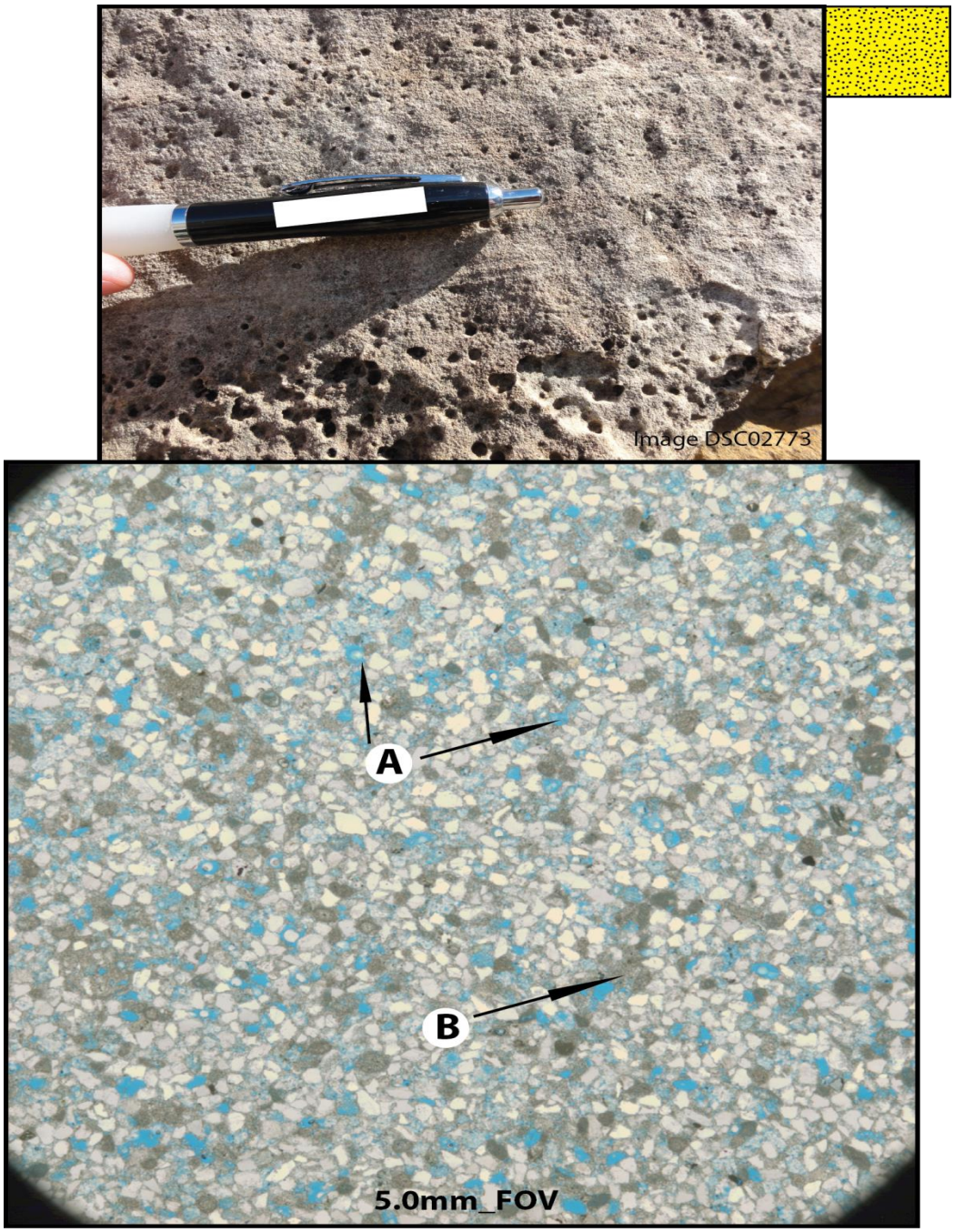

Facies Plate 7: Siltstone-to-v.fine grained quartz sandstone: There is up to 20% interparticle porosity (A) preserved. Dolomitic cement (B) occludes porosity and is a relic of the moderately abundant fine peloids. The peloids are darker relative to the light colored quartz grains in the photomicrograph above.

FACIES TRACTS AND VERTICAL FACIES SUCCESSION

Fundamental to outcrop-based sequence stratigraphic model construction is the documentation of the lateral facies transitions and delineation of facies tracts on the shelf-to-basin depositional profile (Kerans 1995). The lithofacies and associated diagnostic sedimentary structures used to delineate the facies tracts in this study have been used by previous authors with general consensus to define facies tracts on the Grayburg shelf-to-basin profile (Tye 1986, Franseen and Fekete 1989, Kerans and Nance 1991, Sarg et al. 1997, Barnaby and Ward 2007). There is a non-unique mosaic of facies that developed within the facies tracts documented on the Grayburg shelf-to-basin depositional profile (Franseen and Fekete 1989, Kerans and Nance 1991, Sarg et al. 1997, and Barnaby and Ward 2007). Diagnostic facies such as fenestral laminites, ooid-grainstones, and fusulinid-dominated packstones are used to place high-frequency cycles within the proper facies tract (Kerans 1995). The high-frequency cycle is closely analogous to the parasequence of Van Wagoner (1985). The parasequence is defined as a relatively conformable succession of genetically related beds or bedsets bounded by marine flooding surfaces. Facies described as cycle bases were deposited or reworked during marine flooding. Facies described as cycle caps were deposited during the latest stages of individual upward-shoaling events and are overlain by units deposited during the subsequent flooding event.

Grayburg Shelf-to-Basin Depositional Profile

The Grayburg shelf-to-basin depositional profile used for this study was developed using eight vertical measured sections from a well-constrained interval within the lower portion of the G12 HFS highstand systems tract at the Shattuck Escarpment in the Guadalupe Mountains (Figure 13). Within this interval, thin (0.5- to 1.0-m-thick) peloid mud-dominated packstone and fenestral laminite high-frequency cycles developed at Shattuck section 1 transition seaward into 1.0- to 1.5-m-thick peloid mud-dominated packstone cycles developed at Shattuck section Sh4 and Lost G (Figure 13B). The peloid mud-dominated packstone cycles transition seaward into the 1.5- to 3.5-m-thick, peloid-ooid grain-dominated and cross-bedded ooid grainstone cycles developed at sections Ot,

Sh7, and Xr (Figure 13B). The cross-bedded ooid-grainstone-capped high-frequency cycles grade downdip into 5.0-m-thick, peloid-ooid grain-dominated packstone, ooid-grainstone, and fusulinid packstone-dominated cycles at the Indian Vista section. The cycles developed at Indian Vista transition seaward into 6.0- to 6.5-m-thick, peloid-fusulinid packstone-dominated cycles at the Devil's Den section (Figure 13B).The total dip width of the Grayburg depositional profile is ~10 km (Figure 13A). The dip width of the depositional profile was determined by projecting the position of the measured sections on the Shattuck Escarpment to a corrected dip line drawn perpendicular between the trend of the terminal San Andres margin and the Grayburg shelf margin (Figure 14). The length of the profile exposed at the Shattuck Escarpment is ~8 km. An additional 2.0 km was added to the outer shelf portion of the profile to account for the Grayburg outer shelf and slope strata exposed at Bush Mountain on the Western Escarpment (Franseen and Fekete 1989).

The most landward facies tract described in this study was the inner-middle shelf facies tract, which graded seaward into the middle shelf facies tract. The middle shelf tract transitioned seaward to the shelf-crest facies tract. The outer shelf facies tract was the most downdip tract examined in this study (Figure 13A). Lateral facies transitions, average high-frequency cycle thickness, and vertical facies succession were used to define the general dip-dimensions of the facies tracts.

Inner-middle shelf facies tract

The inner-middle shelf facies tract is more than 1 km wide. It was deposited at the lowest accommodation setting on the shelf-to-basin depositional profile (Figure 13A). Average high-frequency cycle (HFC) thickness is from <0.5 m to ~2.0 m (Figure 15). The high-frequency cycle-base is either peloid wackestone to mud-dominated packstone or thin, recessive quartz sandstone. The peloid wackestone to mud-dominated packstone cycle base is typically overlain by a fenestral/algal laminite cycle cap. The sandstone cycle base may be overlain by either a fenestral laminite or a peloidal packstone cycle cap (Figure 15). Thinly bedded mud-dominated carbonate rocks such as the peloid wackestone to mud-dominated packstone indicate deposition in intertidal to low-energy

subtidal settings (Kerans and Nance 1991, Barnaby and Ward 2007). The fenestral/algal laminite is the key facies used to identify inner-middle shelf facies tract cycles (Kerans 1995). Key allochems and sedimentary structures documented within the fenestral laminite facies, such as pisoids, fenestrae, rare tepee structures, and sheet cracks, are known to develop in upper intertidal-to-supratidal depositional settings (Kendall 1969, Scholle and Halley 1980). The fenestral laminite cycle caps are typically slightly more resistant than the bases of the thin (2-10-cm) bedded peloid mud-dominated packstone cycles (Figure 15D).

Middle shelf facies tract

The middle shelf facies tract is ~ 4 km wide. It was deposited in a higher accommodation setting on the shelf-to-basin depositional profile relative to the inner-middle shelf facies tract (Figure 13A). Average high-frequency cycle thickness is from <1.0 m to 6.0 m (Figure16). The cycle base is typically thinly bedded (2-10 cm) peloid mud-dominated packstone or ooid-peloid grain-dominated packstone. Similar to the inner-middle shelf HFCs; thin recessive quartz sandstone units may represent the cycle base in middle shelf HFCs (Figure 16). Middle shelf HFC caps are commonly low-angle current stratified ooid-peloid grain-dominated packstones and grainstones. The winnowed grain-supported texture of the ooid-peloid grain-dominated packstone is indicative of a depositional setting within fair-weather wave base (Barnaby and Ward 2007). Grain-rich facies of the Grayburg middle shelf depositional environment are analogous to the grain-rich facies found in the Persian Gulf within the lagoon at the Khor al Bazam (Ward and Kendall 1986). The vertical transition from 2-10-cm-bedded ooid-peloid mud-dominated packstone units up into 5-20-cm-bedded low-angle current stratified ooid-peloid grain-dominated packstone units indicates increased energy related to upward shoaling or sea-level fall (Harris and Kerans 1993). Current-stratified ooid-peloid grain-dominated packstone cycle caps are typically more resistant units than the thin-bedded peloid mud-dominated cycle bases (Figure 16C). The evolution from thin 0.2 m to 1.0 m thick laminite capped cycles at section Sh1 to thicker 1.0 to 1.5 m peloid packstone cycles at

sections Sh4 and Lost Grayburg was used to delineate the transition from the inner-middle shelf to middle shelf facies tract.

Shelf-crest facies tract

The shelf crest facies tract is~ 3 km wide, and it was deposited at the highest energy position on the shelf-to-basin profile (Sonnenfeld 1993, Kerans and Nance 1991, Kerans 1995) (Figure 13A). The mixed carbonate-siliciclastic shelf crest high-frequency cycles have an average thickness of between 1.0 and 3.5 m (Figure 17). The cycle bases are typically current-stratified ooid-peloid grain-dominated packstones, massive current stratified quartz sandstones, or peloid-fusulinid packstones (Figure 17). Shelf crest facies tract cycle caps are ooid grainstone units with planar cross stratification, trough cross stratification, and sheet stratification. Shelf-crest cycle bases are typically moderately recessive, and the cycle caps are resistant bench-forming units (Figure 17D). Cross-bedded ooid grainstone facies are an excellent indicator of that depositional setting. Ooid grainstone facies are known to develop in high-energy settings within fair-weather wave base (Sarg and Lehmann 1986, Kerans and Nance 1991, Sonnenfeld 1993, Kerans and Fitchen 1995, Sarg et al. 1997, Barnaby and Ward 2007). Sedimentary structures observed within the ooid grainstone units are analogous to features attributed to modern processes active in tidally dominated ooid bar belts in the Bahamas (Rankey 2006). Ooid grainstone units have been used to identify the shelf-crest depositional environment within the San Andres and Grayburg Formations in numerous previous studies (Sarg and Lehmann 1986, Sonnenfeld 1993, Kerans and Nance 1991, Kerans et al. 1994, Barnaby and Ward 2007).

Siliciclastic-dominated cycles within the shelf-crest facies tract are between 1.0 and 4.0 m thick (Figure 17C). Siliciclastic shelf-crest cycle bases are typically low-angle current-stratified to massive fine quartz sandstones or siltstones. Overlying the current cycle bases are sandstone units with sedimentary structures including: planar cross stratification, trough cross stratification, ripple lamination, and sheet stratification (Barnaby and Ward 2007, this study). Shelf-crest facies tract sandstone cycles are typically resistant tan to rust-colored successions.

The transition from 1.0- to 1.5-m-thick peloid packstone dominated high-frequency cycles at sections Sh4 and Lost Grayburg seaward to 1.0- to 3.5-m-thick cross-bedded ooid grainstone capped cycles at sections Ot, Sh7, and Xr was used to delineate the transition from the middle shelf facies tract to the shelf-crest facies tract (Figure 14A).

Outer shelf facies tract

The outer shelf facies tract is ~ 4 km wide. It occupies the highest accommodation position on the shelf-to-basin profile examined in this study (Figure14 A). The mixed carbonate-siliciclastic outer shelf facies tract high-frequency cycle average thickness is between 3.0 and 8.0 m (Figure 18). Outer shelf cycle bases are typically massive, fusulinid-bearing quartz sandstones. The lack of preserved sedimentary structures within the massive sandstone cycle bases may be a result of the bioturbation that is common in low-energy outer shelf subtidal settings. The sandstone cycle base is typically recessive, and the overlying peloid-fusulinid packstone cycle cap is resistant (Figure 18D). The peloid-fusulinid packstone units are typically massive toward the base and grade up into faint low-angle current stratification. Low-angle current stratification developed within the fusulinid packstone units indicates that these cycles were deposited in a moderate-energy setting within storm-weather wave base (Kerans and Fitchen 1995, Kerans and Tinker 1999). Previous studies of both San Andres and Grayburg strata have linked fusulinid-dominated facies to the outer shelf depositional environment (Franseen and Fekete 1989, Kerans and Nance 1991, Sonnenfeld 1993, Kerans and Fitchen 1995, Kerans and Tinker 1999, Ruppel and Bebout 2001, Barnaby and Ward 2007).

Outer shelf facies tract siliciclastic-dominated high-frequency cycle thicknesses range from 1.0 to 7.0 m. Siliciclastic outer shelf cycle bases are typically recessive bioturbated fusulinid-bearing quartz sandstones overlain by massive to low-angle current-stratified fusulinid-bearing sandstone units with minor bioturbation. The abundance of fusulinids within these sandstone cycles supports depositional marine reworking within the outer

shelf facies tract (Franseen and Fekete 1989, Kerans and Nance 1991, Sonnenfeld 1993, Kerans and Fitchen 1995, Kerans and Tinker 1999, Ruppel and Bebout 2001, Barnaby and Ward 2007). The transition from 1.0- to 3.5-m-thick cross-bedded ooid grainstone-capped cycles at sections Sh7 and Xr seaward to 3.0- to 8.0-m-thick fusulinid packstone-dominated cycles at the Devil's Den section was used to delineate the transition from the shelf-crest facies tract to the outer shelf facies tract (Figure 14B)..

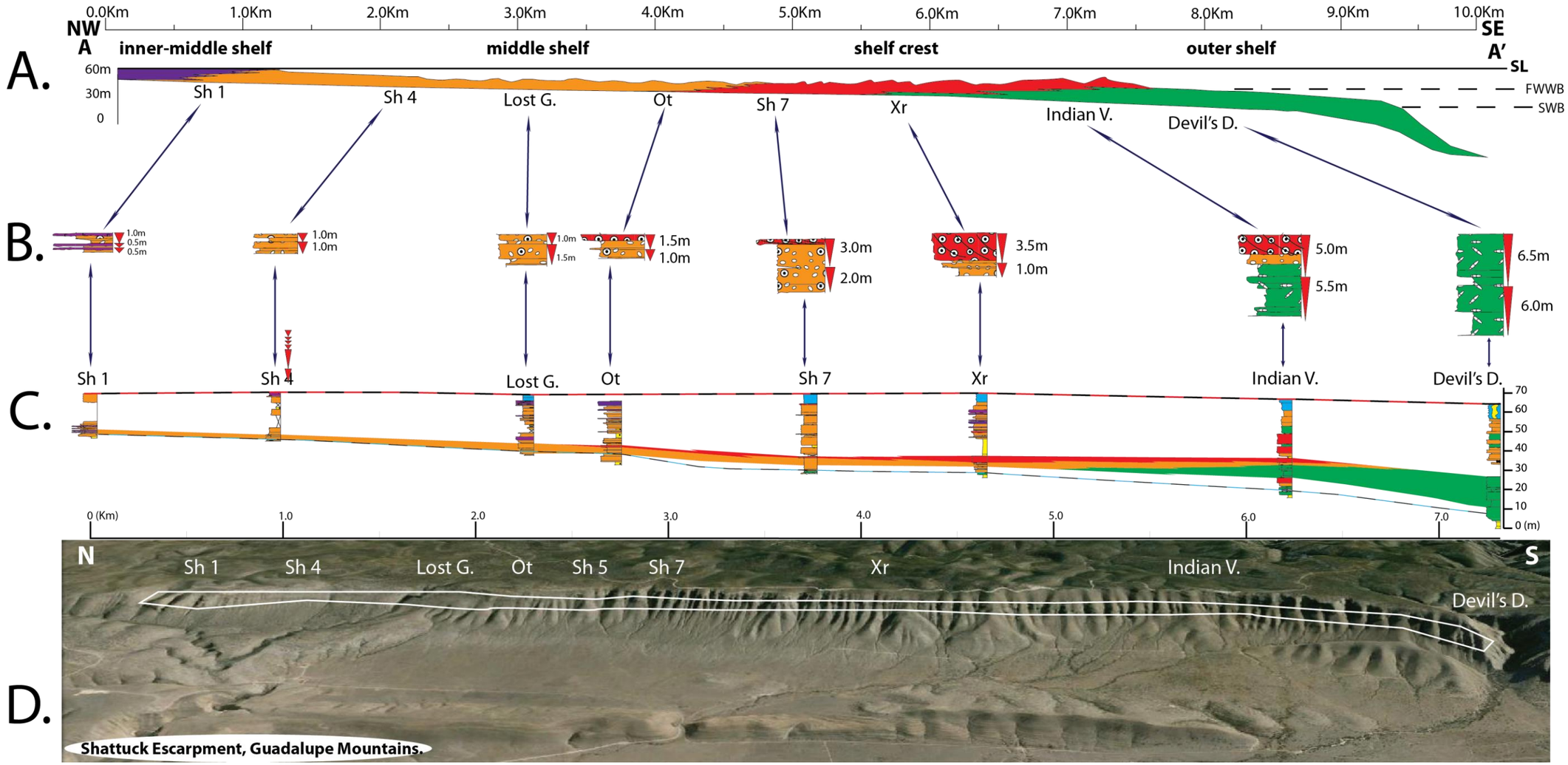

Figure 13: Grayburg Fm Dip-Corrected Depositional Profile: The shelf-to-basin depositional profile was developed using data from 8 of the 9 vertical measured sections measured along the Shattuck Escarpment in the Guadalupe Mountains (D). The profile was constructed within a well-constrained interval of the G12 HFS highstand systems tract (C) Inner-middle shelf facies tract laminite capped cycles at section Sh1 transition seaward to low-energy subtidal middle shelf peloid packstone cycles at sections Sh4 and Lost Grayburg. The ooid-grainstone capped shelf-crest cycles at sections Ot, Sh7, and Xr transition seaward to fusulinid dominated outer shelf cycles at the Devil's Den section (B). The dip width of the inner-middle shelf facies tract was >1km (updip limit not defined in this study), the width of the middle shelf was ~4km, the shelf-crest was ~3km, and the outer shelf was ~4km wide (Grayburg Fm margin is mapped ~2km seaward of the Devil's Den section at Bush Mtn. along the Western Esc. See Franseen and Fekete (1989))

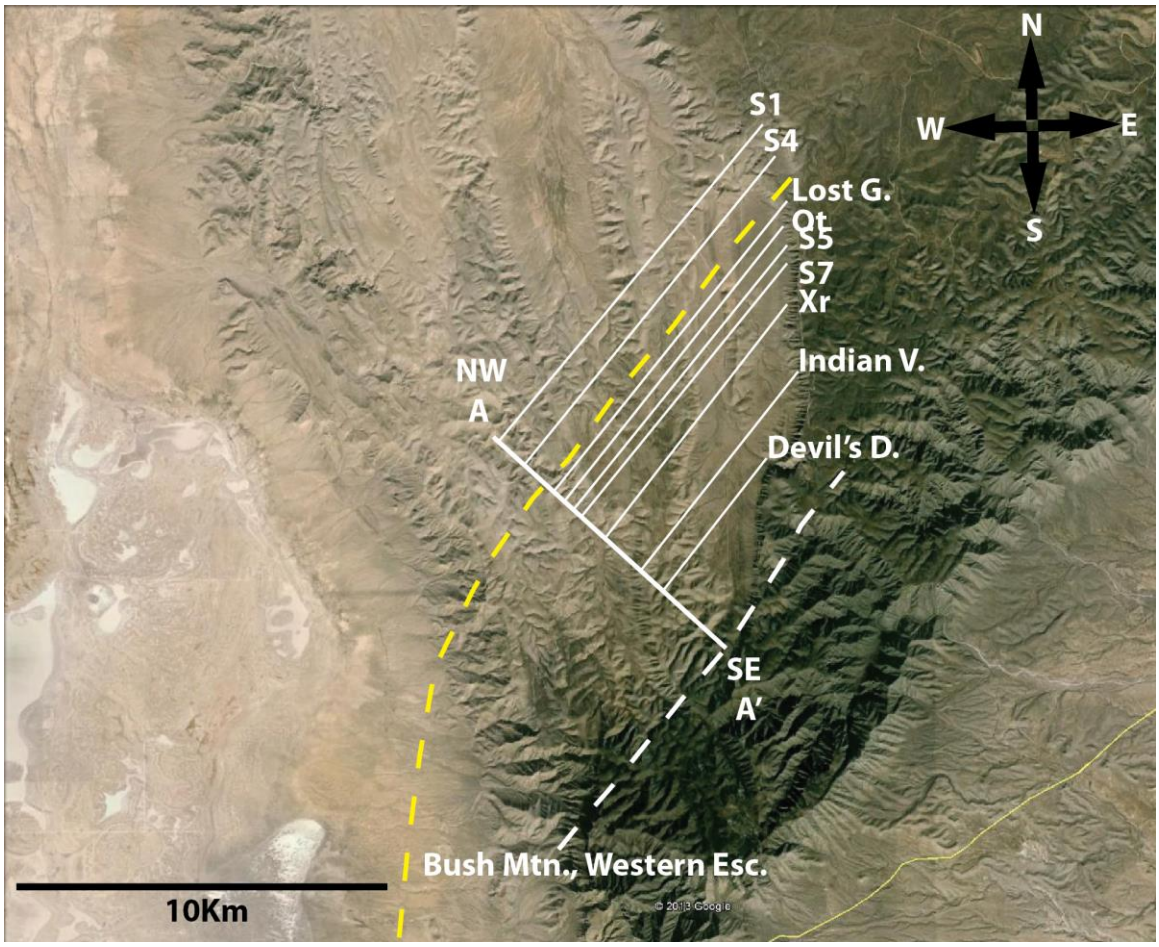

Figure 14: Dip-Corrected Line of Section A-A': The line A-A' is drawn perpendicular to the trend of the terminal San Andres Fm margin (dashed in yellow) and the Grayburg Fm margin (dashed in white). Measured sections collected along the Shattuck Escarpment were projected to this line for construction of the depositional profile and cross-section.

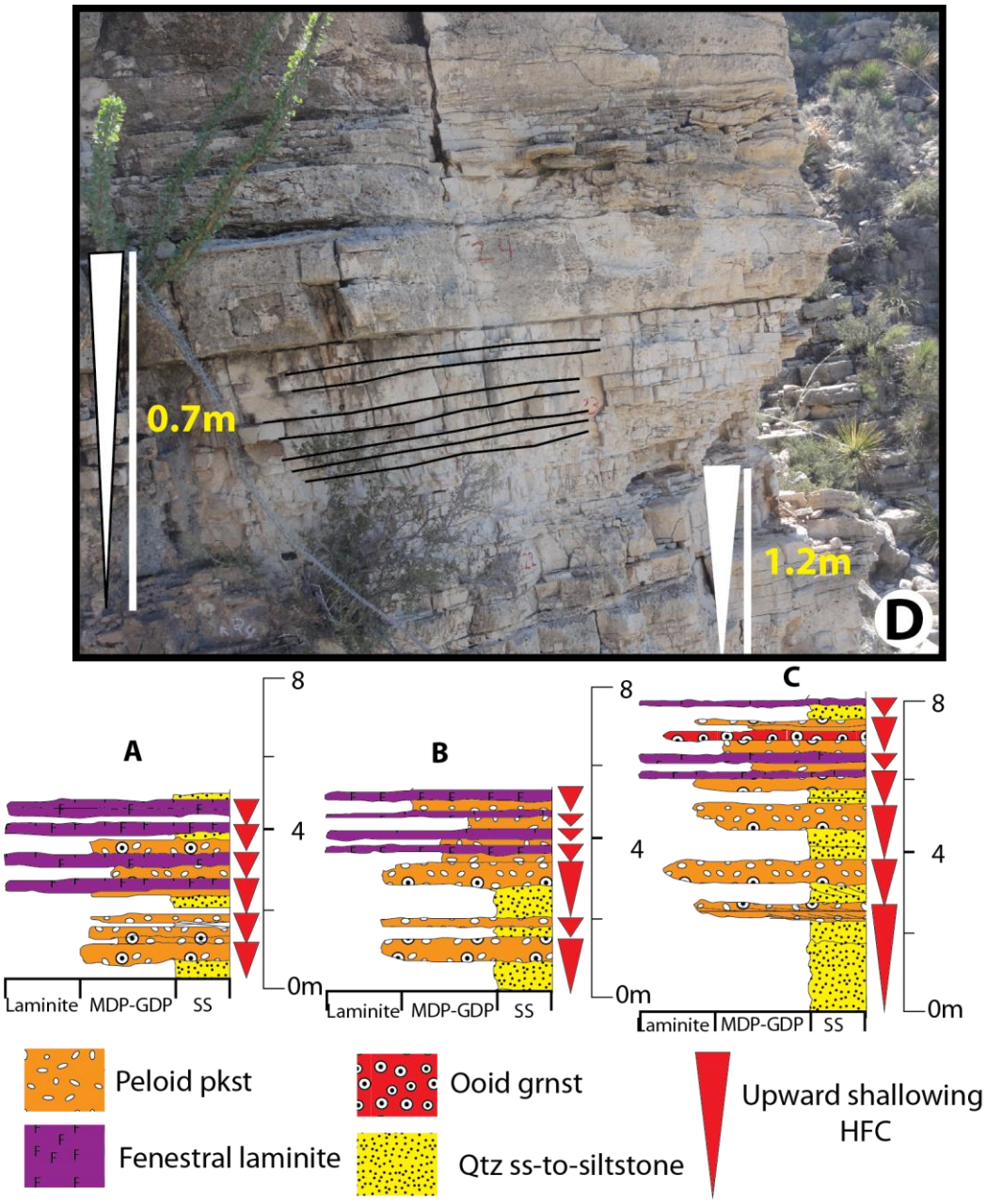

Figure 15: Inner-Middle Shelf Facies Tract Cycles: The inner-middle shelf facies tract is dominated by peloidal packstones, fenestral laminites, and quartz sandstones. The average cycle thickness is between 0.2 and 1.2m. Thin bedded peloid packstone cycle bases are typically recessive compared to the fenestral laminite cycle caps. The cycle stacking pattern (A) is from the G10HFS at section S 1, (B) from the G10 HFS section S7, and (C) the G11 HFS section S7.

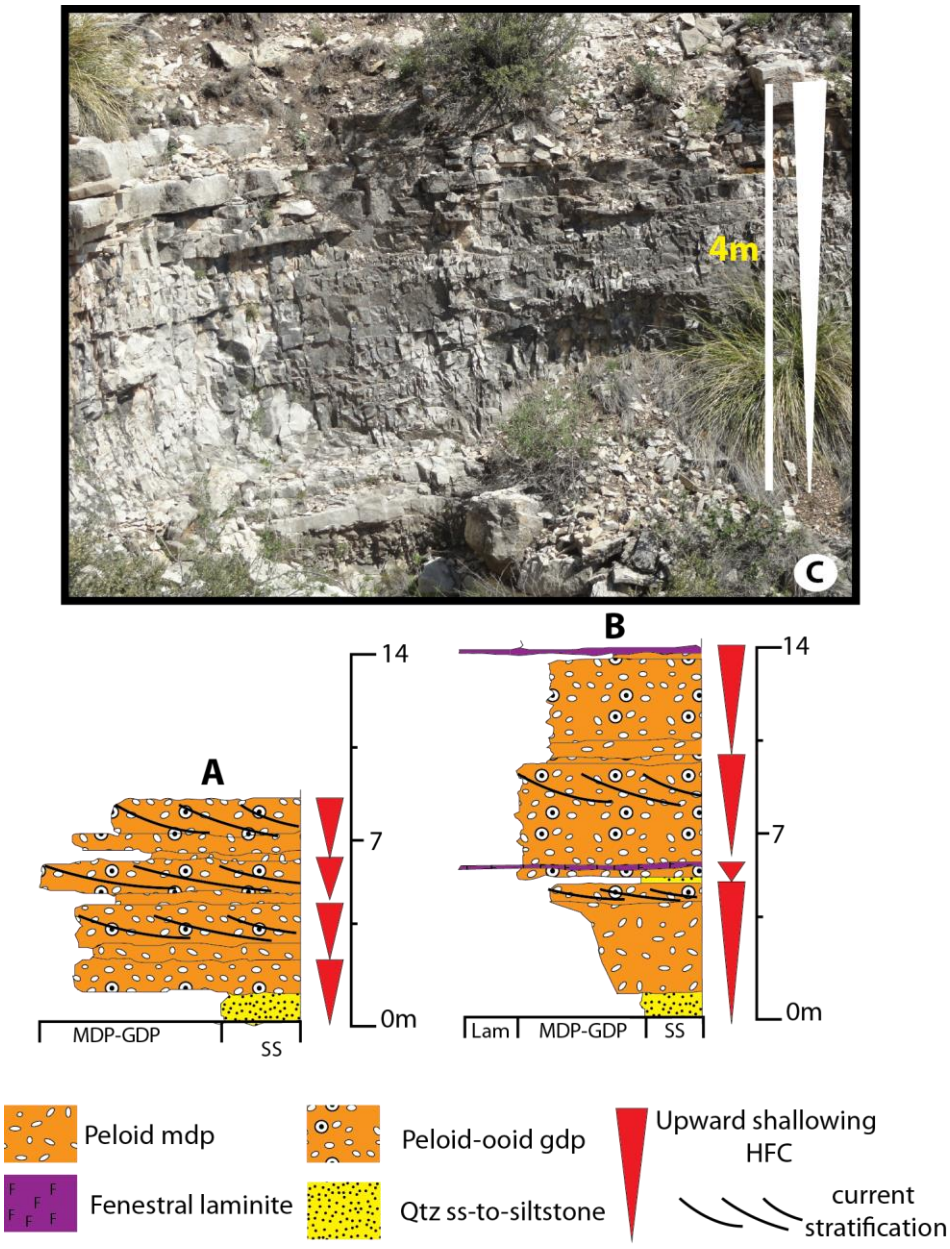

Figure 16: Middle Shelf Facies Tract Cycles: The middle shelf facies tract is dominated by peloidal mud-dominated packstones, peloid-ooid grain dominated packstones, and quartz sandstones. The average cycle thickness is between 1.0 and 6.0m. Cycle bases are quartz sandstones or thin bedded peloid packstones. The cycle caps are peloid-ooid grain-dominated packstones or thin laminites. The cycle stacking pattern (A) is from the G12 HFS at section Sh 1 and (B) is from the G12 HFS at section Ot.

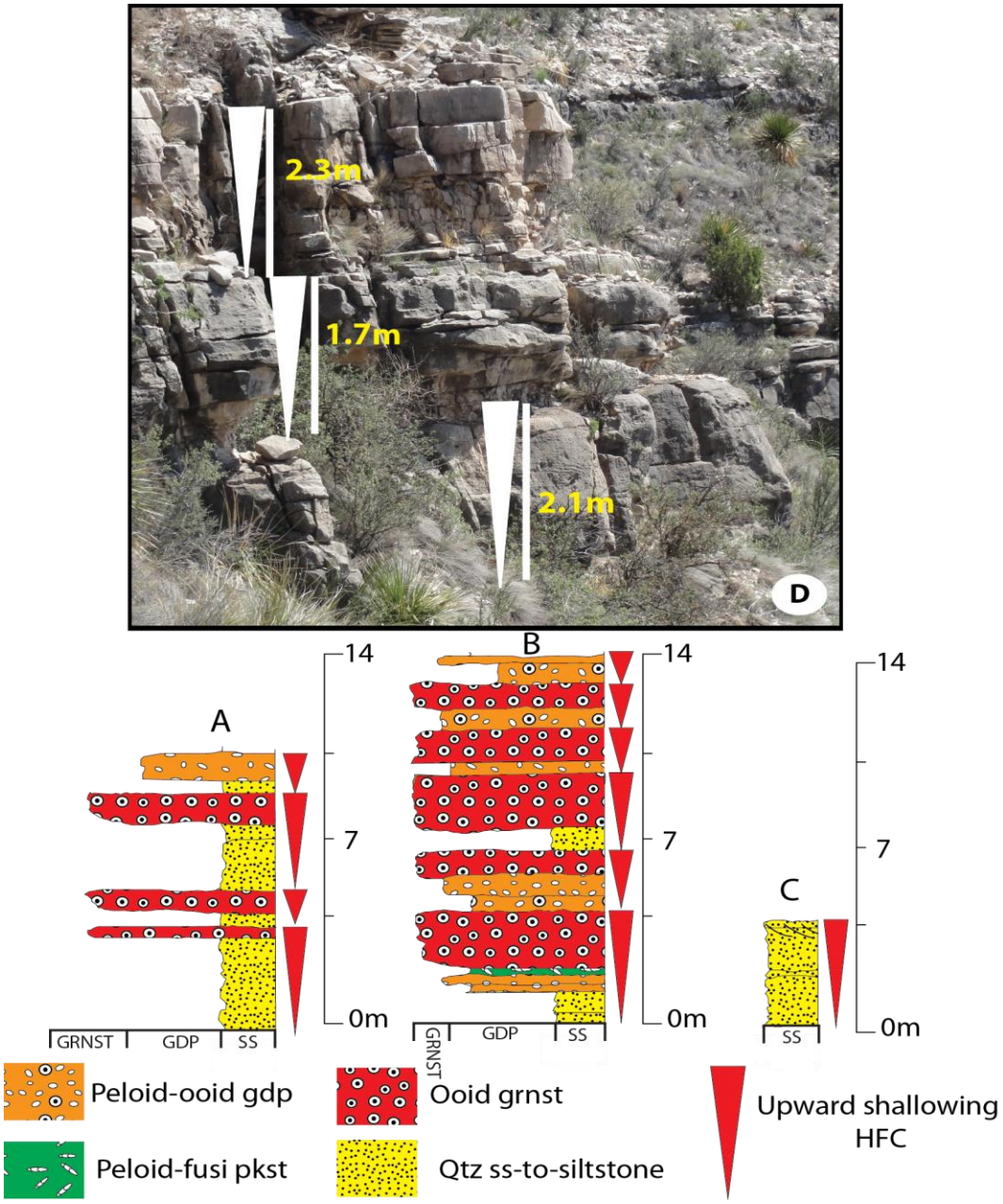

Figure 17: Shelf-Crest Facies Tract Cycles: The shelf-crest facies tract is dominated by peloid-ooid grain dominated packstones, ooid grainstones, and quartz sandstones. The average cycle thickness is between 1.5 and 3.5m. Cycle bases are quartz sandstones or peloid-ooid grain-dominated packstones. The cycle caps are peloid-cross-bedded ooid grainstones. The cycle stacking pattern (A) is from the G10 HFS at section S7, (B) is from the G12 HFS at section S7, and (C) is from the G11HFS at section Xr.

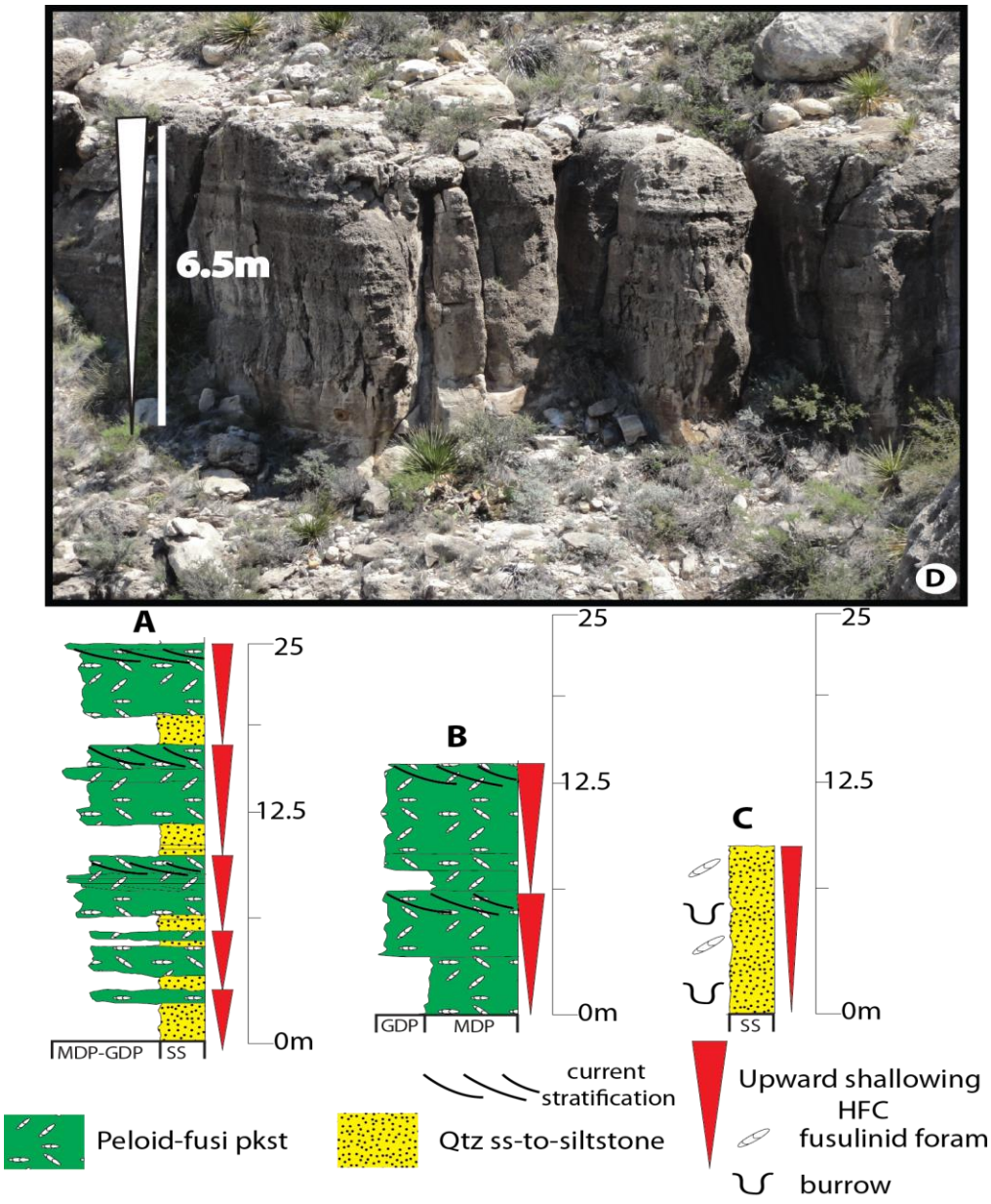

Figure 18: Outer Shelf Facies Tract Cycles: The outer shelf facies tract is dominated by peloid-fusulinid grain dominated and mud-dominated packstones and quartz sandstones. The average cycle thickness is between 3.5 and 8.0m. Cycle bases are quartz sandstones or peloid-fusulinid mud-dominated packstones. The cycle caps are peloid-fusulinid grain-dominated packstones or sandstones. The cycle stacking pattern (A) is from the G10 HFS at section S7, (B) is from the G12 HFS at the Devil's Den section, and (C) is from the G11HFS at Indian Vista.

GRAYBURG SEQUENCE STRATIGRAPHIC FRAMEWORK

The stratigraphic framework of the Grayburg Formation was first examined in the Brokeoff Mountains by Boyd (1958) and in the Guadalupe Mountains by Hayes (1959, 1964). The San Andres-Grayburg contact is exposed at the Algerita Escarpment, Last Chance Canyon, and the Shattuck Escarpment in the Guadalupe Mountains (Hayes 1964, Kerans and Nance 1991, Sonnenfeld 1993, Kerans and Fitchen 1995) The San Andres-Grayburg contact is exposed at Big Ridge, Plowman Ridge, and Cutoff Ridge in the Brokeoff Mountains (Boyd 1958, Fitchen 1993, Sarg et al. 1997, Barnaby and Ward 2007, and this study).

One of the best locations to observe the San Andres-Grayburg contact in the Guadalupe Mountains is on the northern end of the Shattuck Escarpment. Kerans and Nance (1991) documented Grayburg sands within karst pits cut into San Andres Formation fenestral laminites. The San Andres-Grayburg contact is difficult to track in the seaward direction at the Shattuck Escarpment due to significant basinward slope related to the progressive thinning of the upper San Andres highstand during composite sequence scale sea-level fall (Kerans and Nance 1991, Sonnenfeld 1993, Fitchen 1993, Kerans and Fitchen 1995). The Grayburg-Queen contact at the Shattuck Escarpment was picked by Hayes (1964) at the base of a "locally conspicuous sandstone" (Hayes 1964, p. 29). In this study the Grayburg-Queen contact is correlated along the base of a conspicuous, recessive, slope-forming sandstone unit underlain by a thick carbonate bench with sporadically developed breccia-filled karst pits.

Boyd (1958) picked the San Andres-Grayburg contact at an abrupt change in "lithologic character" coinciding with a sharp color change at Big Ridge in the Brokeoff Mountains. He used these criteria to map the contact throughout the El Paso Gap quadrangle. Boyd (1958) treated the Grayburg-Queen interval as a single sequence and thus did not define a contact between the two formations in the Brokeoff Mountains. Subsequent outcrop-based studies of the Grayburg Formation have addressed internal sequence framework and facies distribution patterns in an effort to better understand the subsurface heterogeneity that affects reservoir performance. Sequence stratigraphic

models of the Grayburg Formation developed at outcrops in the southern Guadalupe Mountains and Brokeoff Mountains have divided the formation into three and four high-frequency sequences (Kerans and Nance 1991, Kerans and Kempter 2002, Barnaby and Ward 2007, this study).

Sequence framework development using 1 and 2-dimensional cycle analysis

The Grayburg sequence stratigraphic framework was constructed using nine vertical measured sections collected along the Shattuck Escarpment in the Guadalupe Mountains (Figure 19). High-frequency sequence boundaries and maximum flooding surfaces were picked using the methods outlined by Kerans (1995) for construction of sequence stratigraphic frameworks in carbonate successions using one- and two-dimensional cycle analysis. Individual high-frequency cycles were systematically interpreted at each measured section. High-frequency cycles (HFC) record deposition at the most frequent scale of retrogradation and progradation (Figure20) The high-frequency cycles were then grouped into high-frequency cycle sets defined by retrogradational, progradational, or aggradational stacking pattern (Van Wagoner 1985). High-frequency cycle sets record retrogradation and progradation on a longer duration relative to the HFC (Figure 20).

High-frequency cycle sets were correlated between measured sections. Key facies with well-constrained depositional origins were present throughout the sections, which facilitated two-dimensional comparison of facies tract distribution. High-frequency sequence-scale maximum flooding surfaces were picked within fusulinid-dominated outer shelf cycle sets correlated to the furthest updip positions (Figure 21). High-frequency sequence boundaries were picked at the top of fenestral laminite dominated inner-middle shelf cycle sets correlated to the furthest downdip positions. Lateral and vertical distribution of ooid grainstone-capped shelf-crest cycles were used to track retrogradation and progradation within the high-frequency sequences (Figure 21). Shattuck S7 is the reference section used to describe the one-dimensional cycle stacking patterns within the Grayburg G10, G11, and G12 high-frequency sequences (Figure 22).

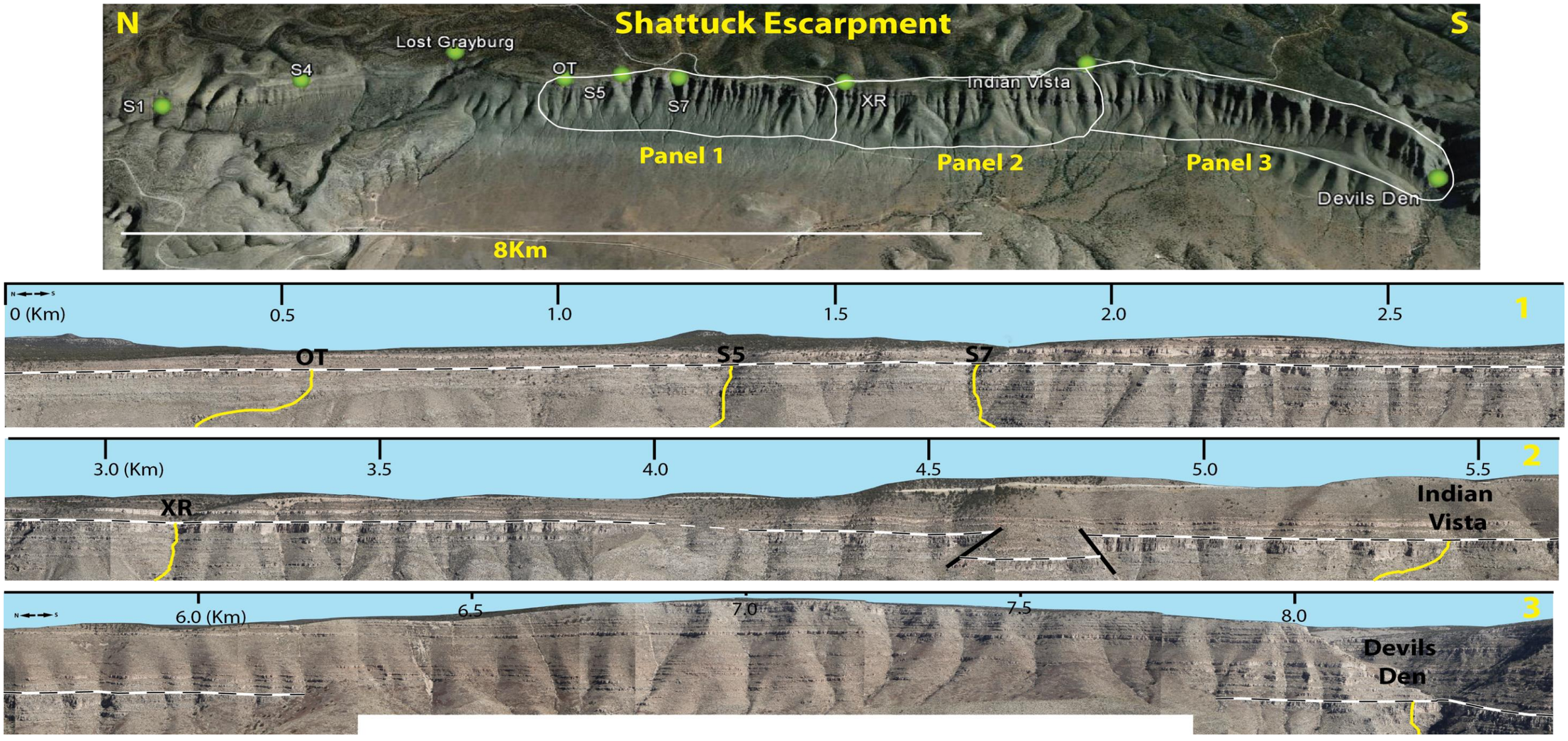

Figure 19: Vertical Measured Section Locations along the Shattuck Escarpment: Nine vertical sections were measured within the Grayburg interval along the Shattuck Escarpment in the Guadalupe Mountains. Section S1 is the most landward and the Devil's Den section is the most seaward. The locations of downdip sections Ot, S5, S7, Xr, Indian Vista, and Devil's Den are shown on the aerial photopan. Sections S1, S4, and Lost Grayburg are located updip of the aerial photopan coverage.

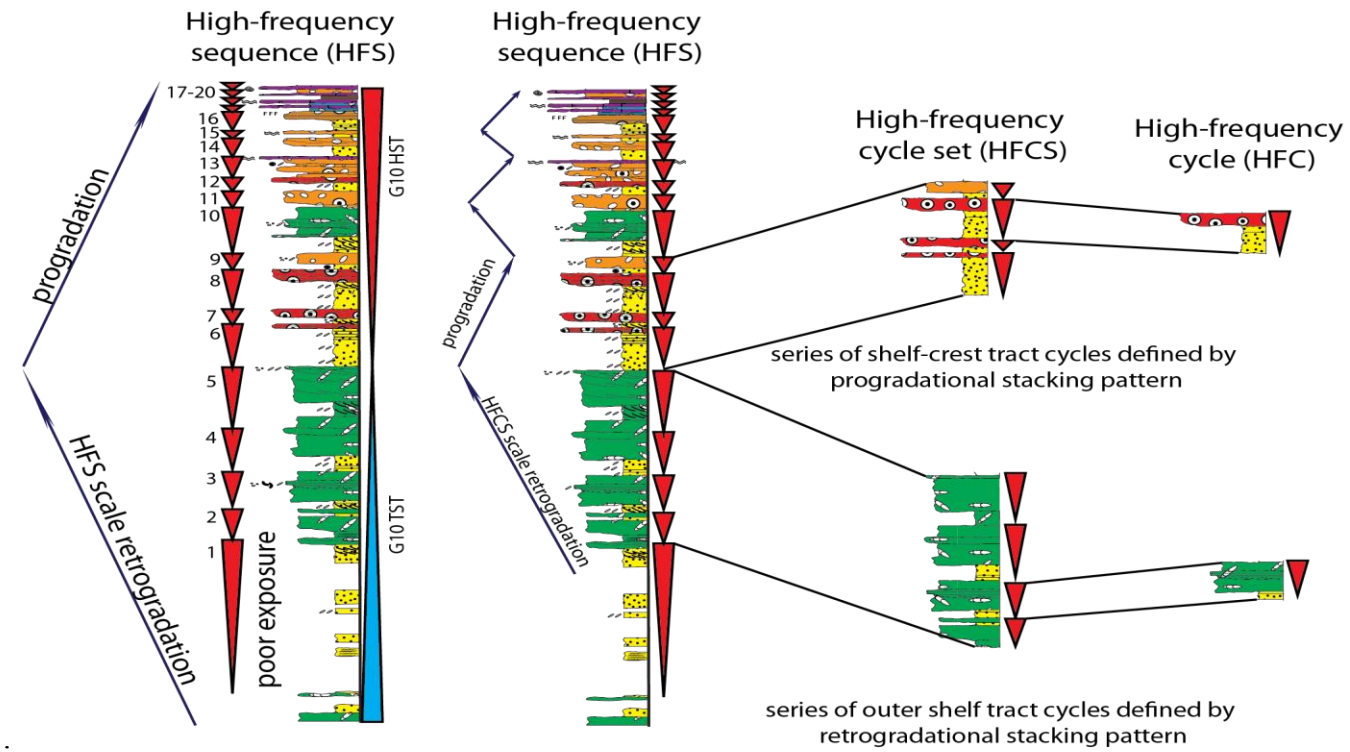

Figure 20: 1-Dimensional Scales of Retrogradation and Progradation: High-frequency cycles (HFC) record deposition at the most frequent scale of retrogradation and progradation. The cycles are grouped into high-frequency cycle sets (HFCS) that record retrogradation and progradation on a longer duration that the HFC. High-frequency cycle sets comprise the high-frequency sequence (HFS). Compared to the HFC and HFCS, the high-frequency sequence scale retrogradation and progradation occurs over the longest duration.

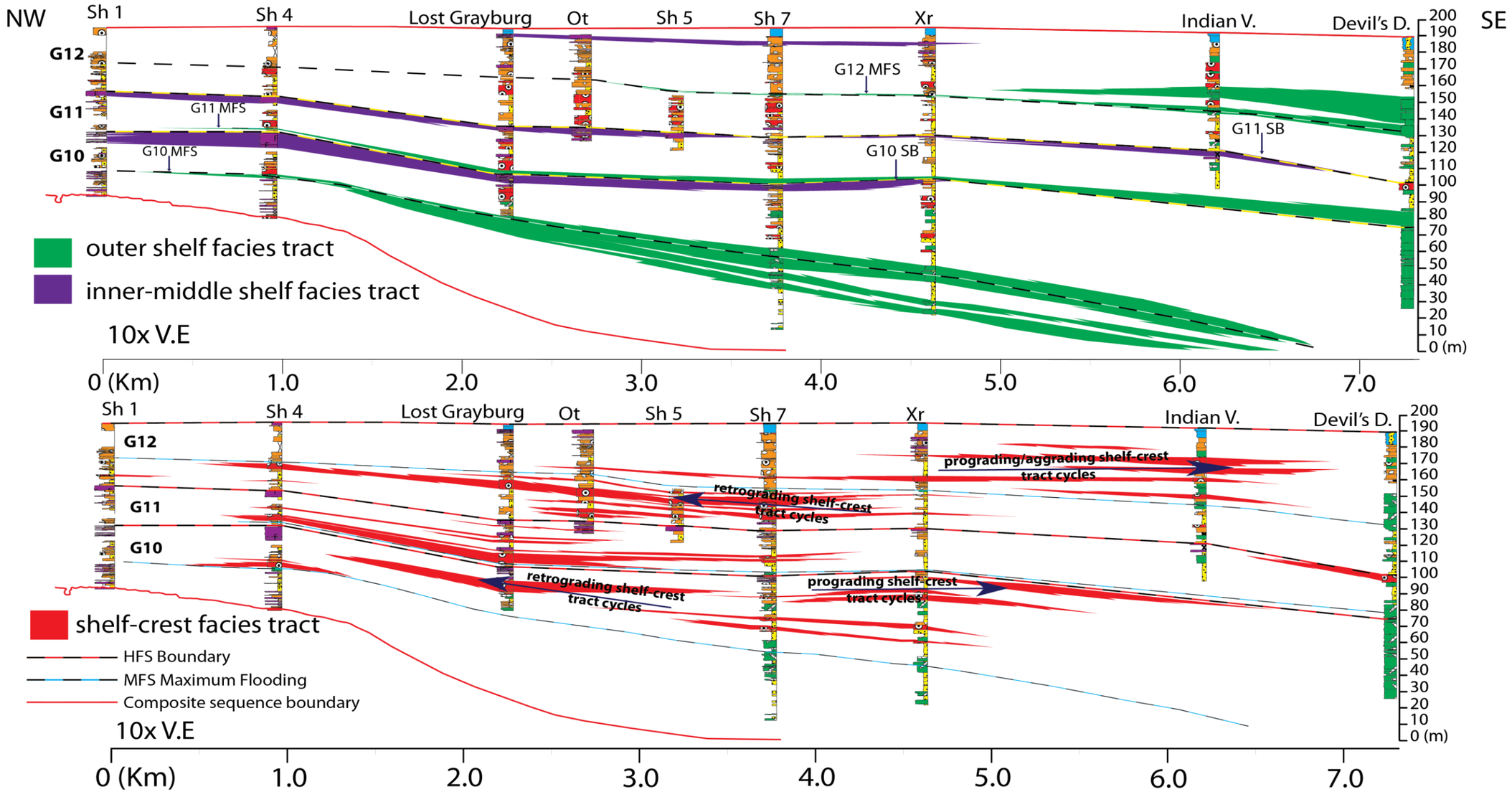

Figure 21: 2-Dimensional Analysis of Facies Tracts: Correlation of fenestral laminite dominated inner-middle shelf tract cycle sets between sections was one of the criteria used to pick the G10 and G11 high-frequency sequence boundaries. Correlation of fusulinid dominated outer shelf cycle sets between sections was used to pick the maximum flooding surfaces within the G10, G11, and G12 high-frequency sequences. Correlation of ooid grainstone capped shelf-crest facies tract cycles between sections was used to tract retrogradation and progradation within the high-frequency sequences

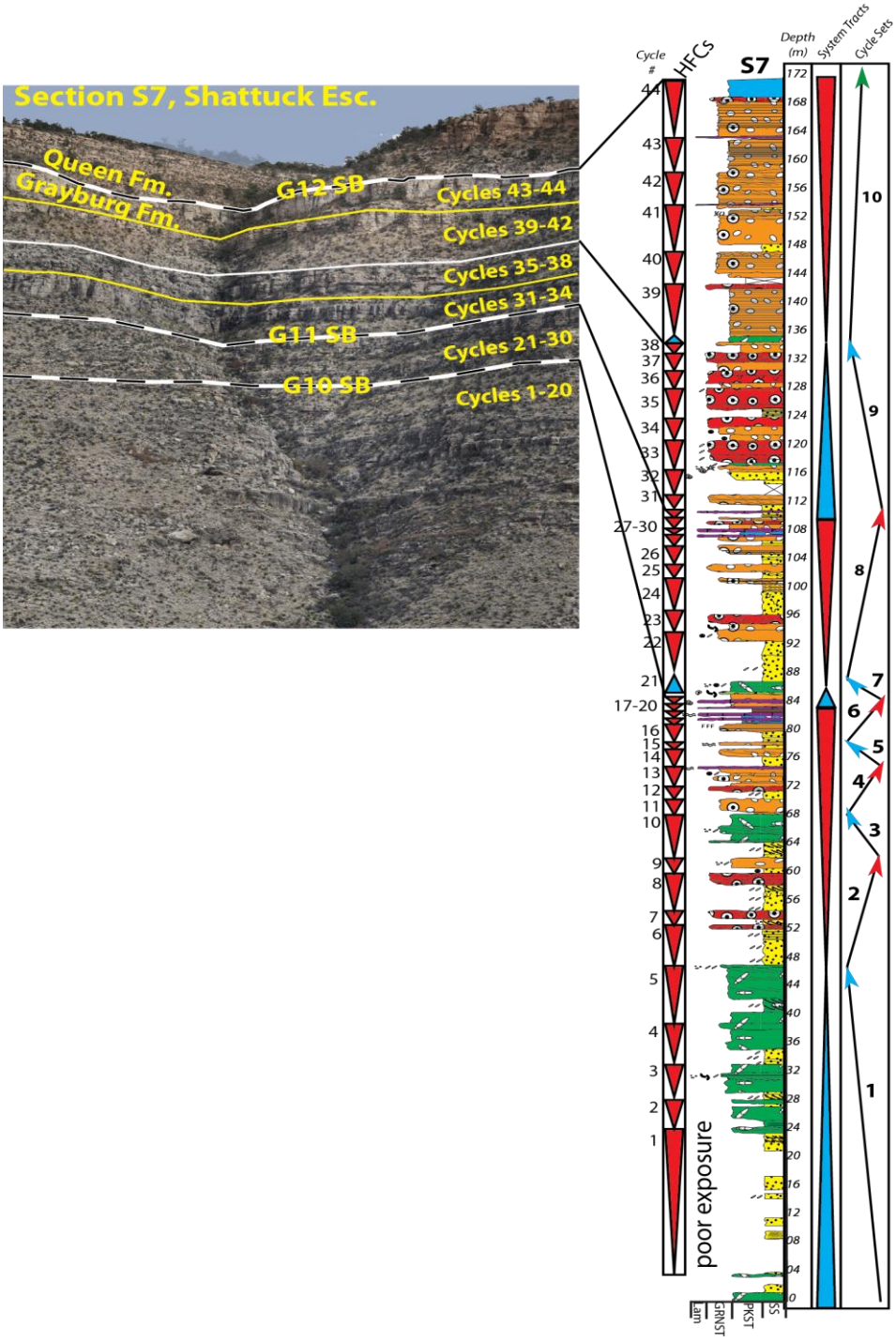

Figure 22: Reference section Shattuck S7: Shattuck section S7 was used to document the one-dimensional cycle stacking patterns within the Grayburg G10, G11, and G12 high-frequency sequences

Grayburg G10 high frequency sequence

The vertical evolution from fusulinid-dominated outer-shelf facies tract cycles (1-5) at the base of section S7, up into ooid-grainstone capped shelf-crest cycles (6-8) and eventually up into fenestral-laminite-dominated inner-middle shelf cycles (17-20) records the sequence scale retrogradation and progradation during deposition of the Grayburg G11 high-frequency sequence (Figure 23) Internal to the larger retrogradational to progradational pattern are a series of more frequent increases and decreases in accommodation that are documented by cycle sets stacked in prograding and retrograding patterns.

The transgressive systems tract of the Grayburg G10 HFS at section S7 is composed of five retrogradational, fusulinid-dominated, outer-shelf high-frequency cycles. Outer shelf facies tract cycles 1-5 are grouped into high-frequency cycle set 1 (Figure 23). Cycles 1-5 are correlated updip from section S7 to a fusulinid-dominated outer shelf tract cycle at section 4; and downdip to outer shelf facies tract cycles at section Xr (Figure 24). The fusulinid-dominated cycles developed at section 4 are the most landward occurrence of the outer shelf facies tract cycles within the Grayburg Formation (Figure C). The G10 maximum flooding surface is picked within cycle 5 at section S7 and is correlated updip to the fusulinid-dominated cycle at section 4; and downdip to the outer shelf cycles at section Xr (Figure 24).

The G10 maximum flooding surface separates the transgressive systems tract from the highstand systems tract. The G10 highstand at section S7 is composed of 15 high-frequency cycles (cycles 6-20) that are divided into 5 high-frequency cycles sets (cycles sets 2-6) (Figure 23). Shelf-crest tract cycles 6-9 constitute progradational high-frequency cycle set 2. Developed above the shelf-crest cycles of HFCS 2 is the retrograding fusulinid-dominated outer shelf facies tract cycle 10. HFC 10 constitutes retrogradational high-frequency cycles set 3. Cycles 11-13 are progradational middle shelf, and shelf crest cycles grouped into HFCS 4. Cycles 14-16 are retrograding middle shelf to shelf-crest tract cycles within HFCS 5. Cycles 17-20 are prograding fenestral laminite-dominated inner-middle shelf facies tract cycles (Figure 25). The fenestral

laminite complex developed within cycles 17-20 at section S7 is correlated updip to fenestral laminite-capped cycles at sections Lost Grayburg, S4, and S1; and downdip to laminite capped inner middle shelf cycles at section Xr (Figure 24). The Grayburg G10 high-frequency sequence boundary is picked at the top of fenestral laminite-capped cycle 20 at section S7 (Figure 23) Fusulinid-dominated outer shelf tract cycle 21 is developed directly above fenestral laminite-capped cycle 20 at section S7. Fusulinid-rich outer shelf tract cycle 21 was deposited during G11 HFS maximum flooding.

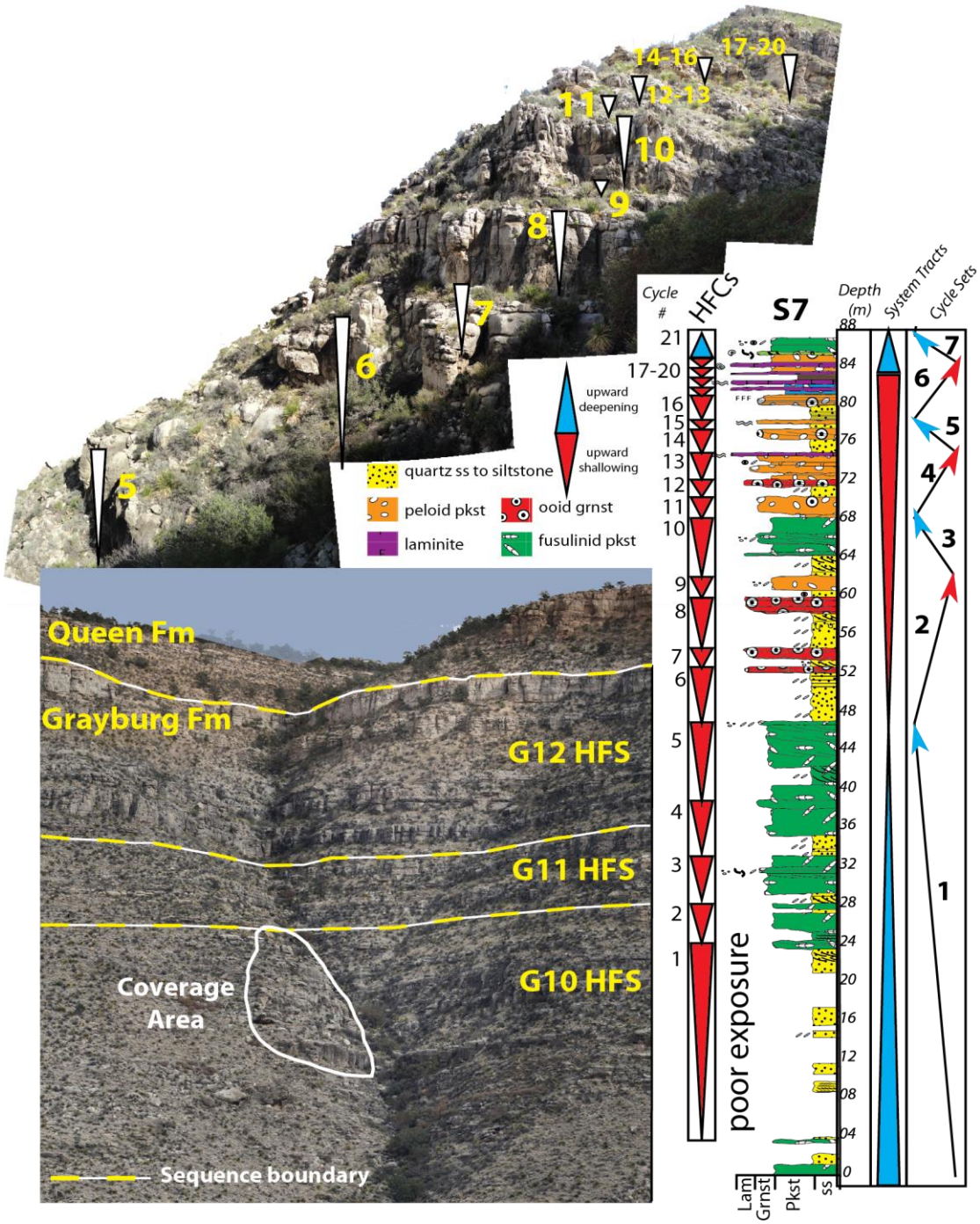

Figure 23: Shattuck S7 Cycles 1-21: Sequence scale retrogradation is recorded in the vertical evolution from the outer shelf tract cycles 1-5 of HFCS 1, up into middle shelf and shelf crest cycles 6-9 of HFCS 2, and eventually up into fenestral laminite capped inner-middle shelf tract cycles 17-20 of HFCS 6.

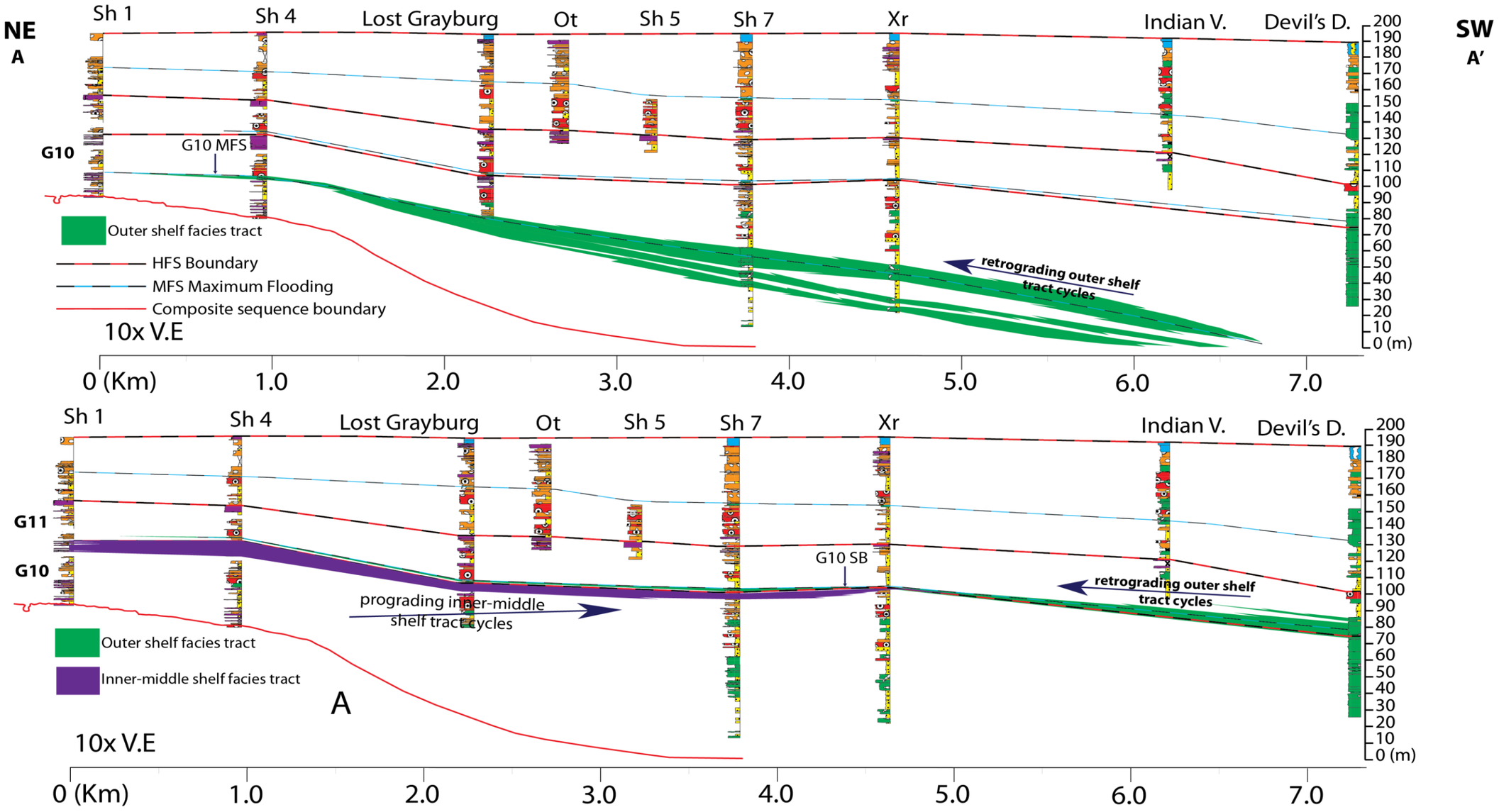

Figure 24: G10 HFS 2-Dimensional Facies Tract Correlation: The G10 maximum flooding surface is picked within outer shelf tract cycles 1-5 at section S7. The surface is correlated updip to a fusulinid unit at section S4 and downdip to outer shelf tract cycles at section Xr. The G10 sequence boundary is picked at the top of inner-middle shelf tract cycle 20 at section S7. Inner-middle shelf cycles at section S7 are correlated updip to section S1 and downdip to section Xr. Laminite capped cycle 20 at section S7 is overlain by fusulinid dominated outer shelf cycle 21.

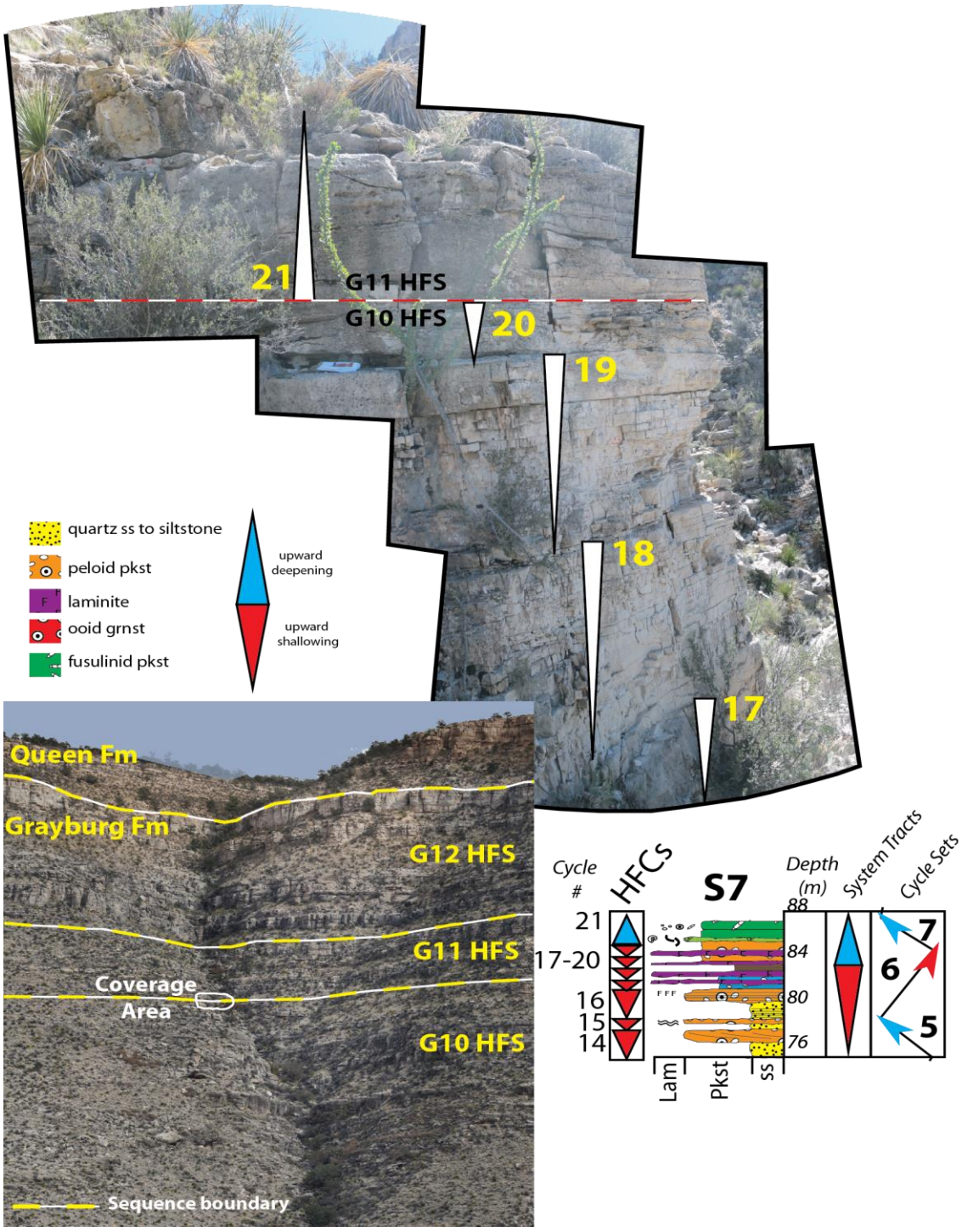

Figure 25: Shattuck S7 Cycles 17-21: The G10 high-frequency sequence boundary is picked at the top of cycle 20. Fenestral laminite capped cycle 20 is overlain by the fusulinid dominated outer shelf tract cycle 21.

Grayburg G11 high frequency sequence

The vertical evolution from fusulinid-dominated outer-shelf (cycle 21), up into the shelf-crest (cycles 22-23), into the middle shelf facies tract (cycles 24-26), and eventually up into inner-middle shelf facies tract cycles (27-30) records the sequence-scale retrogradation and progradation during deposition of the G11 HFS.

The G11 HFS transgressive systems tract at section S7 is a fusulinid-dominated outer shelf cycle (cycle 21) developed above the G10 inner-middle shelf cycles 17-20 (Figure 26). Outer shelf tract cycle 21 is correlated updip to a thin fusulinid unit at section S4. Downdip cycle 21 thickens to a massive fusulinid-dominated outer shelf tract cycle at the Devil's Den section (Figure 27). The G11 HFS maximum flooding surface is picked within outer shelf tract cycle 21 at section S7. The G11 maximum flooding surface separates the G11 transgressive systems tract from the G11 highstand systems tract.

The G11 highstand systems tract is composed of the high-frequency cycles 22-30 that define progradational HFCS 8 (Figure 28). Cycles 22 and 23 at section S7 are progradational shelf-crest cycles that are overlain by middle shelf facies tract cycles 24-26. Fenestral laminite inner-middle shelf tract cycles 27-30 are correlated updip to fenestral laminite capped cycles at section 1; and downdip to inner-middle shelf tract cycles at the Indian Vista section (Figure 27). The sequence boundary separating the Grayburg G11 from the overlying G12 high-frequency sequence is picked at the top of the prograding inner-middle shelf facies tract laminite succession at section S7. Overlying the G11 laminite complex at section S7 is a series of retrogradational ooid grainstone- capped shelf-crest tract cycles.

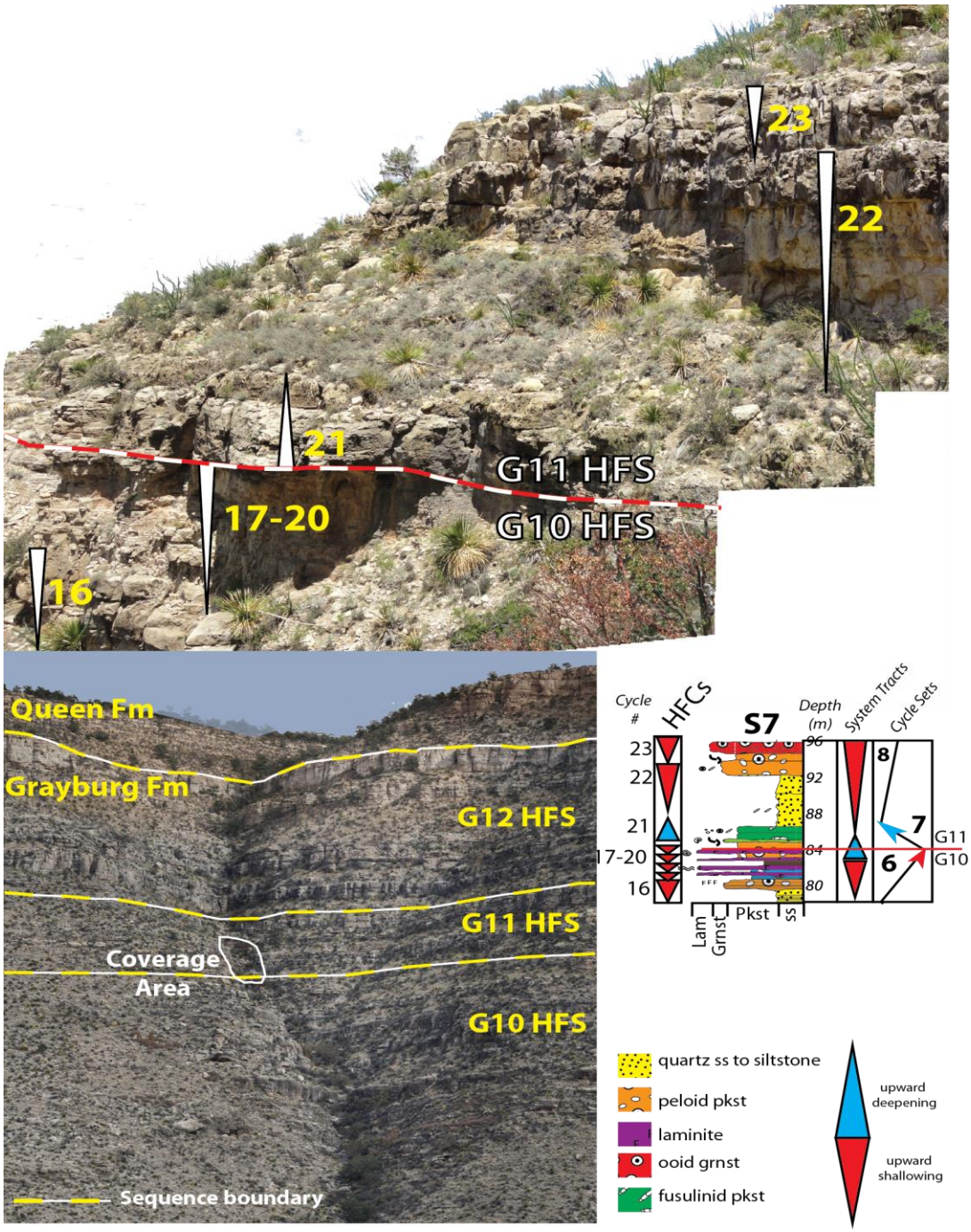

Figure 26: Shattuck S7 Cycles 14-23: The G11 HFS transgressive systems tract at section S7 is a fusulinid dominated outer shelf cycle (cycle 21) developed above inner-middle shelf cycles 17-20. G11 cycles 22 and 23 are shelf-crest tract cycles within progradational HFCS 8.

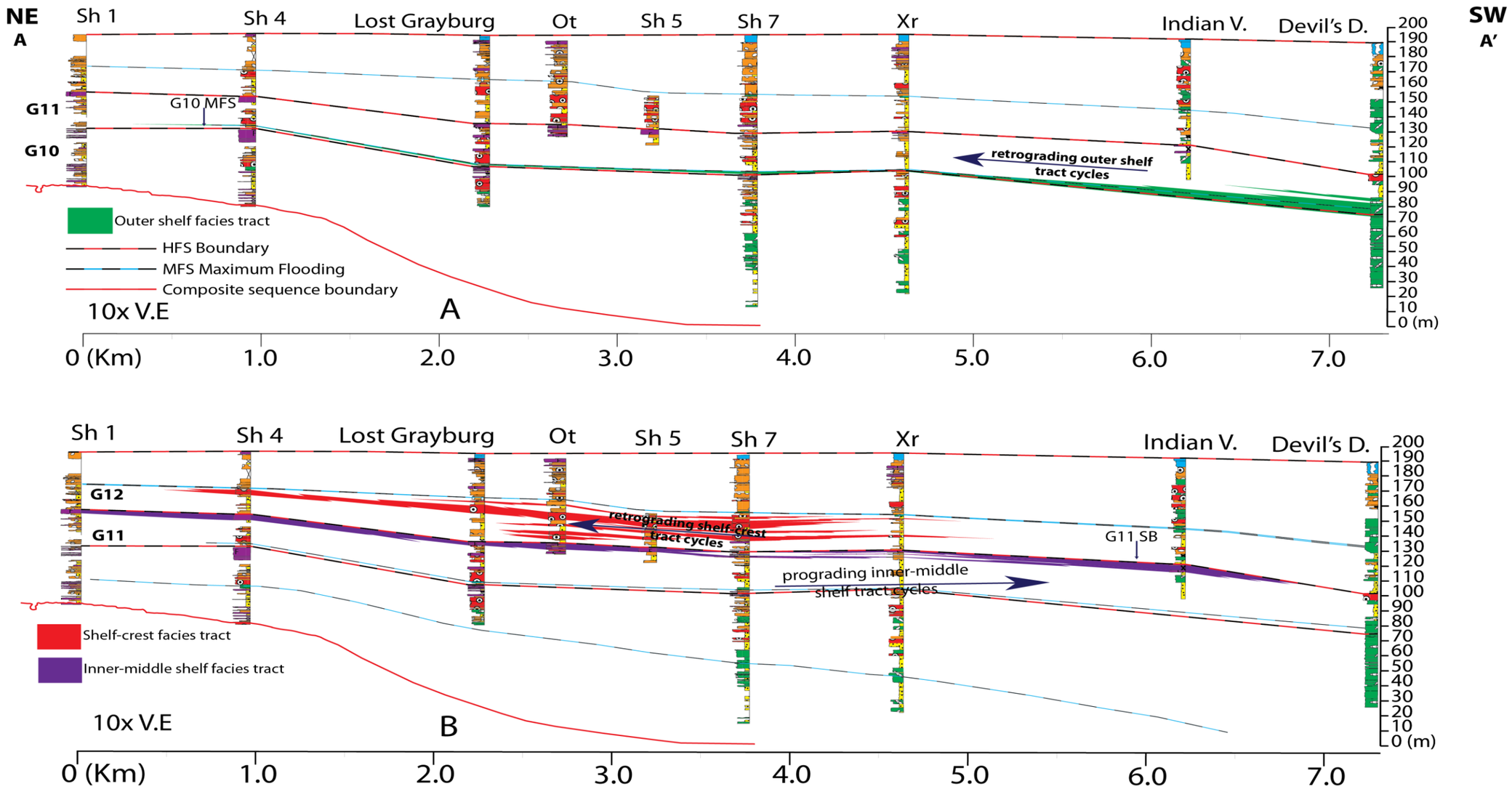

Figure 27: G11 HFS 2-Dimensional Facies Tract Correlation: The G11 maximum flooding surface is picked within outer shelf tract cycles 21 at section S7. The surface is correlated updip to a fusulinid unit at section S4 and downdip to a massive fusulinid dominated outer shelf tract cycle at the Devil's Den section. The G11 sequence boundary is picked at the top of inner-middle shelf tract cycle 30 at section S7. Inner-middle shelf cycles at section S7 are correlated updip to section S1 and downdip to the Indian Vista section. The G11 laminite complex is overlain by G12 retrogradational ooid grainstone capped shelf-crest tract cycles.

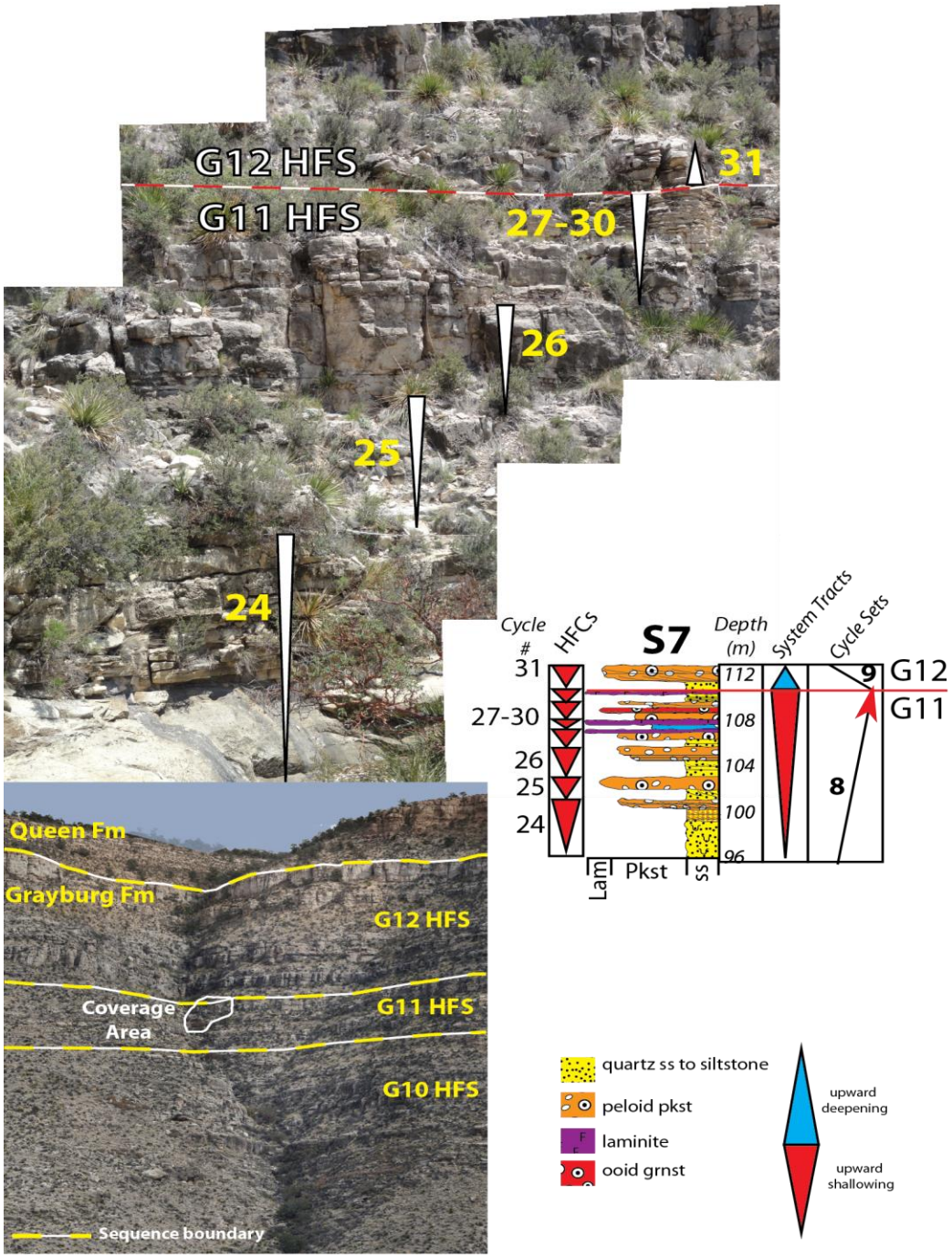

Figure 28: Shattuck S7 Cycles 22-31: Middle shelf tract cycles 24-26 are overlain by fenestral laminite capped inner-middle shelf cycles 27-30. The G11 sequence boundary is picked at the top of laminite capped cycle 30. Cycle 31 is the lowest cycle within retrogradational high-frequency cycle set 9.

Grayburg G12 high frequency sequence

The vertical evolution from shelf-crest cycles 33-38 into middle shelf cycles 39-44 capped by a karst-modified skeletal packstone unit records the sequence-scale retrogradation and progradation during deposition of the G11 HFS. The Grayburg G12 transgressive systems tract at section S7 is composed of middle-shelf and shelf-crest high-frequency cycles 31-38 (Figures 29-30). Cycles 31-38 define retrogradational high-frequency cycle set 9. Cycles 31 and 32 are middle shelf cycles overlain by ooid-grainstone-capped shelf-crest facies tract cycles 33-37? Ooid-grainstone-capped shelf-crest cycles 33-37 are correlated updip to ooid grainstone capped shelf shelf-crest cycles at sections S5, Ot, Lost Grayburg, and S4; and downdip to ooid-grainstone capped shelf-crest cycles at section Xr (Figure 31). The total dip width of the grainstone complex within the G12 transgressive systems tract is ~4 km. Overlying cycle 38 at section S7 is a thin fusulinid packstone unit at the base of cycle 39 (Figure 32). The outer shelf tract fusulinid unit at the base of cycle 39 at section S7 is correlated downdip to fusulinid-dominated outer shelf cycles at Indian Vista and Devil's Den (Figure 31). Updip the fusulinid unit developed at the base of cycle 39 at section S7 transitions to a middle shelf peloid packstone cycle at sections Ot and Lost Grayburg. The Grayburg G12 maximum flooding surface is picked within the fusulinid packstone at the base of cycle 39 at section S7 (Figure 31). The G12 maximum flooding surface separates the Grayburg G12 transgressive systems tract from the G12 highstand systems tract.

The G12 HST is composed of high-frequency cycles 39-44. Cycles 39-44 define aggradational to progradational high-frequency cycle set 10 (Figures 32-34). Middle shelf facies tract peloid packstone cycles 39-43 at section S7 are correlated updip to middle-shelf cycles at section Ot, Lost Grayburg, S4, and S1 (Figure 31). The peloid packstone-dominated middle shelf cycles 39-43 are correlated downdip to middle shelf cycles at section Xr, Indian Vista, and Devil's Den (Figure 31). Middle shelf cycle 44 is capped by a brecciated skeletal packstone unit that is correlated updip to sections Ot and Lost Grayburg; and downdip to section Xr, Indian Vista, and Devil's Den (Figure 31). The ~2-m-deep karst pit developed within the skeletal packstone unit at the Devil's Den section

is evidence of subaerial exposure at the top of cycle 44 (Figure 35). Overlying the skeletal packstone unit at the top of cycle 44 at section S7 is 6 m of recessive slope-forming sandstones (Figure 36). The Grayburg-Queen contact is correlated at the base of the thick, recessive sandstone unit.

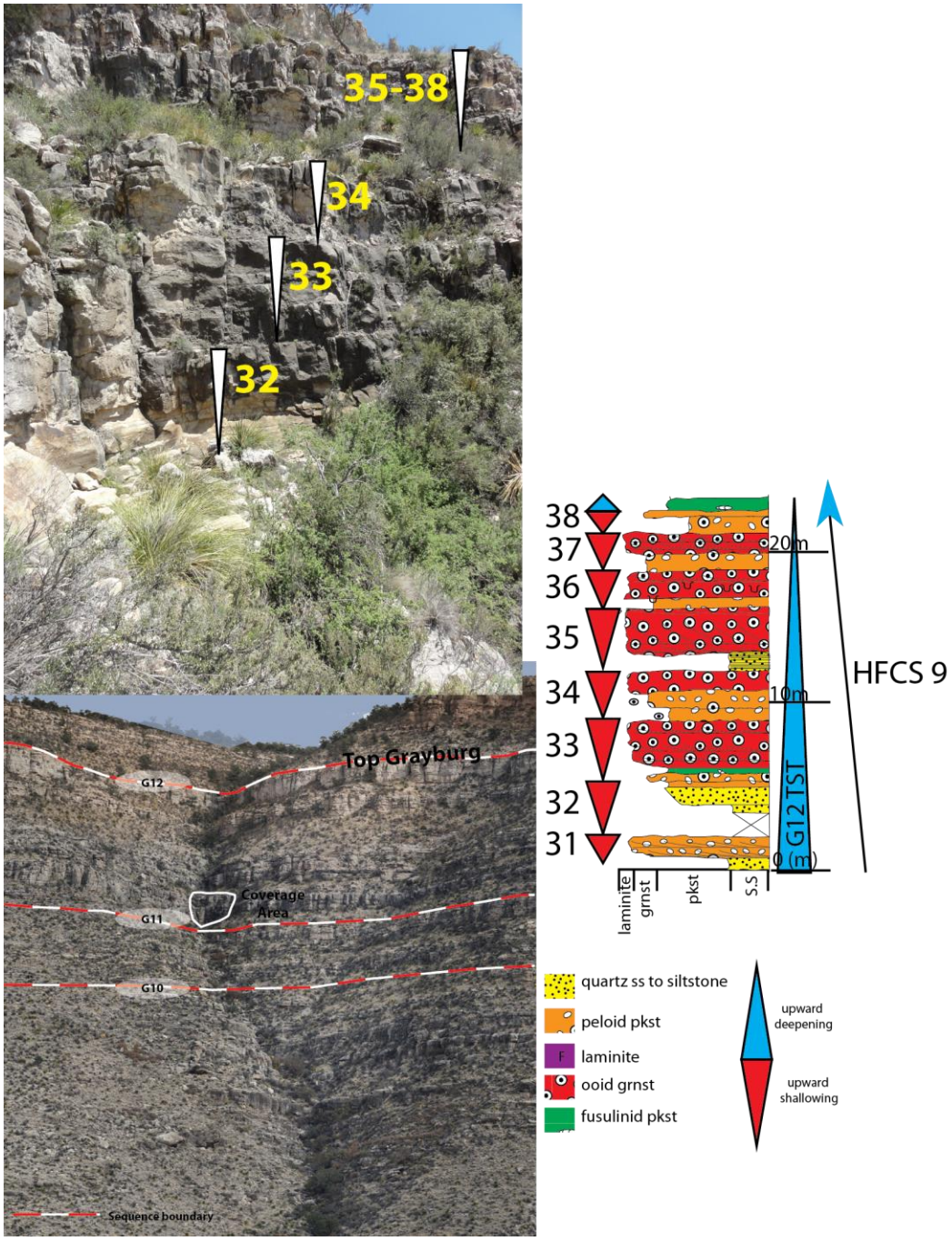

Figure 29: Shattuck S7 Cycles 32-38: The Grayburg G12 transgressive systems tract is includes the 7 high-frequency cycles of retrograding high-frequency cycle set 9. HFCS 9 is composed of middle shelf cycles 31 and 32 and grainstone capped shelf-crest cycles 33-38.

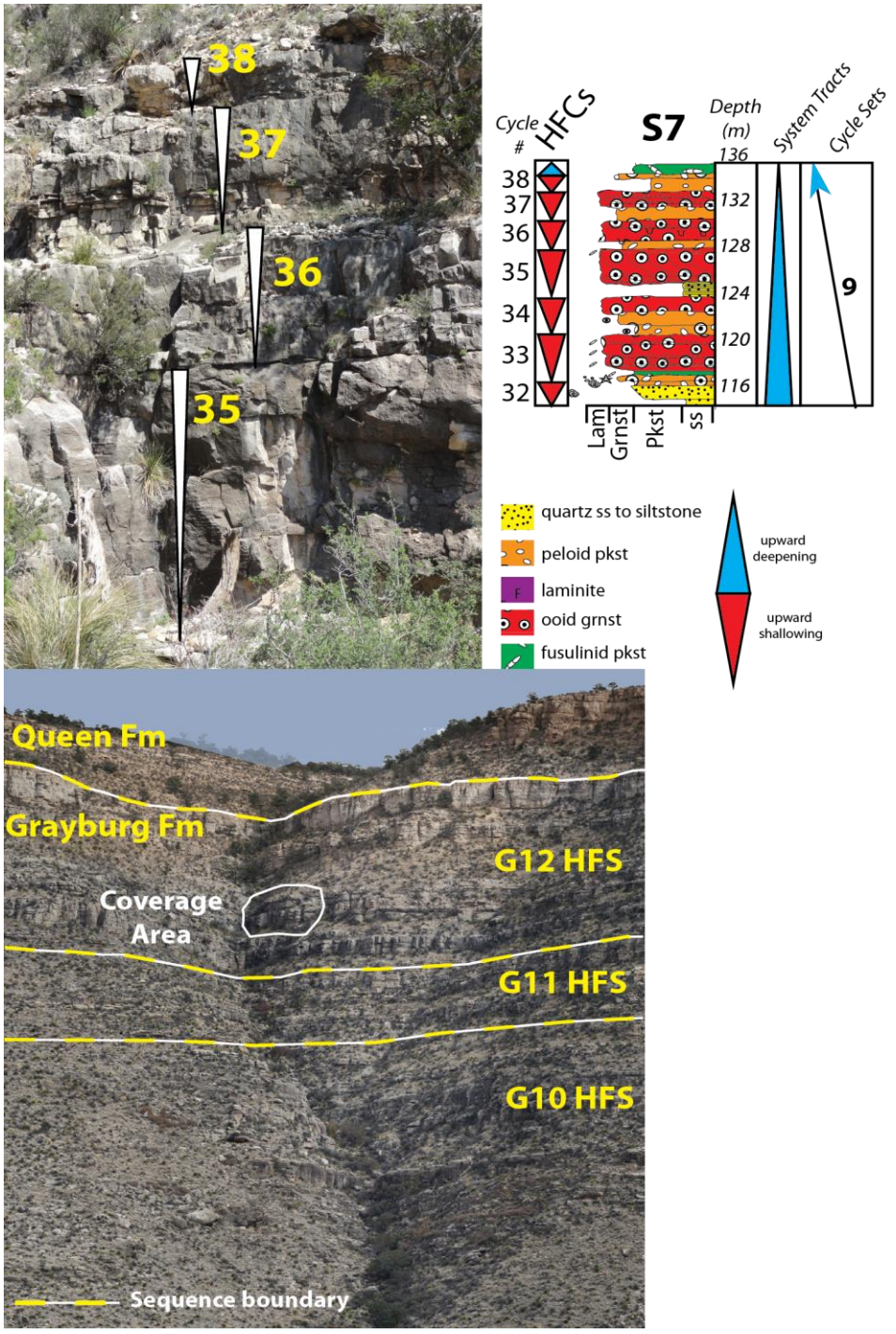

Figure 30: Shattuck S7 Cycles 35-38: Ooid grainstone capped shelf-crest cycles 35-37 are correlated updip to section S4 and downdip to section Xr. The total dip-width of the G12 TST retrograding shelf-crest facies tract is ~4km.

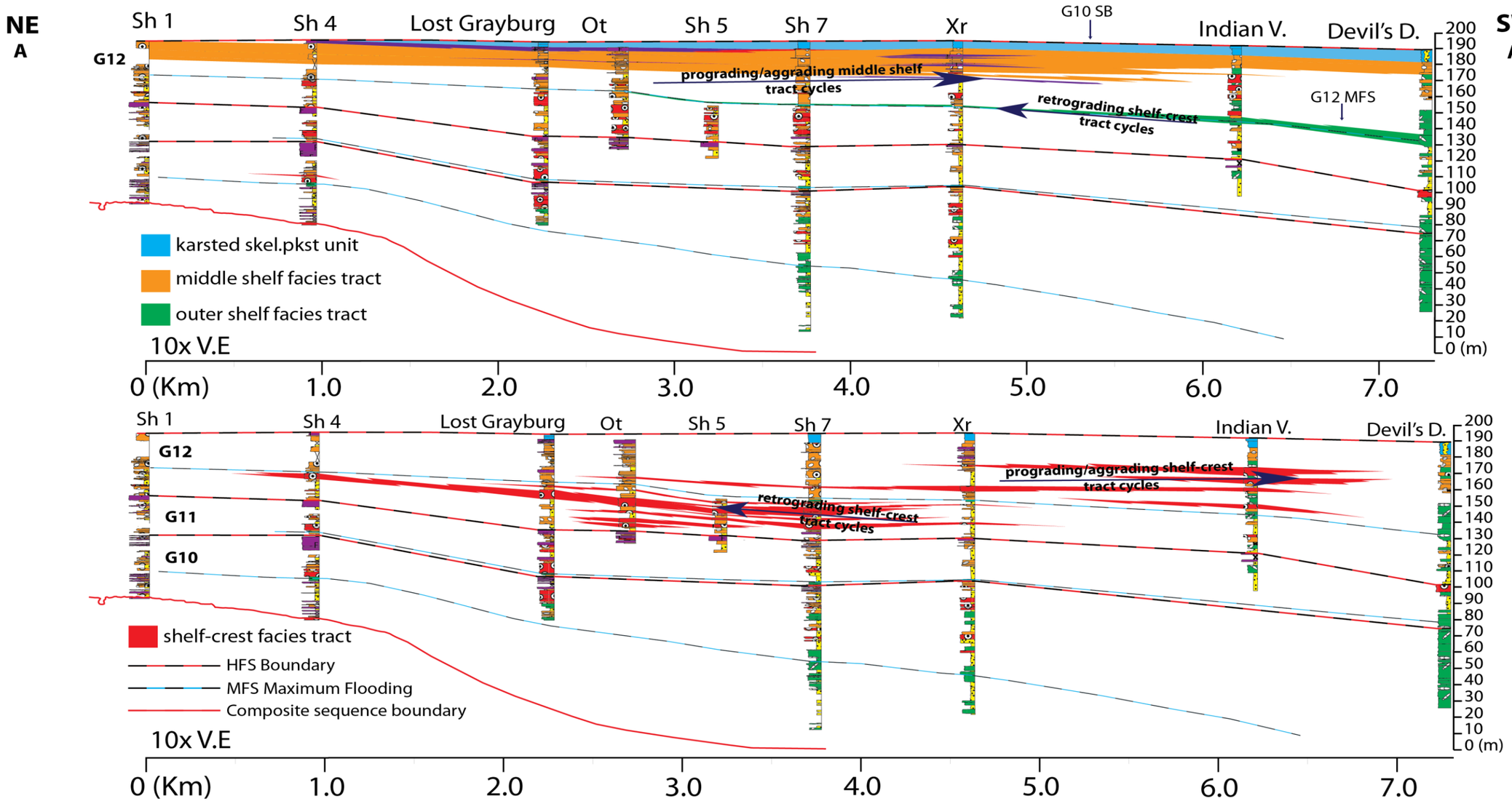

Figure 31: G12 HFS 2-Dimensional Facies Tract Correlation: The G12 maximum flooding surface is picked within the outer shelf fusulinid packstone unit at the base of cycle 39. The surface is correlated downdip fusulinid dominated outer shelf tract cycles at sections Xr and Devil's Den. Retrogradational shelf-crest tract cycles at section S7 are correlated updip to section S4 and downdip to section Xr. Progradational to aggradational shelf crest cycles are correlated between section Xr and Indian Vista. The G12 sequence boundary is picked at the top skeletal packstone unit that is correlated from the top of cycle 44 at section S7 downdip to the Devil's Den section where a 2m deep chaotic matrix supported breccia filled karst pit is documented.

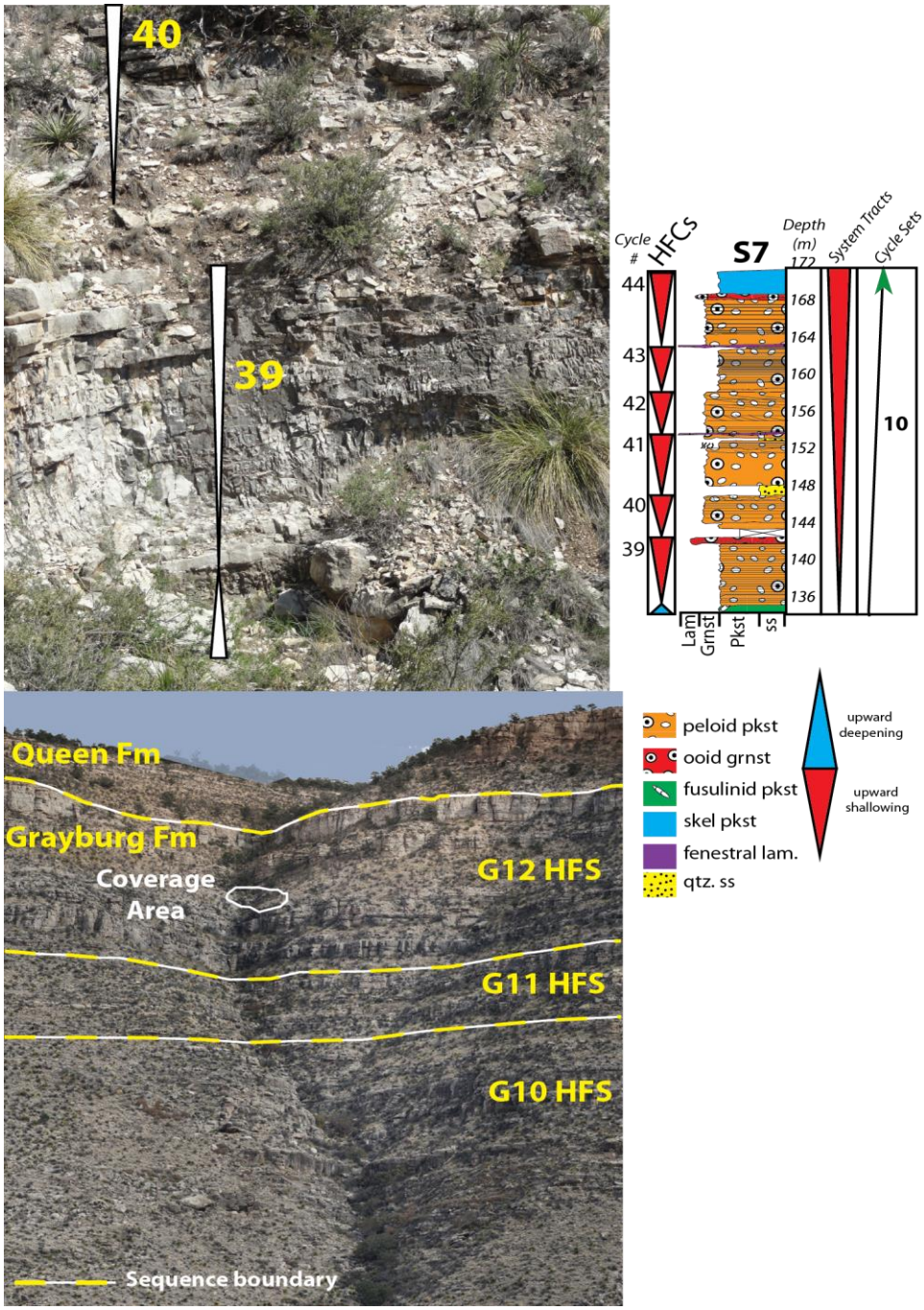

Figure 32: Shattuck S7 Cycles 38-40: The G12 maximum flooding surface is correlated within the outer shelf fusulinid unit at the base of cycle 39.

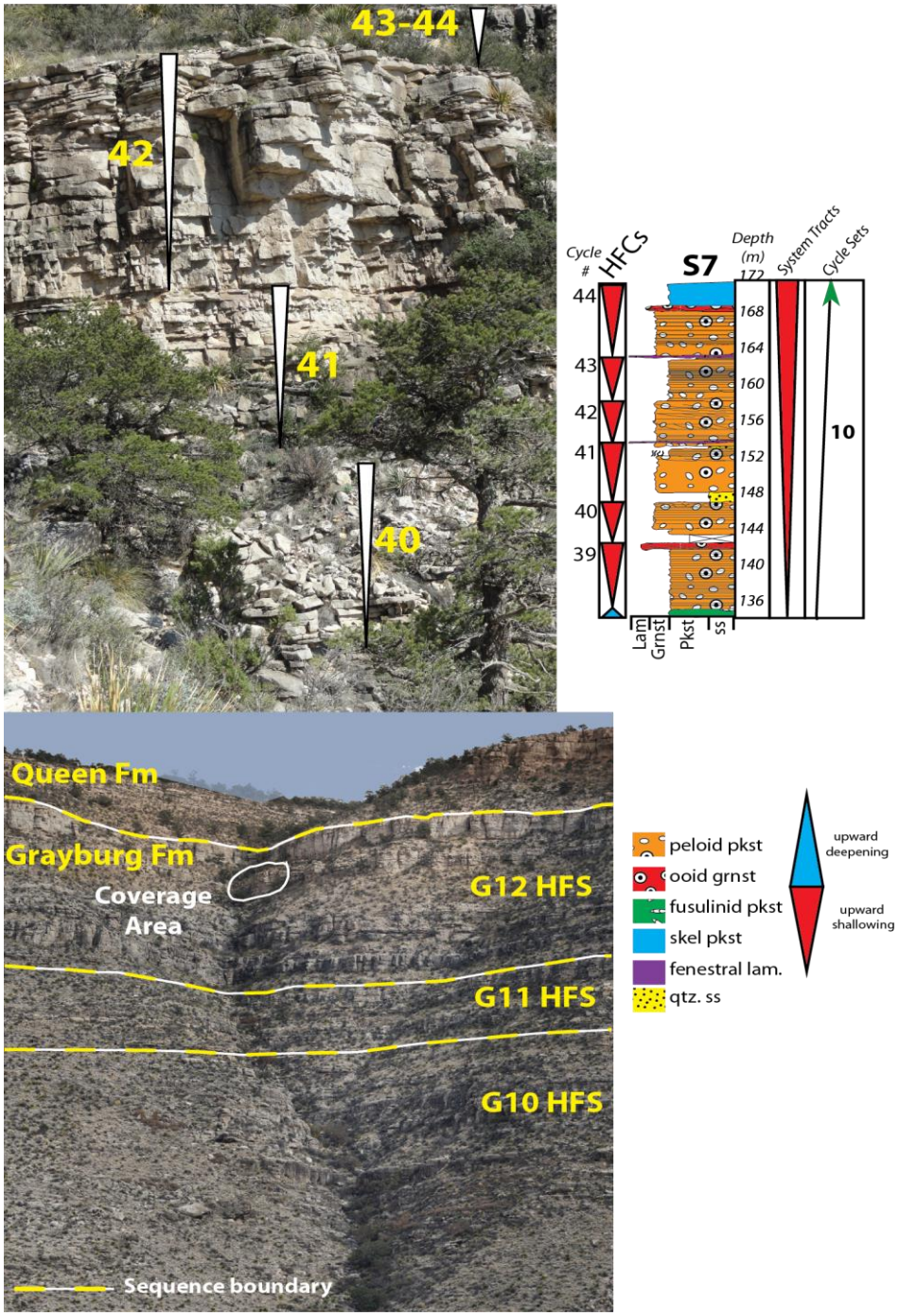

Figure 33: Shattuck S7 Cycles 40-44: The Grayburg G12 highstand systems tract is composed of high-frequency cycles 39-44. Middle shelf tract cycles 39-44 comprise the aggrading to prograding high-frequency cycle set 10.

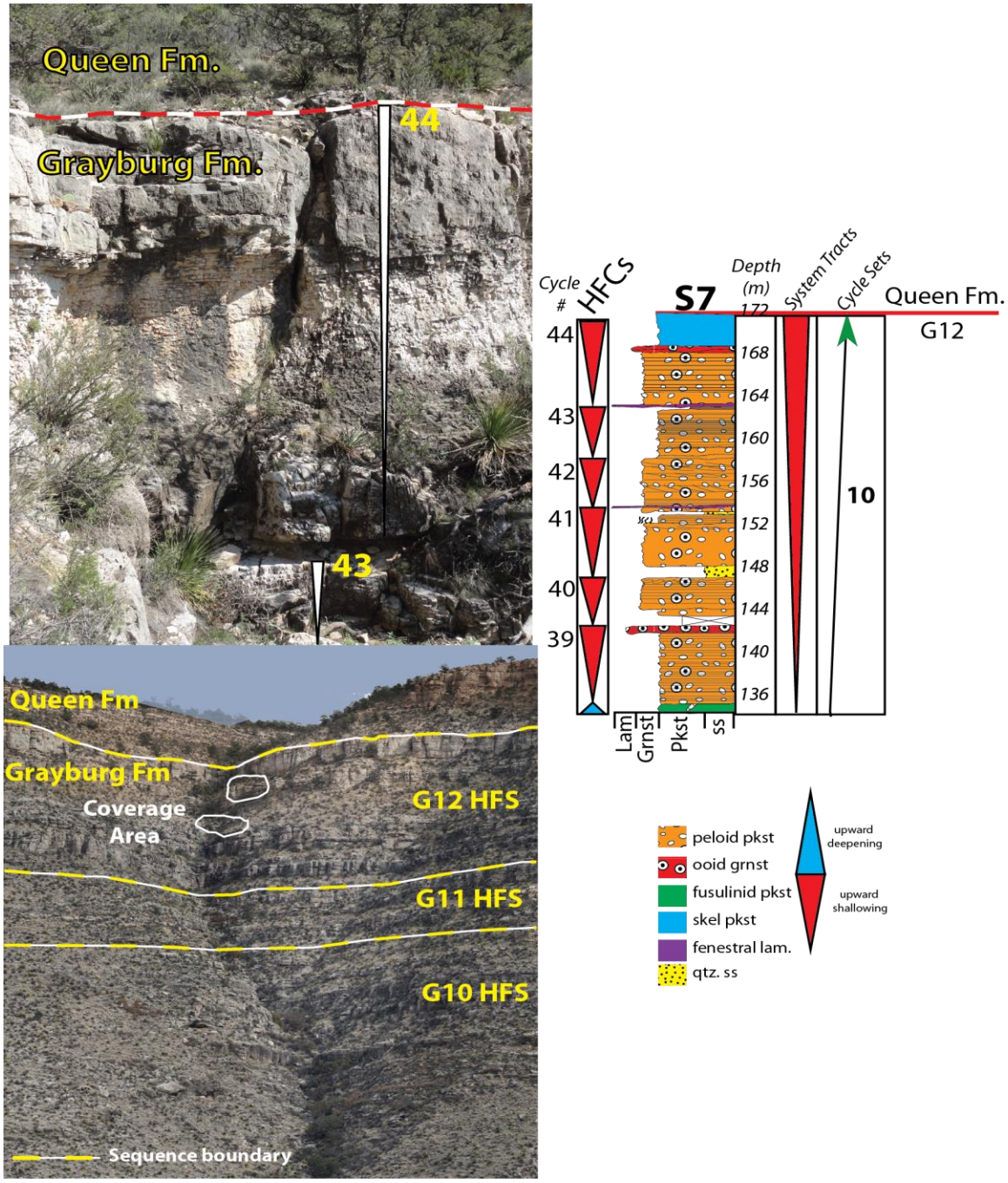

Figure 34: Shattuck S7 Cycles 43-44: The skeletal packstone unit at the top of cycle 44 at section S7 is picked as the top of the Grayburg Fm. The skeletal packstone unit at the top of cycle 44 is correlated downdip to the Devil's Den section where the unit is karsted.

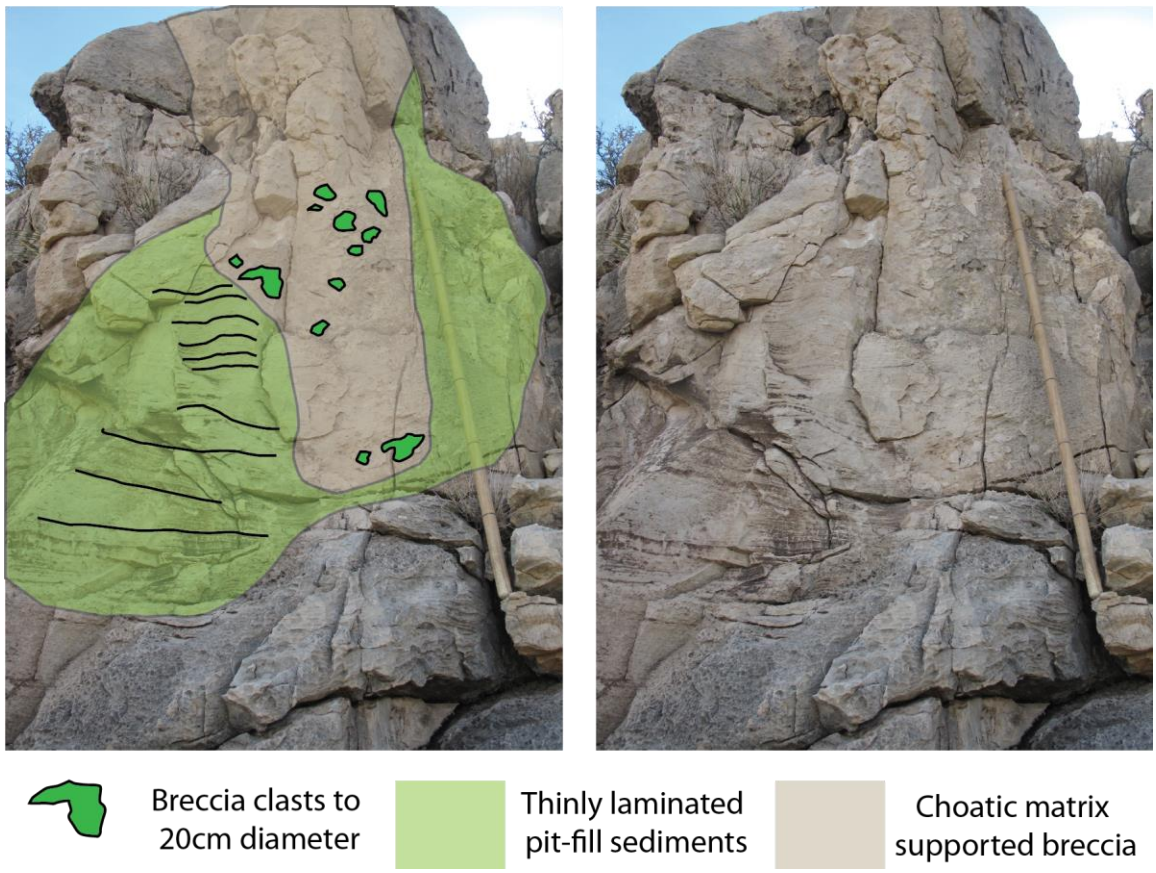

Figure 35: Karsted G12 HFS Boundary at Grayburg-Queen Contact: The ~2m deep (Jacob's staff is 1.5m) breccia filled karst pit documented at the Devil's Den section is evidence of subaerial exposure prior deposition of Queen Fm sandstones.

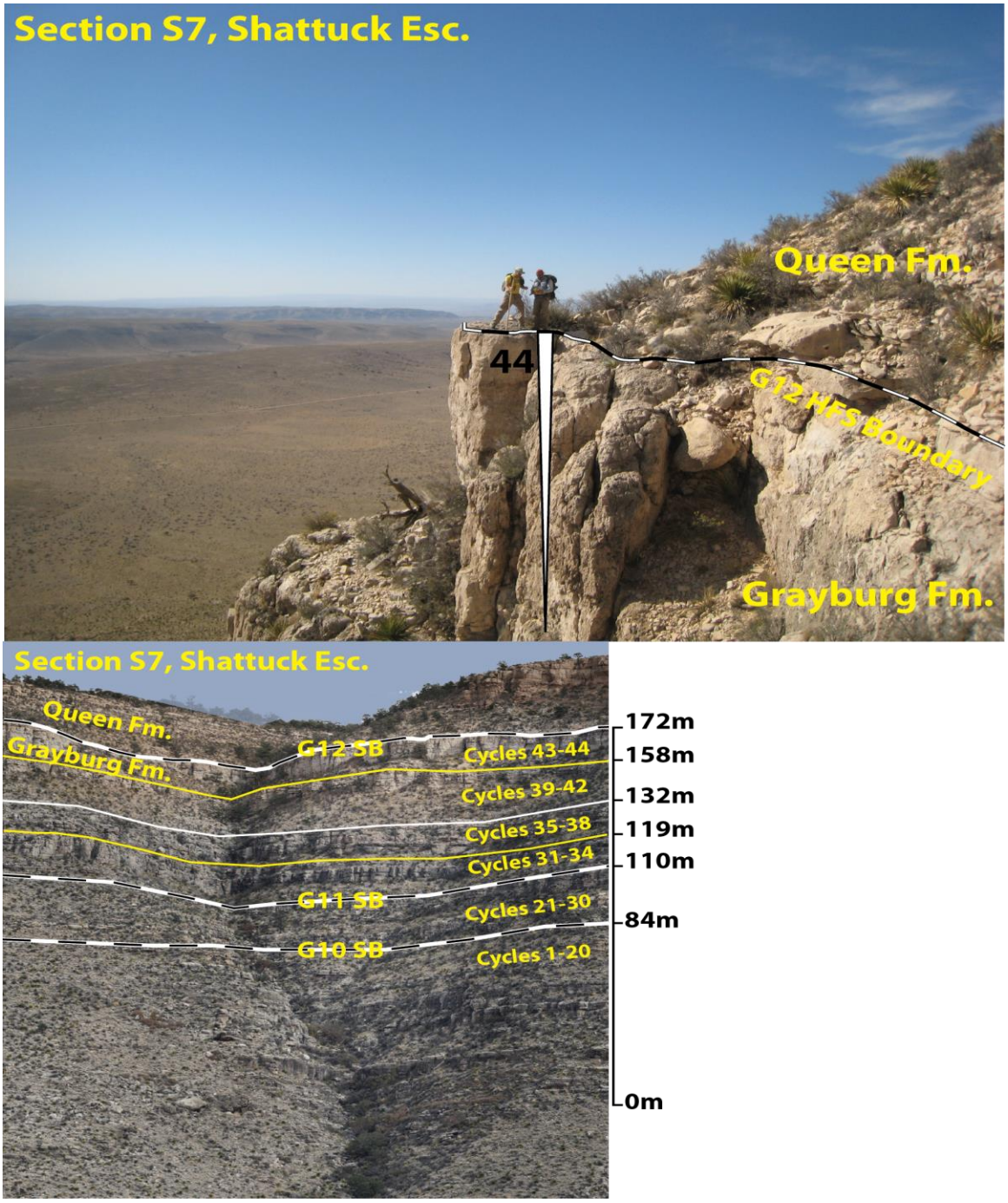

Figure 36: Grayburg-Queen Contact at Shattuck Section 7: The G12HFS boundary is picked above the skeletal packstone unit at the top of cycle 44. Overlying cycle 44 are 6.0m of recessive slope forming sandstones deposited during Queen Fm transgression.

CORRELATION: SHATTUCK SECTION S7 AND PLOWMAN SECTION PR1

One- and two-dimensional cycle stacking patterns documented within the Grayburg G10, G11, and G12 high-frequency sequences at reference section S7 in the Guadalupe Mountains were compared to the one-dimensional cyclostratigraphic architecture documented at section PR1 in the Brokeoff Mountains (Figure 37). Correlation of Grayburg strata between section S7 in the Guadalupe Mountains and section PR1 in the Brokeoff Mountains was made at high-frequency sequence, high-frequency cycle set, and when feasible, high-frequency cycle scale. The correlation between section PR1 and section S7 was based on comparison of high-frequency sequence thickness, cycle number, cycle thickness, vertical facies succession, and facies proportion (Figure 38).

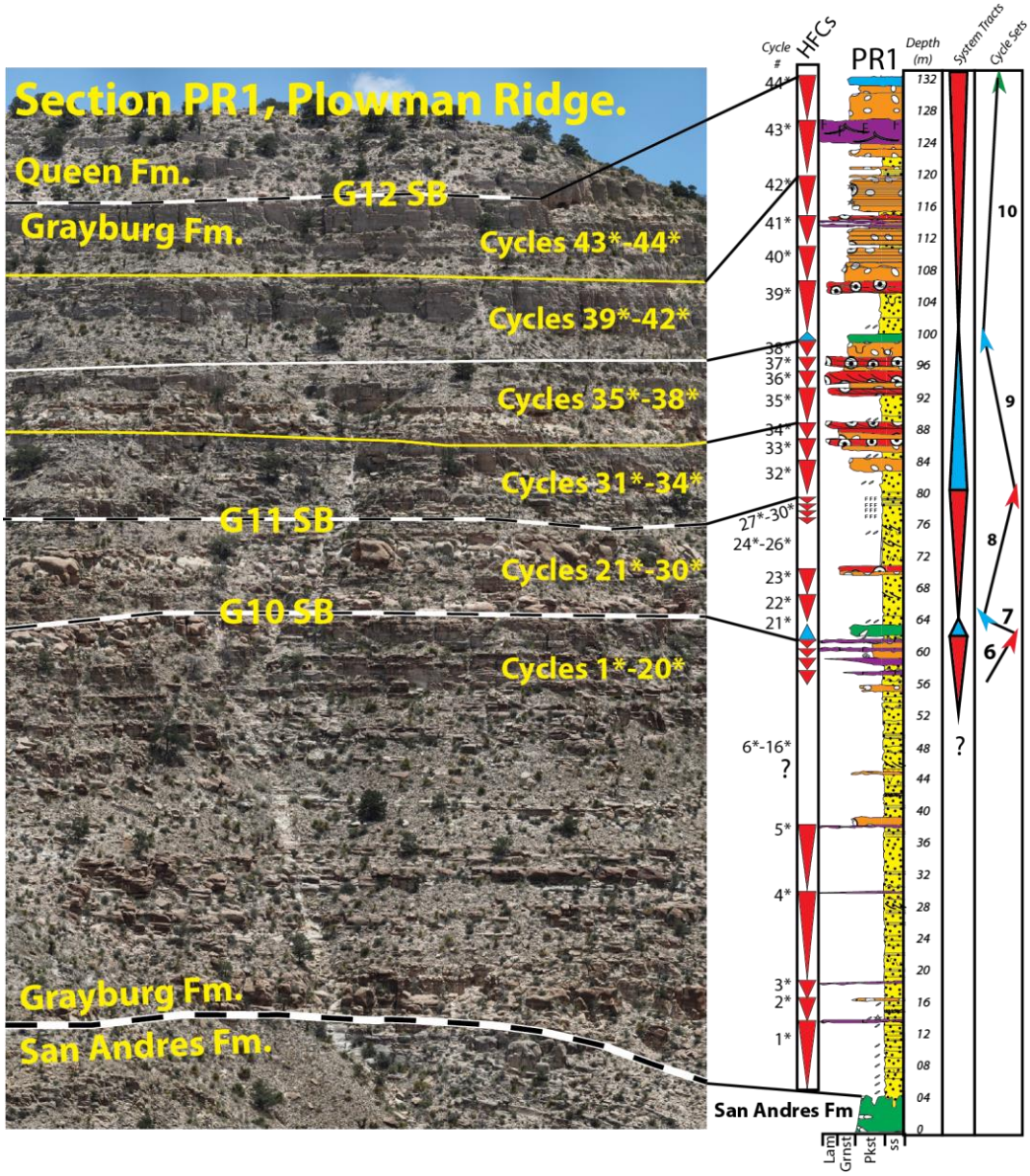

Figure 37: Reference section Plowman PR1: The one-dimensional cyclostratigraphic architecture documented at Plowman Ridge section PR1 was compared against the one-dimensional cycle stacking patterns within the Grayburg G10, G11, and G12 high-frequency sequences documented at Shattuck section S7.

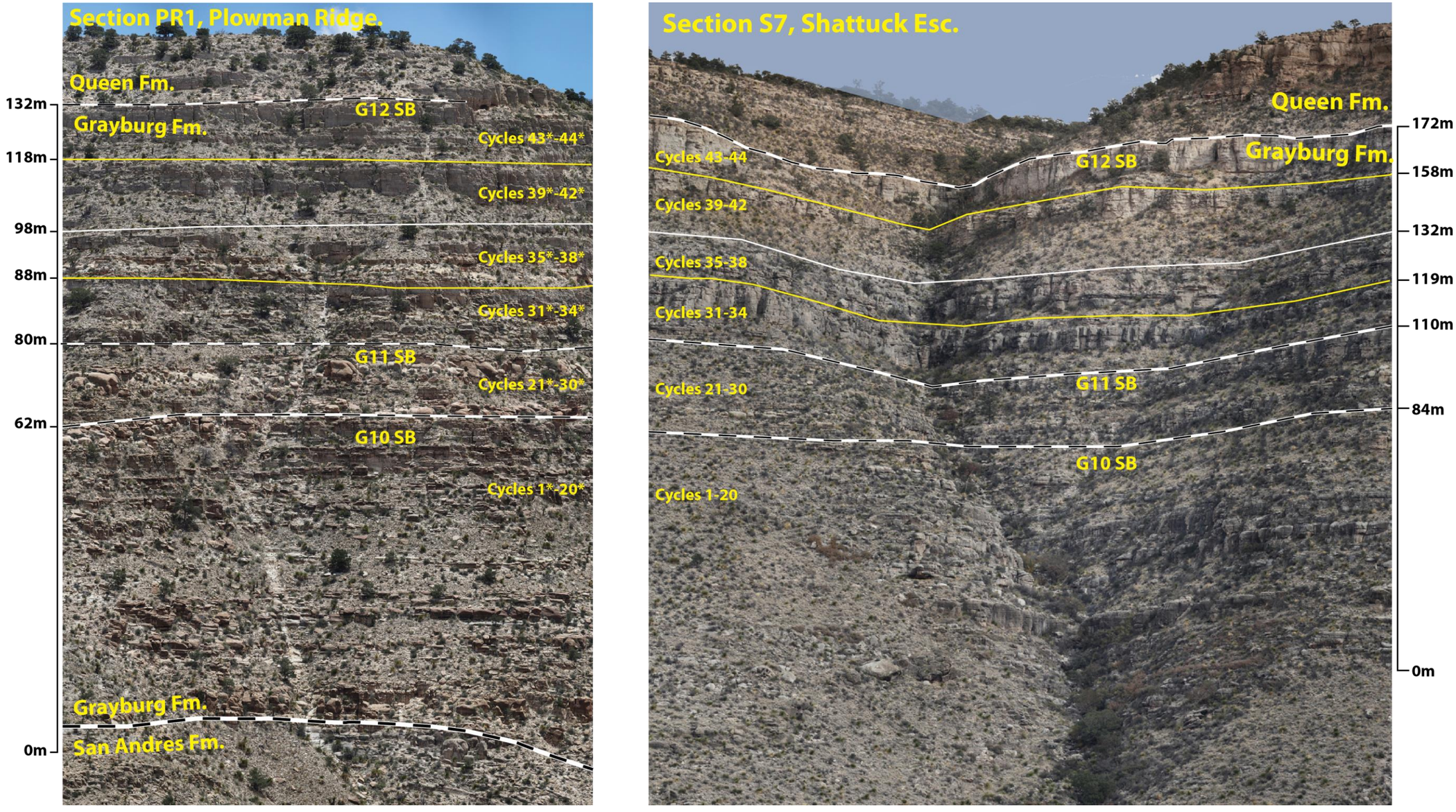

Figure 38: Vertical Comparison of High-Frequency Sequence Thicknesses: The Grayburg G10 HFS at section S7 is 84m thick, the G11 is 26m thick, and the G12 is 62m thick. The Grayburg G10 HFS at section PR1 is 62m thick, the G11 is 18m thick, and the G12 is 52m thick.

Grayburg G10 high-frequency sequence correlation

The vertical evolution from fusulinid-dominated outer shelf cycles 1-5, up into shelf-crest grainstone-capped cycles 6-8 and eventually up into inner-middle shelf fenestral laminite cycles 17-20 records the sequence scale retrogradation and progradation within the G10 HFS at Shattuck section S7. Sequence-scale retrogradation and progradation within the Grayburg G10 HFS at Plowman section PR1 is recorded in the vertical evolution from amalgamated shelf-crest and middle shelf sandstone cycles within the lower G10 up into fenestral laminite-capped, inner-middle shelf cycles 17*-20*.

The 3rd-order composite sequence boundary separating the San Andres Formation from the overlying Grayburg Formation was picked at the contact between gray, seaward-dipping fusulinid-dominated outer shelf high- frequency cycles and tan, middle shelf sandstone cycle 1* at the base of Plowman section PR1 (Figure 39).The Grayburg G10 HFS at section S7 is composed of cycles 1-20, which comprise retrogradational and progradational high-frequency cycle sets 1-6. Amalgamated sandstone cycles within the lower portion of the G10 HFS at section PR1are equivalent to the mixed carbonate-siliciclastic cycles of high-frequency cycles sets 1-5 at section S7. Prograding HFCS 6 at section S7 is composed of fenestral laminite capped inner-middle shelf cycles 17-20. The equivalent prograding inner-middle shelf laminite capped cycles at PR1 are cycles 17*-20*. Inner-middle shelf tract cycles 17-20 at S7 provide an excellent match to the inner-middle shelf tract laminite-capped cycles 17*-20* at Plowman section PR1 in terms of cycle number, cycles thickness, and vertical facies succession (Figure40). The Grayburg G10 high-frequency sequence boundary was correlated between cycle 20 at Shattuck section S7 and cycle 20* at Plowman section PR1 (Figure 41). Directly overlying fenestral laminite-capped inner-middle shelf cycle 20* at section PR1 is fusulinid-dominated outer shelf cycle 21* (Figure 40). Cycle 21* at section PR1 is equivalent to fusulinid-rich outer shelf tract cycle 21 at Shattuck section S7. The Grayburg G11 high-frequency sequence maximum flooding surface is correlated within cycle 21 at section S7 to within cycle 21* at section PR1 (Figure 41).

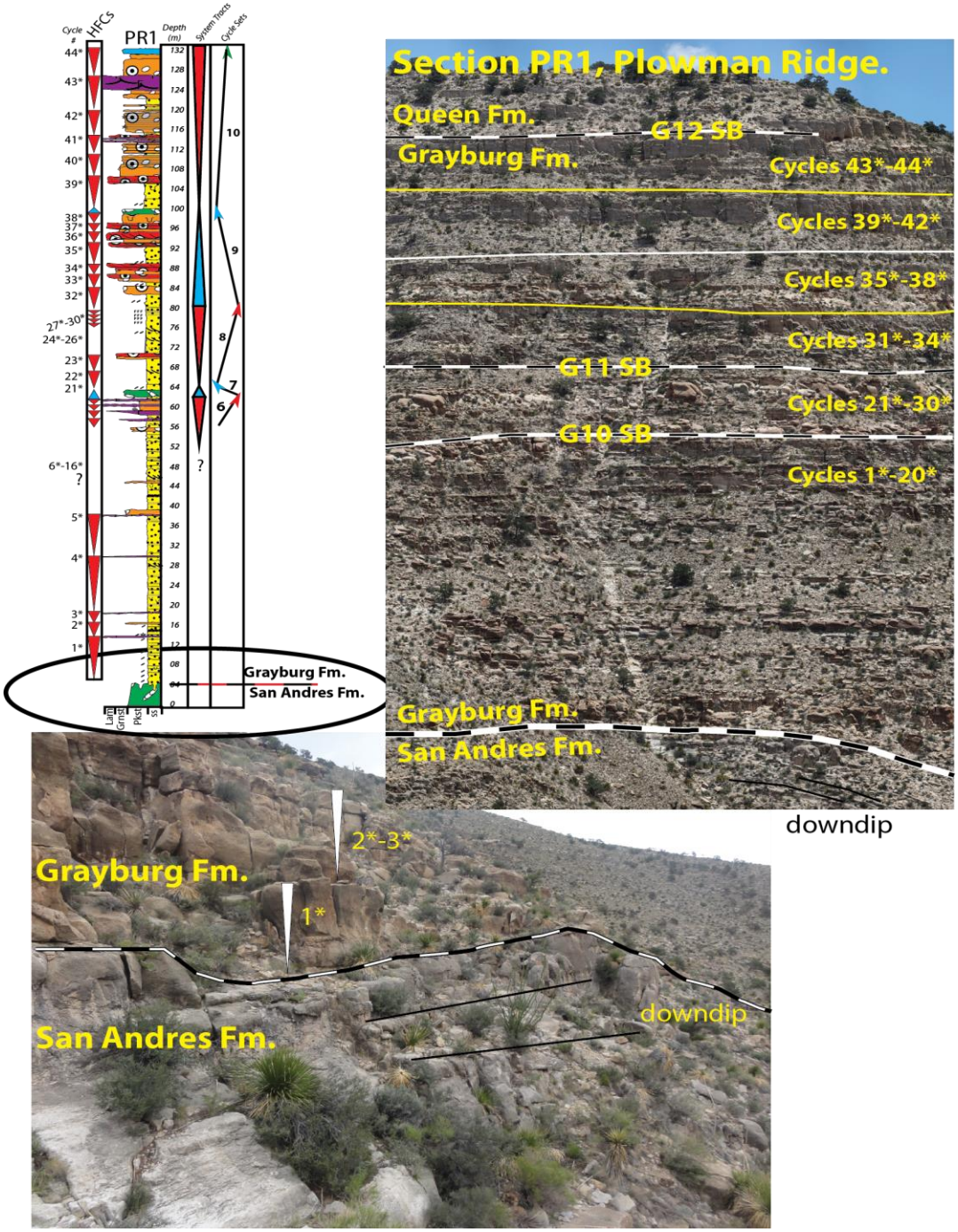

Figure 39: San Andres-Grayburg Contact: The San Andres-Grayburg contact is picked at the base of section PR1 where seaward dipping grey outer shelf tract fusulinid dominated cycles are onlapped by tan colored inner-middle shelf and middle shelf tract Grayburg sandstone cycles.

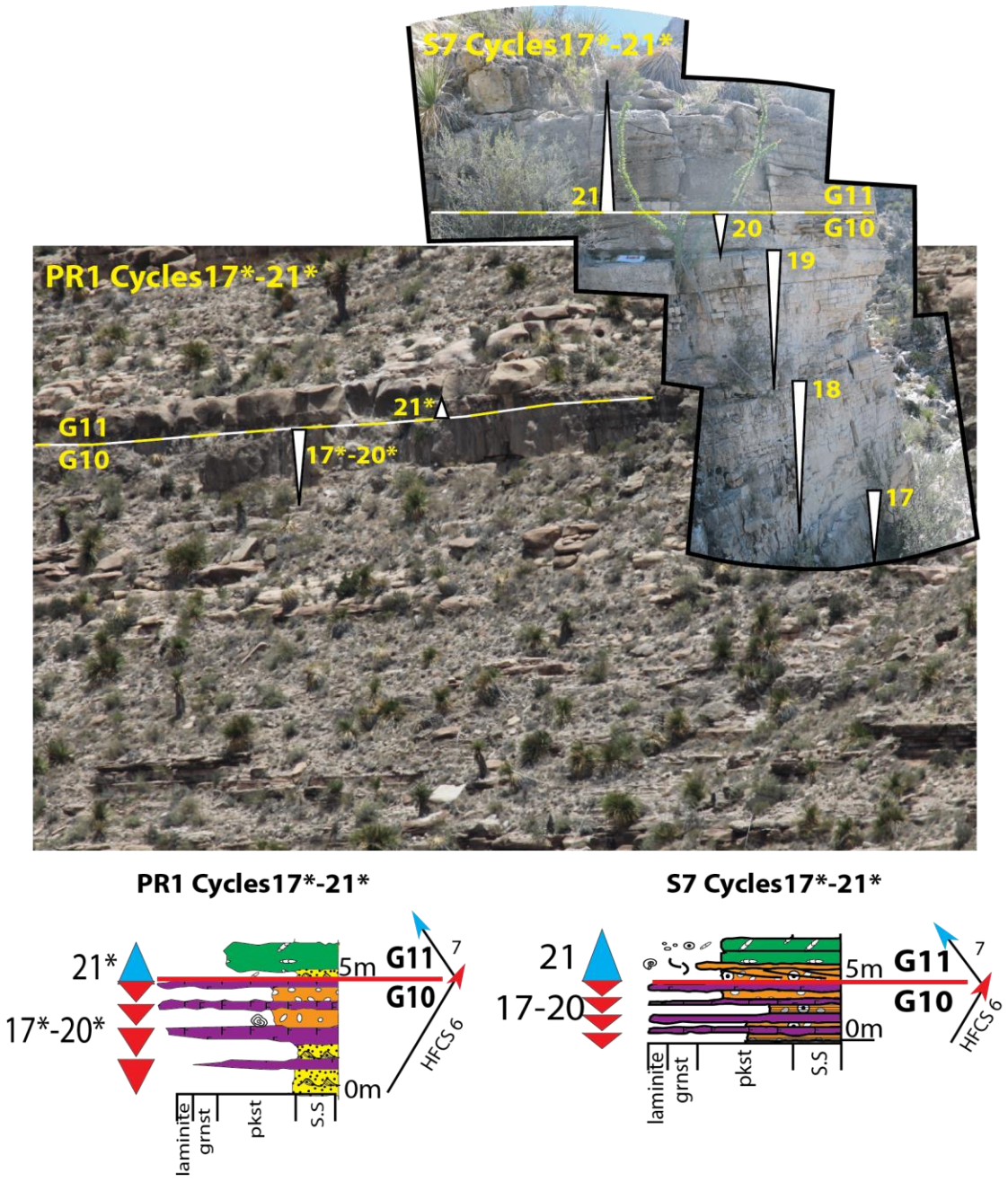

Figure 40: Plowman PR1 Cycles 17*-21*: Fenestral laminite capped inner-middle shelf tract cycles 17*-20* at Plowman section PR1 are an excellent match to the laminite capped inner-middle shelf tract cycles 17-20 at Shattuck section S7 in terms of cycle number, cycles thickness, and vertical facies succession. The G10 HFS boundary is correlated between sections at the top of the laminite successions. Inner-middle shelf tract cycle 20* is overlain by fusulinid dominated outer shelf cycle 21*. The Grayburg G11 MFS is correlated between cycle 21* at section PR1 and fusulinid dominated outer shelf cycle 21 at section S7.

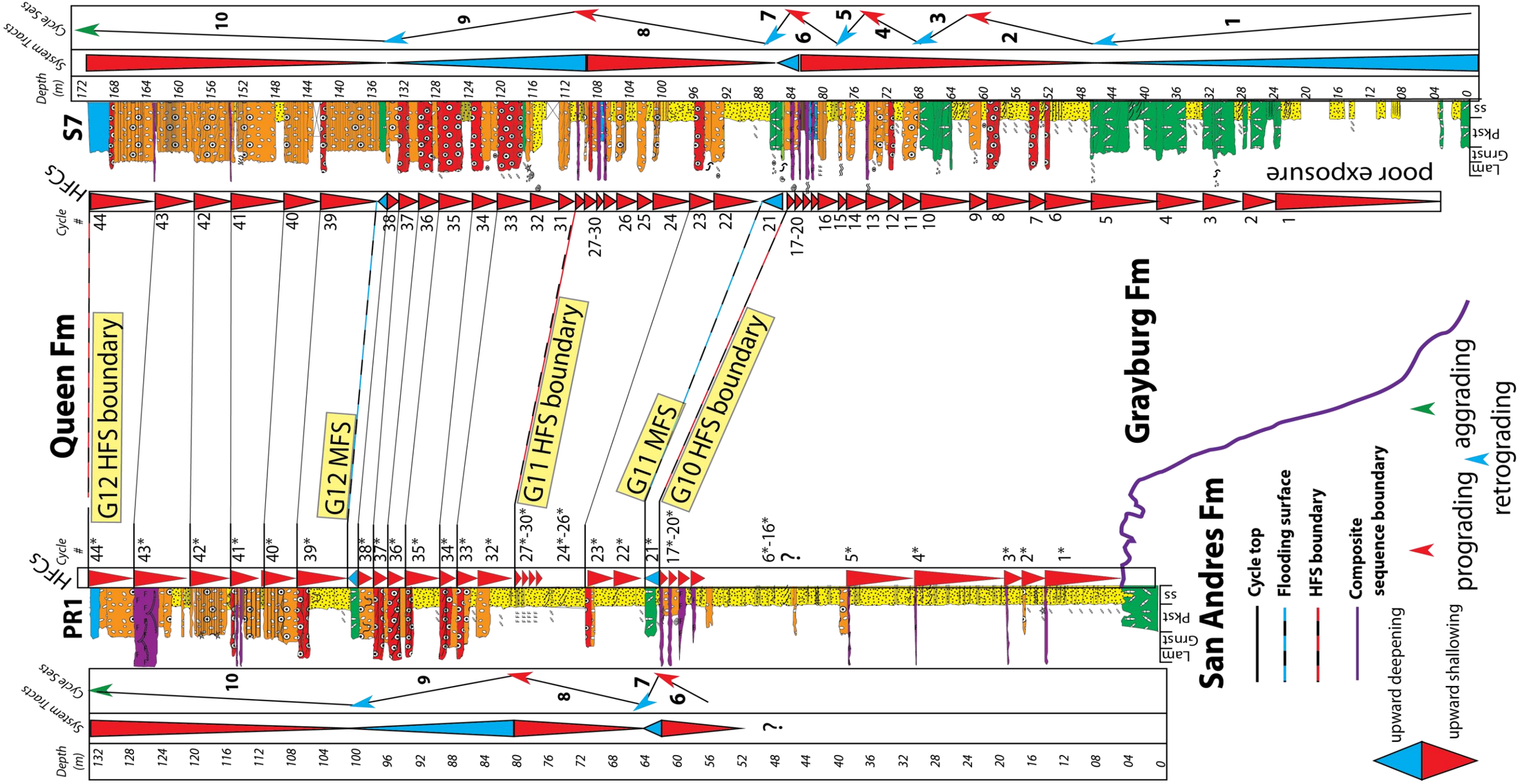

Figure 41: Correlation of Grayburg Strata between S7 and PR1: The Grayburg G10 HFS boundary is correlated between the top of cycle 20 at Shattuck section S7 to the top of cycle 21* at Plowman section PR1. The G11 MFS is correlated within cycle 21 at S7 to cycle 21* as PR1. The G11 HFS boundary is correlated between the top of cycle 30 at S7 to the top of cycle 30* at PR1. The G12 MFS is correlated within the base of cycle 39 at S7 to the base of cycle 39* at PR1. The Grayburg-Queen contact (G12 HFS boundary) is correlated at the top of cycle 44 at S7 to the top of cycle 44* at PR1.

Grayburg G11 high-frequency sequence correlation

The vertical evolution from outer shelf cycle 21 up into the shelf crest cycles 22-23 up into middle shelf tract cycles 24-26, and eventually up into inner-middle shelf facies tract cycles 27-30 records the sequence-scale retrogradation and progradation within the G11 high-frequency sequence at Shattuck section S7. The Grayburg G11 high-frequency scale retrogradation and progradation is recorded at Plowman section PR1 in the vertical evolution from outer fusulinid-dominated outer shelf tract cycle 21* up into shelf crest cycles 22*-23*, and eventually up into algally laminated inner-middle shelf sandstone cycles 27*-30* (Figure 42).

The Grayburg G11 high-frequency sequence maximum flooding surface correlated within cycle 21 at section S7 to cycle 21* at section PR1 separates the G11 transgressive systems tract from the G11 highstand systems tract. The G11 highstand systems tract at Shattuck section S7 is composed of nine high-frequency cycles that define progradational high-frequency cycle set 8. Progradational shelf-crest cycles 22 and 23 are correlated to shelf-crest cycles 22*-23* at section PR1 (Figure 41). Shelf-crest cycles 22 and 23 at S7 are overlain by middle shelf tract cycles 24-26. The equivalent strata at section PR1 are amalgamated middle shelf sandstone cycles that are difficult to differentiate. Overlying cycles 24-26 at section S7 are fenestral laminite-capped inner-middle shelf tract cycles 27-30. The Grayburg G11 high-frequency sequence boundary is picked at the top of laminite-capped cycle 30 at section S7. Cycles 27-30 at section S7 are correlated to algally laminated inner-middle shelf tract sandstone cycles 27*-30*at section PR1. The G11 high-frequency sequence boundary is correlated from the top of cycle 30 at section S7 to the top of cycle 30* at section PR1 (Figure 41).

.

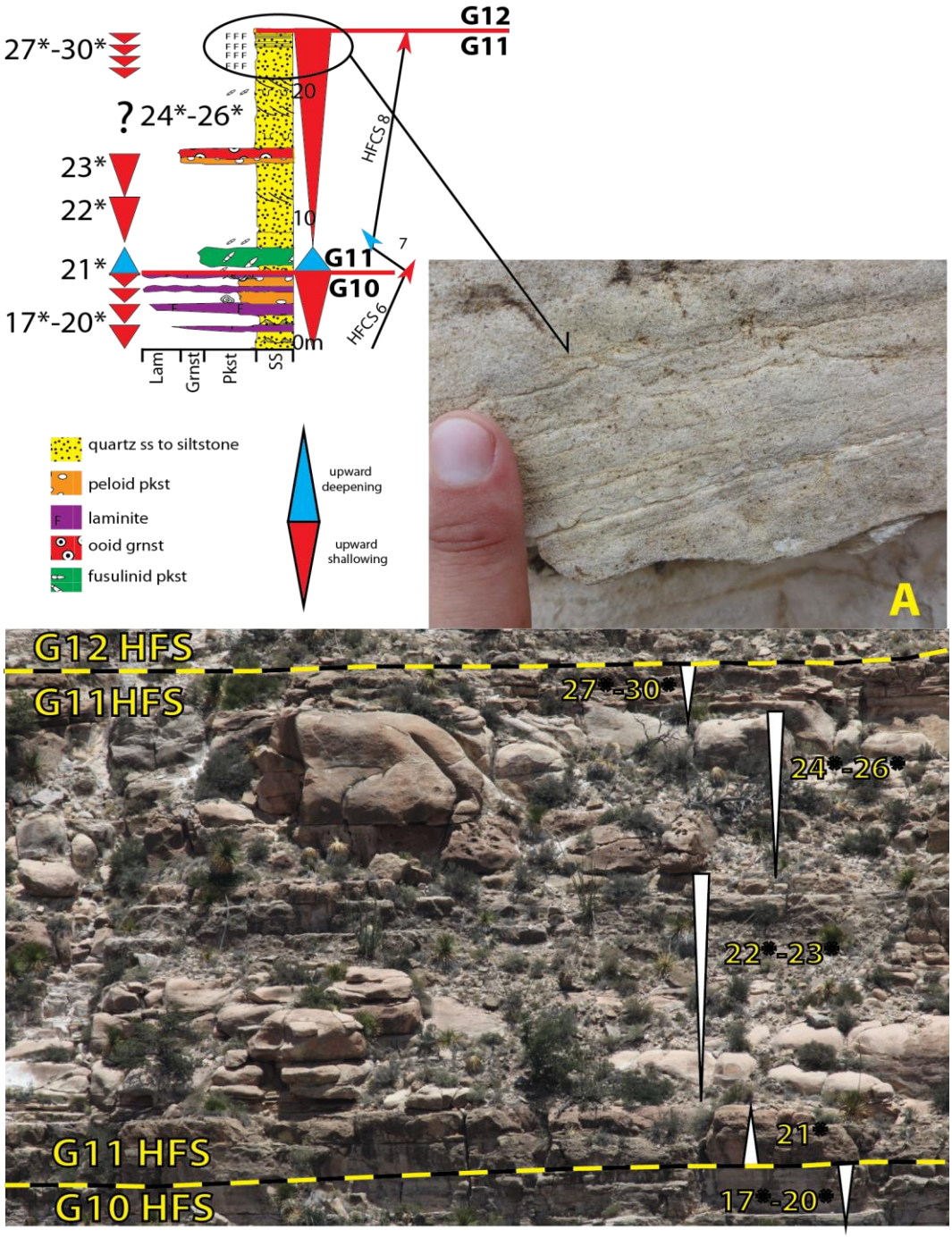

Figure 42: Plowman PR1 Cycles 17*-30*: High-frequency sequence scale retrogradation and progradation within the G11 is recorded in the vertical evolution from: outer shelf tract cycle 21* up into shelf crest tract cycles 22*-23*, and eventually up into algally laminated inner-middle shelf tract sandstone cycles 27*-30*. Photograph (A) documents "crinkly" algal laminations within the sandstone cycles at the top of the G11 HFS.

Grayburg G12 high-frequency sequence correlation

The vertical evolution from shelf-crest cycles (cycles 33-38) up into middle shelf cycles (cycles 39-44) that are capped by a karsted skeletal packstone unit records the sequence scale retrogradation and progradation during deposition of the Grayburg G11 high-frequency sequence. Sequence scale retrogradation and progradation within the Grayburg G12 high-frequency sequence at Plowman Ridge section PR1 is recorded in the vertical evolution from shelf crest cycles 32*-38* up into middle and inner-middle shelf cycles 40*-44* capped by a brecciated skeletal packstone unit.

The G12 transgressive systems tract at section S7 is composed of middle shelf and shelf-crest high-frequency cycles 31-38. Cycles 31-38 at section S7 define retrogradational high-frequency cycle set 9. Shelf-crest cycles 32-37 at section S7 are equivalent to shelf-crest cycles 32*-38* at Plowman section PR1 (Figure 43). The ooid-grainstone capped shelf crest cycles 32*-37* at section PR1 are an excellent match in terms of cycle number, cycle thickness, vertical facies succession, and facies proportion to the ooid-grainstone shelf-crest cycles 32-37 at section S7 (Figures 44-45). Overlying shelf-crest cycle 38 at section S7 is a thin fusulinid packstone unit at the base of cycle 39. The G12 high-frequency sequence maximum flooding surface is picked within the outer shelf tract fusulinid unit at the base of cycle 39. The fusulinid unit at the base of cycle 39 at section S7 is equivalent to the outer shelf tract fusulinid unit at the base of cycle 39* at section PR1 (Figure 44). The Grayburg G12 high-frequency sequence maximum flooding surface is correlated within the fusulinid outer shelf tract unit at the base of cycle 39 to the fusulinid-dominated outer shelf tract unit at the base of cycle 39*(Figure 41). The G12 high-frequency maximum flooding surface separates the g12 transgressive systems tract from the g12 highstand systems tract. The G12 highstand systems tract at Shattuck section S7 is composed of high-frequency cycles 39-44 which define aggradational to progradational high-frequency cycle set 10. Middle shelf peloid packstone cycles 40-44 are equivalent to inner-middle shelf and middle shelf cycles 40*-44* at Plowman section PR1 (Figure 46). The Grayburg-Queen contact (G12 high-frequency sequence boundary) is picked at the top of cycle 44, where a karsted skeletal packstone unit is overlain by 6 m

of recessive, slope-forming sandstone. The Grayburg-Queen contact is correlated to the brecciated skeletal packstone unit at the top of section PR1 cycle 44* (Figure 41). Cycle 44* is overlain by 3 m of recessive slope-forming sands (Figure 47).

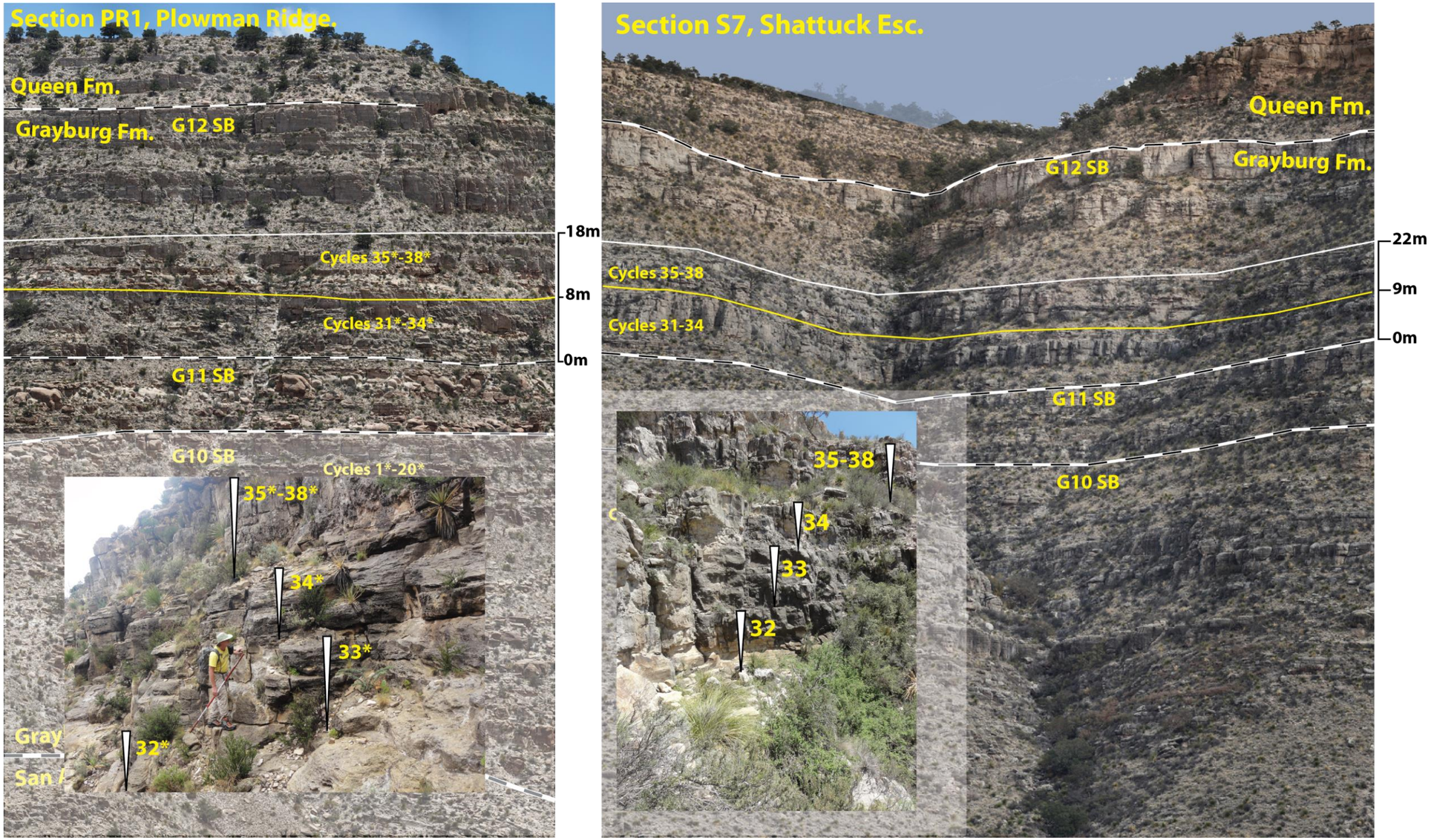

Figure 43: G12 HFS Transgressive Systems Tract Shelf-Crest Tract Cycles: Shelf-crest cycles 31-38 at Shattuck section S7 are 22m thick. The equivalent shelf-crest cycles 31*-38* at Plowman section PR1 are 18m thick.

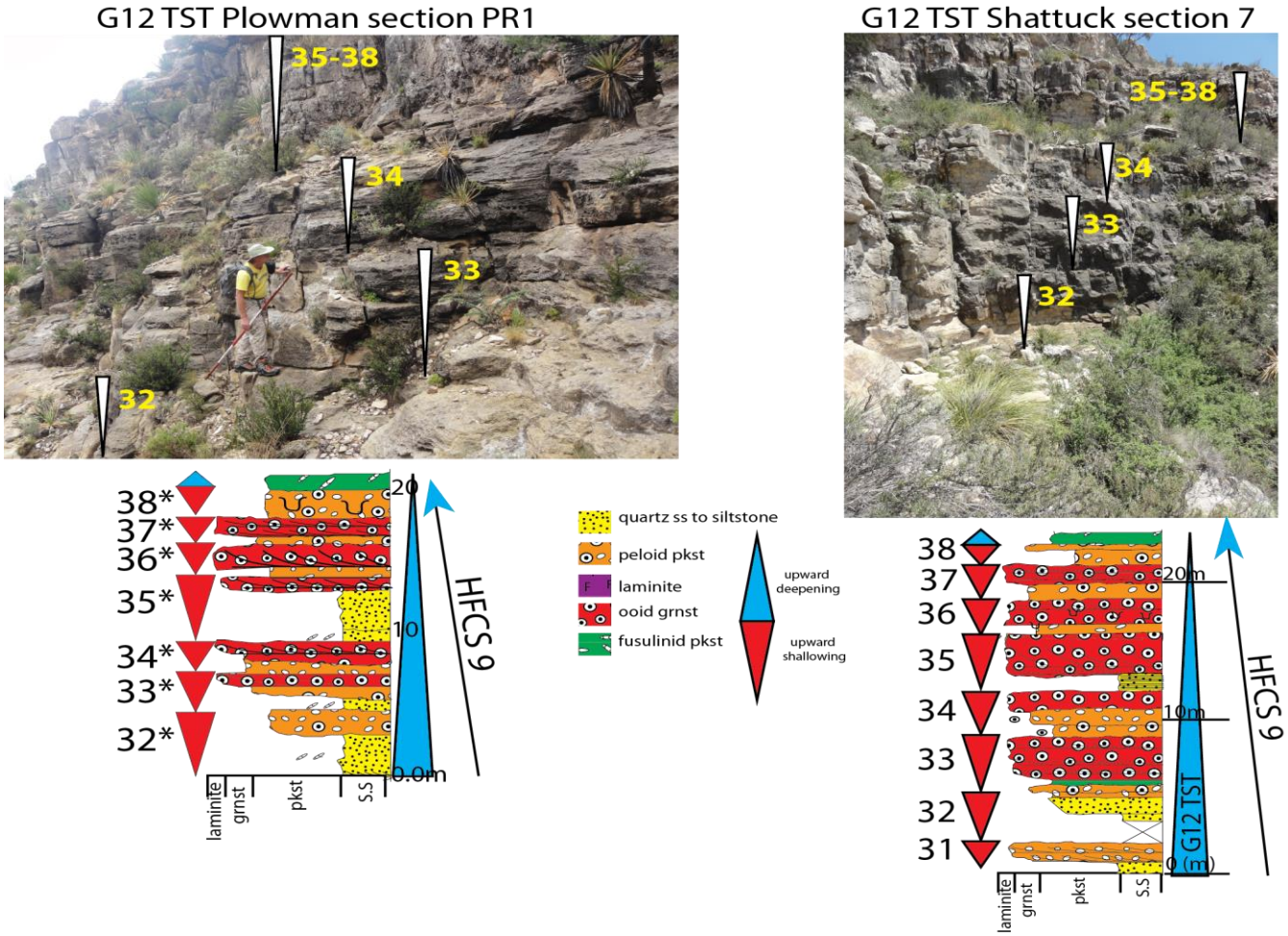

Figure 44: Plowman PR1 Cycles 32*-38*: Shelf crest cycles 32*-38* at section PR1 are an excellent match to the G12 high-frequency sequence shelf-crest cycles 32-38 in terms of cycle number, cycle thickness, and vertical facies succession.

	Plowman section PR1			Shattuck section S7		
	Vertical facies succession	# of HFCs	Avg. cycle thickness	Vertical facies succession	# of HFCs	Avg. cycle thickness
G12 HFCS 9	inner-middle shelf			inner-middle shelf		
	middle shelf	**2**	**3.5m**	middle shelf	**3**	**2.6m**
	shelf crest	**5**	**2.2m**	shelf crest	**5**	**2.8m**
	Total thickness		**18m**	**Total thickness**		**22m**
G12 HFCS 10	inner-middle shelf	**2**	**6.0m**	inner-middle shelf		
	middle shelf	**3**	**5.5m**	middle shelf	**6**	**6.3m**
	shelf crest	**1**	**3.5m**	shelf crest		
	Total thickness		**32m**	**Total thickness**		**38m**

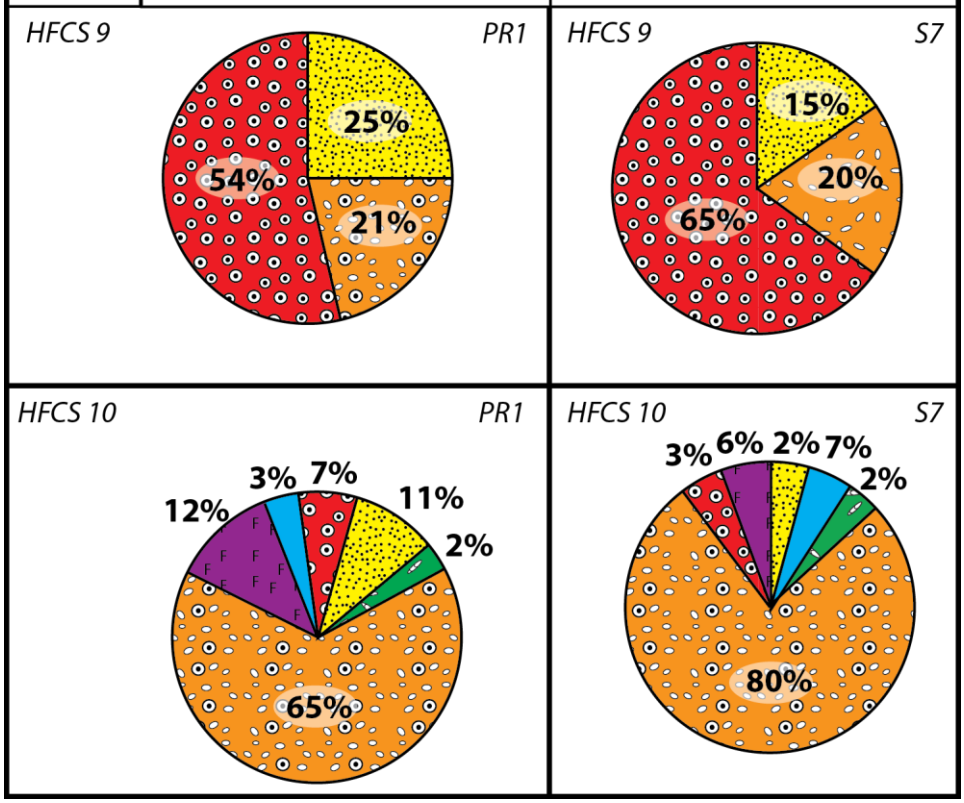

Figure 45: Grayburg G12 HFS Facies Proportion Comparison: High-frequency cycle sets 9 and 10 at section S7 and section PR1 are an excellent match in terms of cycle number, average cycle thickness and facies proportion. For example the average thickness of the 5 shelf-crest tract cycles within HFCS 9 at section S7 is 2.8m. The five shelf-crest cycles within HFCS 9 at section PR1 have average thickness of 2.2m. HFCS 9 is composed of over 50% ooid grainstone facies at section S7 and section PR1.

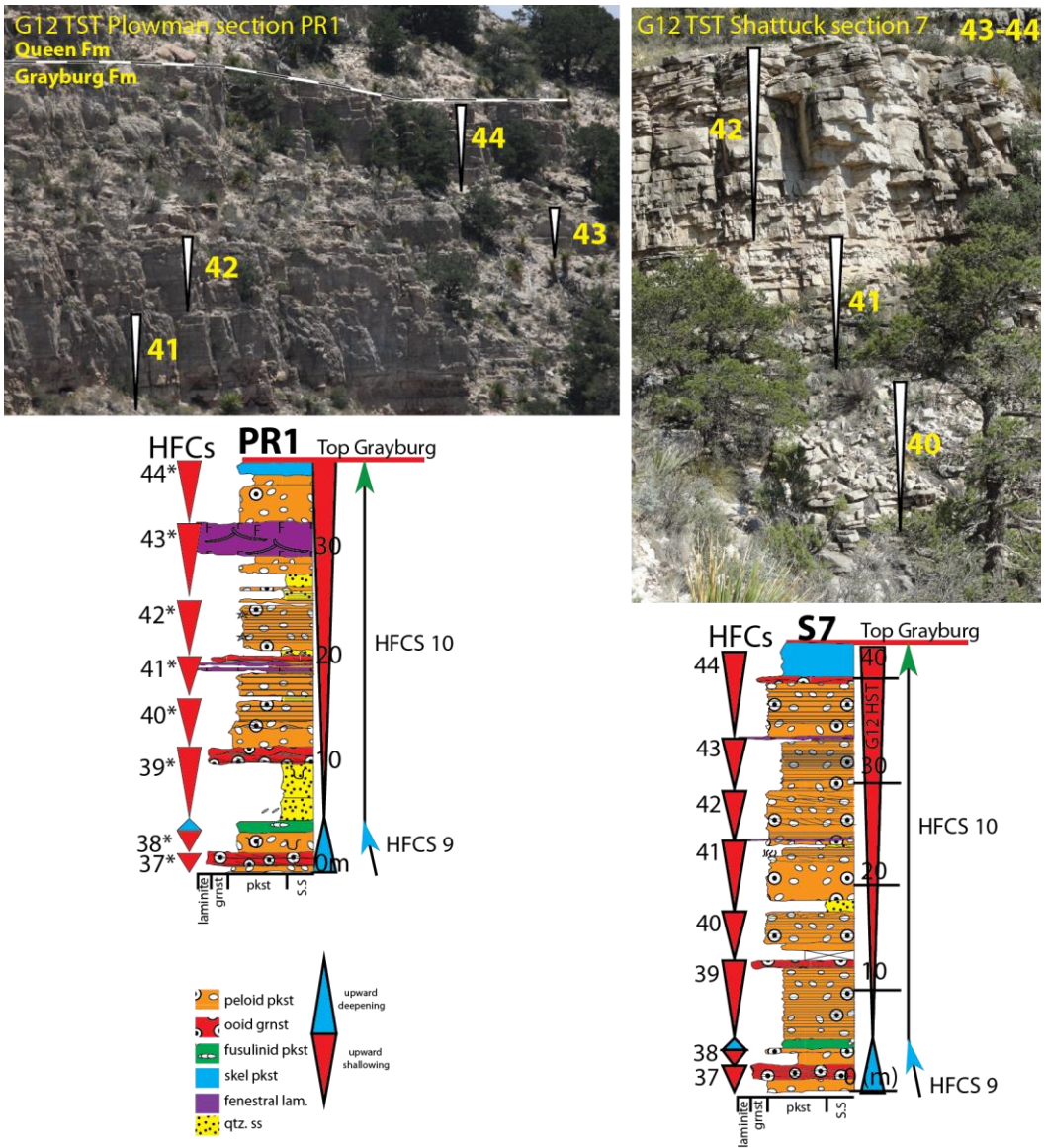

Figure 46: Plowman PR1 Cycles 41*-44*: The G12 highstand systems tract at Shattuck section S7 is composed of high-frequency cycles 39-44 which define aggradational to progradational high-frequency cycle set 10. Middle shelf peloid packstone cycles 40-44 are equivalent to inner-middle shelf and middle shelf cycles 40*-44* at Plowman section PR1

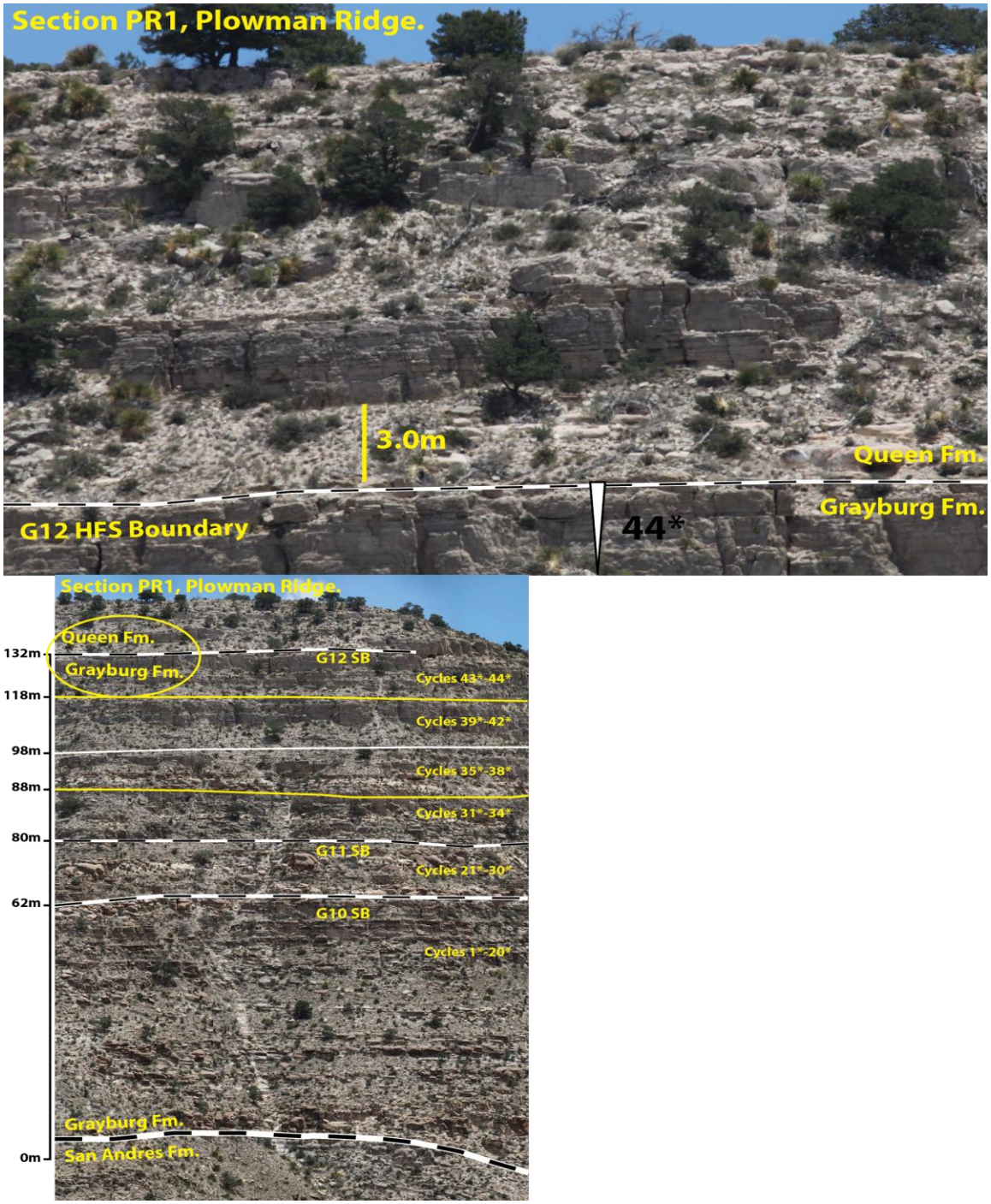

Figure 47: Grayburg-Queen Contact at Plowman Section PR1: The Grayburg-Queen contact (G12 HFS boundary) is picked at the top of a brecciated skeletal packstone that caps middle shelf tract cycle 44*. Cycle 44* is overlain by 3m of recessive slope forming sandstone.

GRAYBURG FM. INORGANIC $\Delta^{13}C$ PROFILES

The $\delta^{13}C_{(inorganic)}$ values at Plowman Ridge section PR1 and Shattuck Escarpment section S7 range from 1.0‰ to +7.0‰. The $\delta^{18}O$ values range from 0.0‰ to -9.0‰ (Figure). The $\delta^{18}O$ and $\delta^{13}C_{(inorganic)}$ values documented in this study are within the range of estimated original Permian-age marine signatures established by Given and Lohmann (1985) (Figure 10). Seventy-nine samples were used to generate the Grayburg $\delta^{13}C_{(inorganic)}$ profile at Shattuck section S7. Twenty-four samples were collected from the G10 HFS, 20 from the G11 HFS, and 35 from the G12 HFS. The $\delta^{13}C_{(inorganic)}$ values for the G10 and G11 high-frequency sequences at section S7 are between +2.0‰ and +6.0‰ (Figure 48). The $\delta^{13}C_{(inorganic)}$ values for the G12 high-frequency sequence at section S7 are between +4.0‰ and +6.0‰ (Figure 48).

Eighty-nine samples were used to generate the Grayburg $\delta^{13}C_{(inorganic)}$ profile for section PR1 at Plowman Ridge. Forty-six samples were collected from the G10 HFS, 10 samples from the G11 HFS, and 33 samples from the G12 HFS. For the G10 HFS at Plowman Ridge the $\delta^{13}C_{(inorganic)}$ values are between +2.0‰ and +6.0‰ (Figure 48). For the G11 HFS at Plowman Ridge the $\delta^{13}C_{(inorganic)}$ values are between +3.0‰ and +4.0‰. Values for the G12 high-frequency sequence are between +2.0 ‰ and 7.0‰.

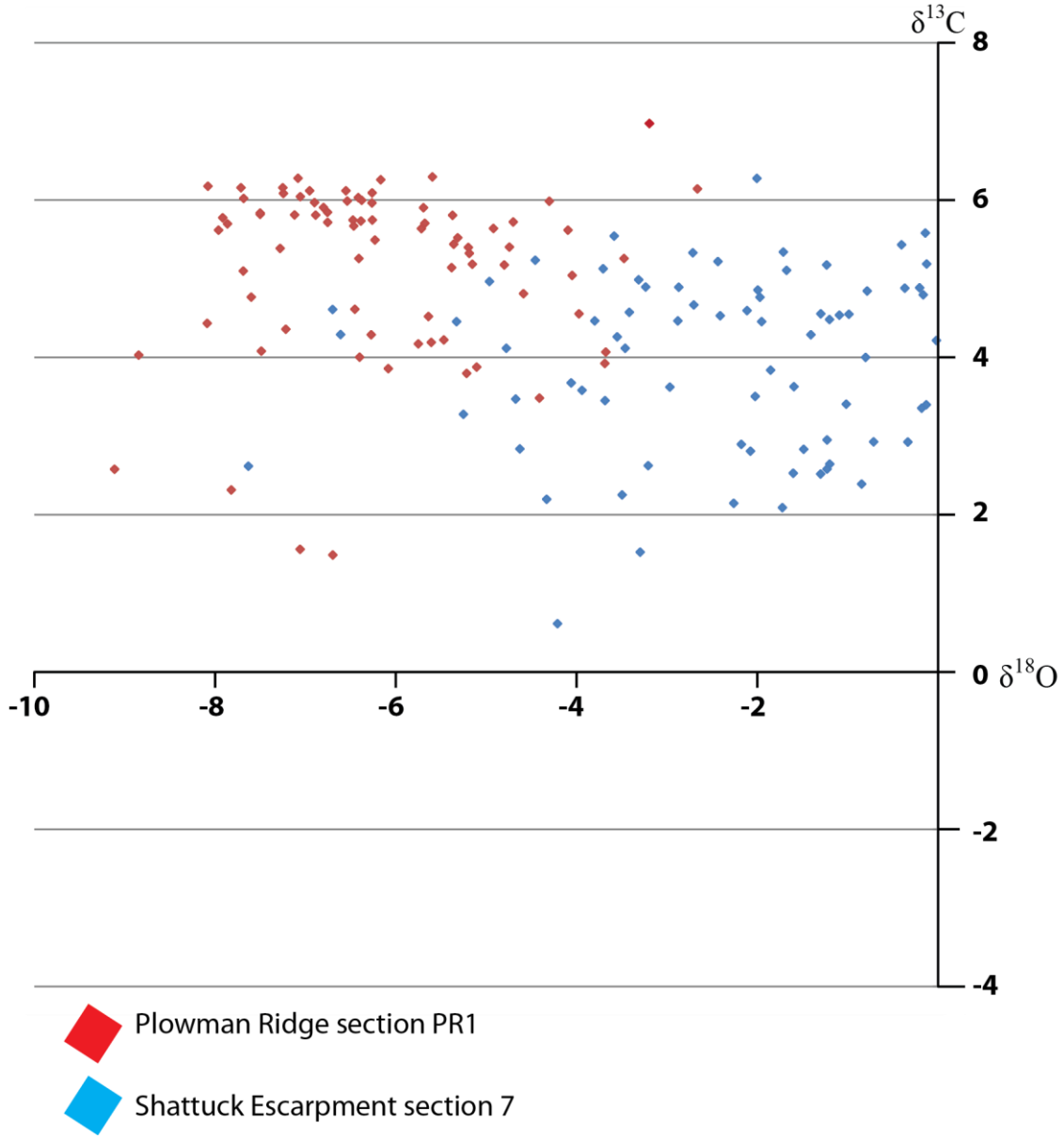

Figure 48: $\delta^{13}C_{(inorganic)}$ Values for Shattuck S7 and Plowman PR1: The $\delta^{13}C_{(inorganic)}$ values generated at sections S7 and PR1 are between +1.0‰ and +7.0‰.

Inorganic $\delta^{13}C$ profile from Shattuck section S7

The Grayburg Formation at Shattuck section S7 has $\delta^{13}C_{(inorganic)}$ values that range from +1.0 ‰ to +6.0‰ (Figure 48). The G10 HFS is composed of high-frequency cycle sets 1-6. The $\delta^{13}C_{(inorganic)}$ values range from +2.0 ‰ to +6.0‰ within the five high-frequency cycles sets of the G10 HFS (Figure 49). Five samples were collected from shelf-crest tract cycles 6-9 that comprise progradational high-frequency cycles set 2. $\delta^{13}C_{(inorganic)}$ values within cycles 6-9 are between +3.0‰ and +6.0‰. There is a 3.0‰ negative trend between cycle 7 (+6.0‰) and cycle 9 (+3.0‰) (Figure 49). Three samples were collected from high-frequency cycle set 2 outer shelf tract cycle 10. There is a 1.0‰ positive trend between shelf-crest cycle 9 (+3.0‰) and outer shelf cycle 10 (+4.0‰) (Figure 49). Thirteen samples were collected from middle shelf and inner-middle shelf high-frequency cycles 11-20. Cycles 11-20 comprise progradational HFCS 4, retrogradational HFCS 5, and progradational HFCS 6. The $\delta^{13}C_{(inorganic)}$ values from cycles 11-20 are tightly clustered around +5.0‰ (Figure 49). There is a 1.0‰ positive trend between outer shelf cycle 10 (+4.0‰) and the middle shelf and inner middle shelf cycles 11-20 (+5.0‰).

The G11 HFS is composed of high-frequency cycle sets 7 and 8. These $\delta^{13}C_{(inorganic)}$ values range from +2.0 ‰ to +6.0‰ within the 2 high-frequency cycles sets of the G11 HFS. Three samples were collected from high-frequency cycles set 7 outer shelf tract cycle 21. The $\delta^{13}C_{(inorganic)}$ values from cycle 21 are tightly clustered around +4.0‰. Eleven samples were taken from cycles 22-30 within progradational high-frequency cycle set 8. Inner-middle shelf, middle shelf, and shelf-crest cycles 22-30 have $\delta^{13}C_{(inorganic)}$ values between +2.0‰ and +6.0‰. There is a negative 3.0‰ trend from +5.0‰ at cycle

24 to +2.0‰ at cycle 26. There is a positive 4.0‰ trend from +2.0‰ at cycle 26 to +6.0‰ at cycle 30 (Figure 49).

The G12 HFS at section S7 is composed of high-frequency cycle sets 9 and 10. The $\delta^{13}C_{(inorganic)}$ values range from +4.0 ‰ to +6.0‰ within the two high-frequency cycles sets of the G12 HFS. Fifteen samples were collected from the middle shelf and shelf-crest high-frequency cycles 31-38 that comprise retrogradational HFCS 9. The $\delta^{13}C_{(inorganic)}$ values are tightly clustered around +6.0‰ (Figure 49). Eleven samples were taken from middle shelf high-frequency cycles 39-44 that comprise aggradational HFCS 10. The $\delta^{13}C_{(inorganic)}$ values from high-frequency cycle set 10 are tightly clustered around +6 (Figure 49).

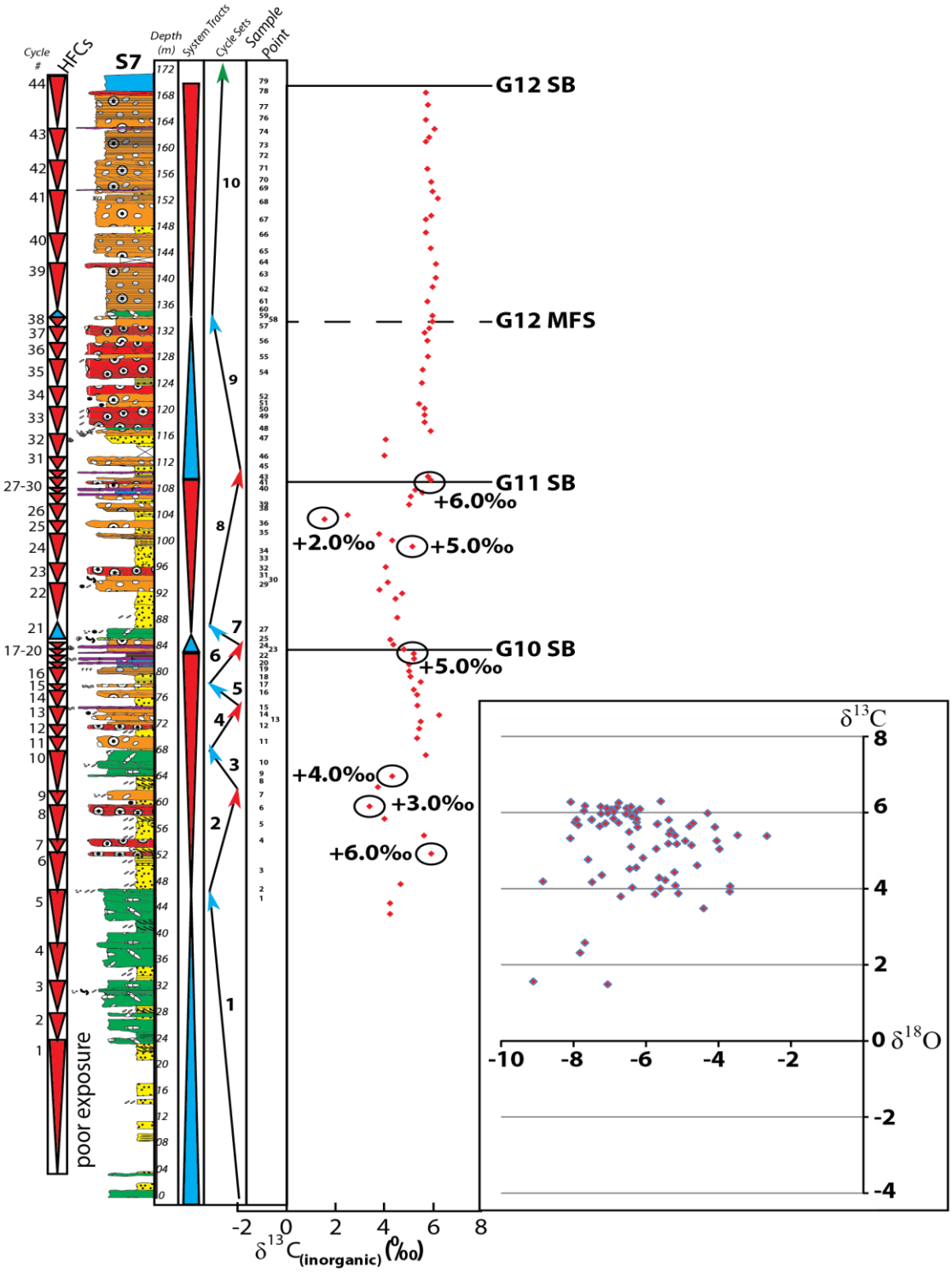

Figure 49: Shattuck Section S7 δ13C (inorganic) Profile: S7 δ13C (inorganic) profile shown was smoothed using a 3 point moving average.

Inorganic $\delta^{13}C$ profile from Plowman section PR1

The Grayburg Formation at Plowman Ridge section PR1 has $\delta^{13}C_{(inorganic)}$ values that range from +2.0 ‰ to +7.0‰ (Figure 48). Grayburg G10 HFS $\delta^{13}C_{(inorganic)}$ values range from +2.0 ‰ to +6.0‰ (Figure 50). Forty-six samples were taken from the 60-m G10 interval. There is a negative 3.0‰ trend from +5.0‰ sample #12 to +3.0‰ sample 16 (Figure 50). Samples 16-25 $\delta^{13}C_{(inorganic)}$ values are grouped around +2.0‰. There is a positive 3.0‰ trend from +2.0‰ sample #25 to +5.0‰ sample 28. Samples 28-46 $\delta^{13}C_{(inorganic)}$ values are grouped between +4.0‰ and +5.0‰.

The G11 HFS at section PR1 is composed of high-frequency cycle sets 7 and 8. Here the $\delta^{13}C_{(inorganic)}$ values range from +3.0 ‰ to +4.0‰ within the two high-frequency cycles sets of the G11 high-frequency sequence at section PR1. Samples 47 and 48 were collected from outer shelf tract cycle 21. The $\delta^{13}C_{(inorganic)}$ values from cycle 21 have a negative 1.0‰ trend from +4.0‰ to +3.0‰. Eight samples were taken from the nine high-frequency cycles 22-30 that comprise progradational HFCS 8. Inner-middle shelf, middle shelf, and shelf-crest cycles 22-30 have $\delta^{13}C_{(inorganic)}$ values between +3.0‰ and +5.0‰. There is a positive 2.0‰ trend from +3.0‰ at cycle 22 to +5.0‰ at cycle 23 (Figure 50). There is a negative 2.0‰ trend from +5.0‰ at cycle 23 to +3.0‰ at cycle 30.

The G12 high-frequency sequence at section PR1 is composed of high-frequency cycle sets 9 and 10. The $\delta^{13}C_{(inorganic)}$ values range from between +2.0 ‰ to +7.0‰ within the two high-frequency cycles sets of the G12 HFS. Twelve samples were collected from middle shelf and shelf-crest high-frequency cycles 32-38. Cycles 32-38 comprise retrogradational HFCS 9. The $\delta^{13}C_{(inorganic)}$ values within HFCS 9 are clustered between +2.0‰ and +4.0‰ (Figure 50). There is a negative 2.0% trend between cycle 33 (+4.0‰) and cycle 36 (+2.0‰) (Figure 50). There is a positive 2.0% trend between cycle

36 (+2.0‰) and cycle 38 (+4.0‰) (Figure 50). Nineteen samples were taken from shelf-crest, middle shelf and inner-middle shelf high-frequency cycles 39-44. Cycles 39-44 comprise aggradational HFCS 10. The $\delta 13C_{(inorganic)}$ values range from +3.0 ‰ to +7.0‰ (Figure 50). There is a pronounced 4.0‰ positive trend within HFCS 10 at section PR1 between cycle 39 (3.0‰) and cycle 43 (7.0‰) (Figure 50).

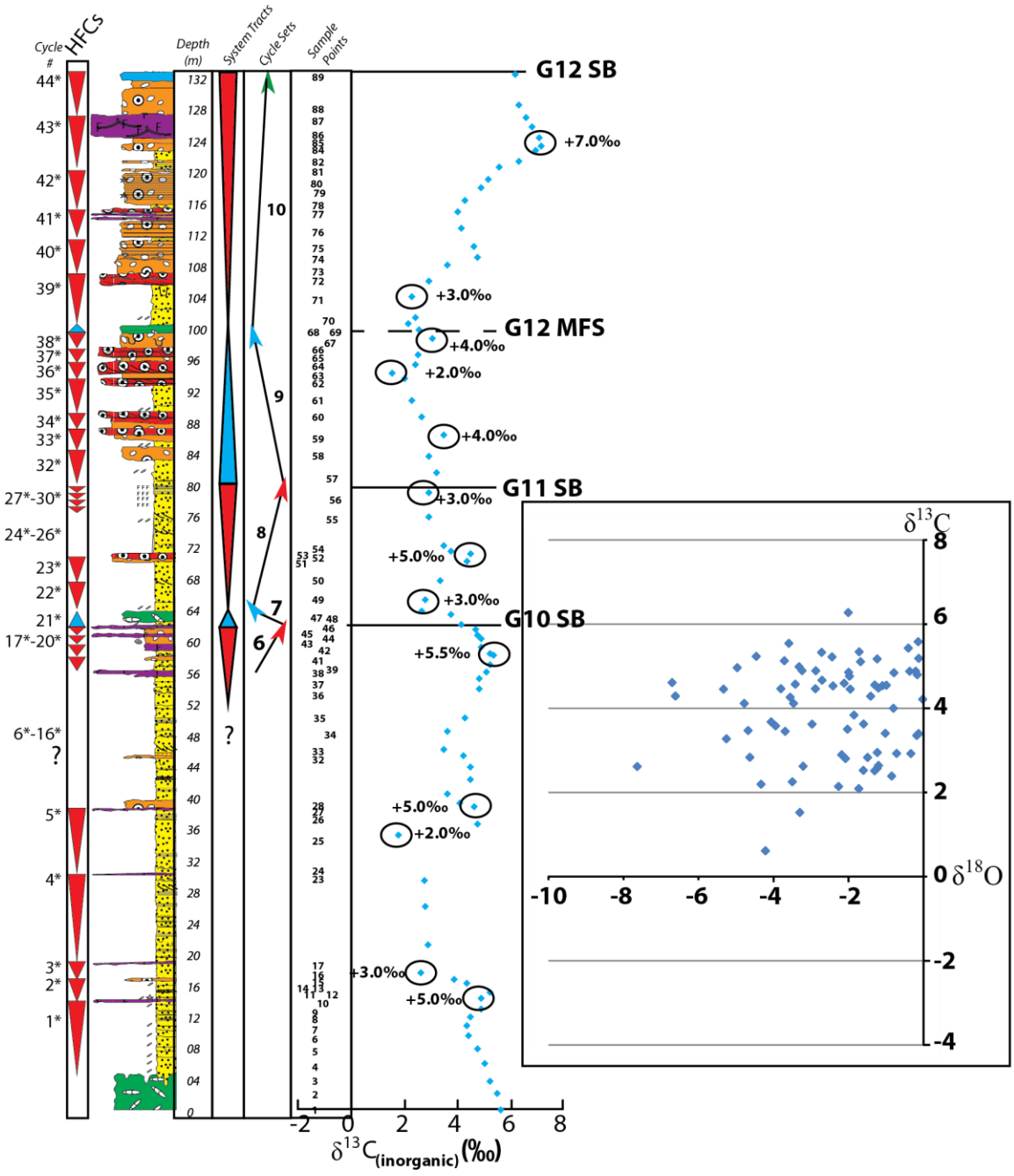

Figure 50: Plowman Section PR1 $\delta^{13}C_{(inorganic)}$ Profile: PR1 $\delta^{13}C_{(inorganic)}$ profile shown was smoothed using a 3 point moving average.

DISCUSSION

Shelf-to-basin correlation frameworks

Documentation of four fundamental observations supports the correlation of Grayburg G10-G12 high-frequency sequences between Shattuck Escarpment section S7 and Plowman Ridge section PR1 in the Brokeoff Mountains as previously proposed by Kerans and Tinker (1999): (1) the 3rd-order composite sequence boundary separating the San Andres Formation from the overlying Grayburg Formation is picked at Plowman Ridge near the base of section PR1, (2) Grayburg G12 HFS transgressive systems tract shelf-crest cycles 32-38 are correlated to shelf crest cycles 32*-38* at Plowman section PR1 on a one-to-one cycle scale, (3) correlation of the Grayburg-Queen contact between the top of cycle 44 at section S7 and the top of cycle 44* at section PR1, and (4) section thickness between the San Andres-Grayburg contact and the Grayburg-Queen contact at section PR1 is very similar to the Grayburg thickness measured at section S7.

Correlation of Grayburg G10-G12 high-frequency sequences between the Shattuck Escarpment and Plowman Ridge can be used to address discrepancies within the San Andres-Grayburg interval of the shelf-to-basin correlation frameworks of Sarg et al (1999) and Kerans and Tinker (1999). Sarg et al (1999) considered the upper two-thirds of Plowman Ridge to be the transgressive and highstand systems tracts of the San Andres GP2 depositional sequence (Figure 51). Sarg et al (1997) ascribed these units to San Andres Formation sequences 4 and 5 that Sonnenfeld (1993) documented at Last Chance Canyon in the Guadalupe Mountains. Kerans and Tinker (1999) correlated the upper two-thirds of Plowman Ridge as Grayburg Formation as equivalent to the G10-G12 high-frequency sequences documented at the Shattuck Escarpment in the Guadalupe Mountains (Figure 51).

Observations made by Sarg et al (1997) at Plowman Ridge are similar to the results documented in this study. Sarg et al (1997) recognized an obvious contact at the base of the section, where seaward-dipping outer shelf strata were onlapped by quartz sandstone units. Sarg et al (1997) called this contact the GP2 sequence boundary within

the San Andres Formation (Figure 51). In this study the contact between seaward-dipping fusulinid outer shelf tract cycles and the overlying sandstone units is picked as the 3rd – order composite sequence boundary separating the San Andres Formation from the overlying Grayburg Formation (Figure 51). Above the San Andres-Grayburg contact Sarg et al (1997) described a series of cyclic, meter -scale, peritidal quartz sand/dolomite parasequences within the San Andres GP2 transgressive systems tract. This study correlated these cycles to the Grayburg G10 high-frequency sequence at section S7 in the Guadalupe Mountains. Sarg et al (1997) described the San Andres GP2 highstand systems tract as a series of inner shelf mud-rich to shelf crest grainstone parasequences. These strata were correlated in this study to the Grayburg G11 and G12 high-frequency sequence cycles at section S7.

Sarg et al's (1999) San Andres Formation GP2 transgressive and highstand systems tracts correlated at Plowman Ridge are depicted as the upper prograding carbonate unit within the San Andres GP2 interval of the shelf-to-basin correlation framework of Sarg et al (1999) (Figure 52). New high-resolution cyclostratigraphic data presented in this thesis support the assertion of Kerans and Tinker (1999) that the upper two-thirds of the strata exposed at the Plowman Ridge in the Brokeoff Mountains should be correlated to the Grayburg Formation exposed at the Shattuck Escarpment in the Guadalupe Mountains; opposed to the correlation proposed by Sarg et al. (1997) of Plowman strata to San Andres strata exposed at Last Chance Canyon in the Guadalupe Mountains. Assigning the upper 2/3rds of the strata at Plowman Ridge to the Grayburg Formation results in the shelf-to-basin framework of Sarg et al (1999) depicting the stratigraphic relationship of Goat Seep Formation overlying Grayburg Formation at the Bush Mountain collapse scarp on the Western Escarpment. The Kerans and Tinker (1999) shelf-to-basin correlation framework shows the Goat Seep Formation overlying the Grayburg Formation at the Bush Mountain collapse scarp on the Western Escarpment (Figure 52).

Potential of $\delta^{13}C_{(inorganic)}$ data for constraining sequence stratigraphic correlations

The results from the bulk rock analysis of $\delta^{13}C_{(inorganic)}$ compiled at Shattuck Section S7 and Plowman section PR1 fall within the +1.0‰ to +6.0‰ range representative of the unaltered $\delta^{13}C_{(inorganic)}$ Permian marine signature (Given and Lohmann 1985). There is as much as +/- 3.0‰ variability between the $\delta^{13}C_{(inorganic)}$ values of equivalent units between Shattuck section S7 and Plowman section PR1. The $\delta^{13}C_{(inorganic)}$ variability documented across the Grayburg shelf is similar to the +/-2.0‰ range of $\delta^{13}C_{(inorganic)}$ values documented in recent sediments deposited across the Bahamian platform near Andros Island (Oehlert et al 2012).

Collection of the isotope data was never intended to facilitate the high-frequency cycle scale correlation between Shattuck section S7 and Plowman section PR1. The isotope sampling was initiated to test whether there would be a pronounced excursion within the Grayburg succession that could be used as a "golden spike" linking the Plowman Ridge and Shattuck Escarpment. There is a -2.0 ‰ $\delta^{13}C_{(inorganic)}$ trend occurs across the Grayburg G10-G11 high-frequency sequence boundary recognized at both Plowman section PR1 and Shattuck section S7 (Figure 53). The $\delta^{13}C_{(inorganic)}$ trend across the G10-G11 sequence boundary is not a stand-alone "golden spike" linking the two sections; but it is geochemical data to corroborate the high-resolution cyclostratigraphic correlation of Grayburg strata between the Guadalupe Mountains and the Brokeoff Mountains.

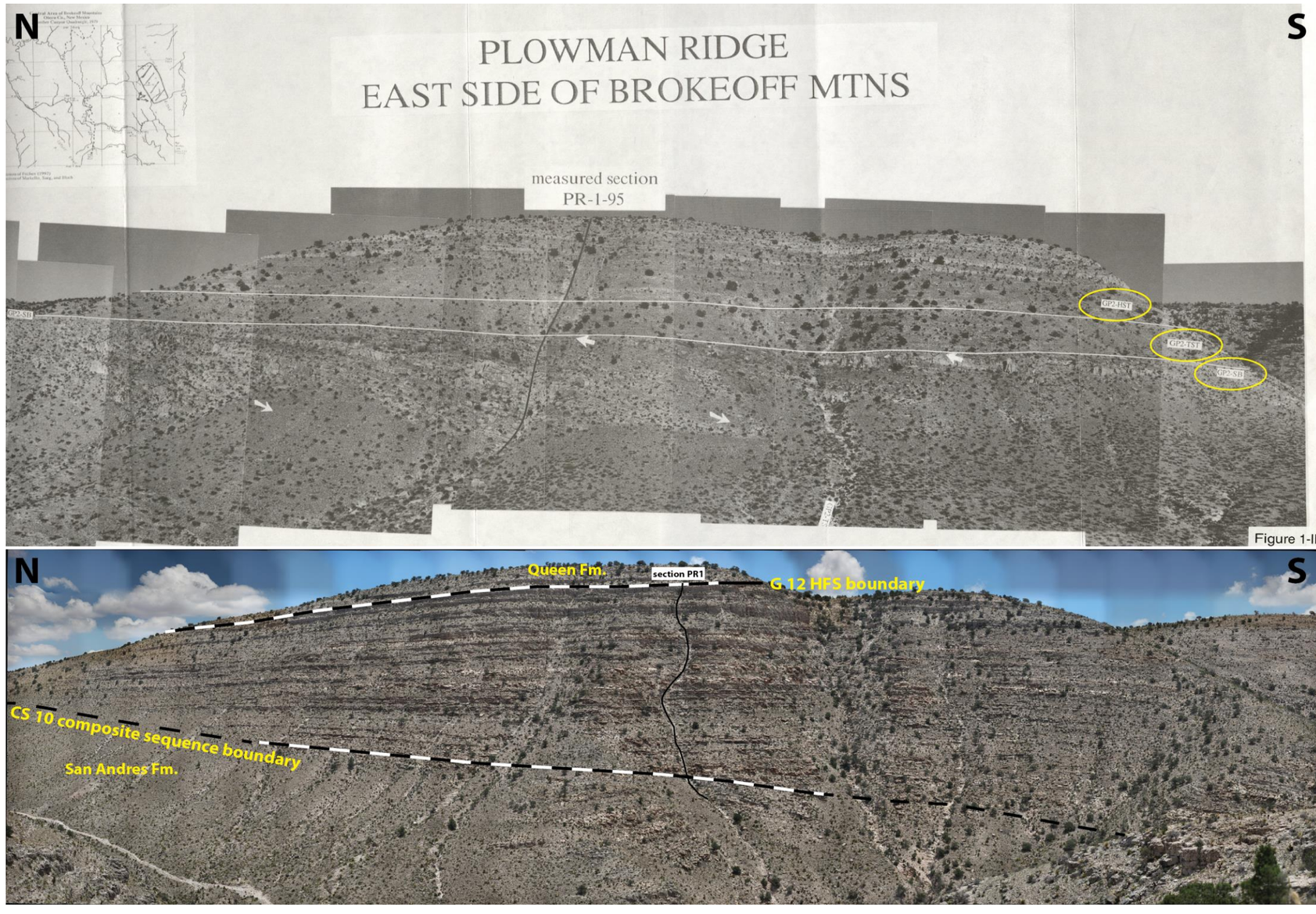

Figure 1-II-5

San Andres Fm
GP2-TST and HST

Sarg et al. (1997)

Grayburg Fm
G10 HFS-G12 HFS

Kerans and Tinker (1999)

Figure 51: Differing Interpretations of Plowman Ridge Strata: Sarg et al (1997) correlated the upper 2/3 of Plowman Ridge as the transgressive and highstand systems tracts of the San Andres GP2 depositional sequence. Kerans and Tinker (1999) correlated the upper 2/3 of the Plowman Ridge as the Grayburg G10-G12 high-frequency sequences.

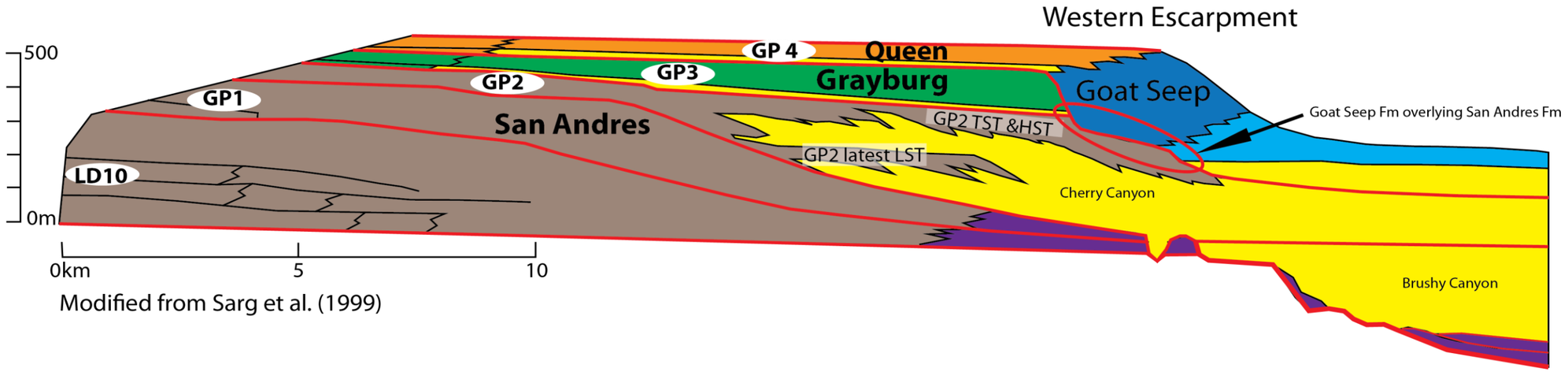

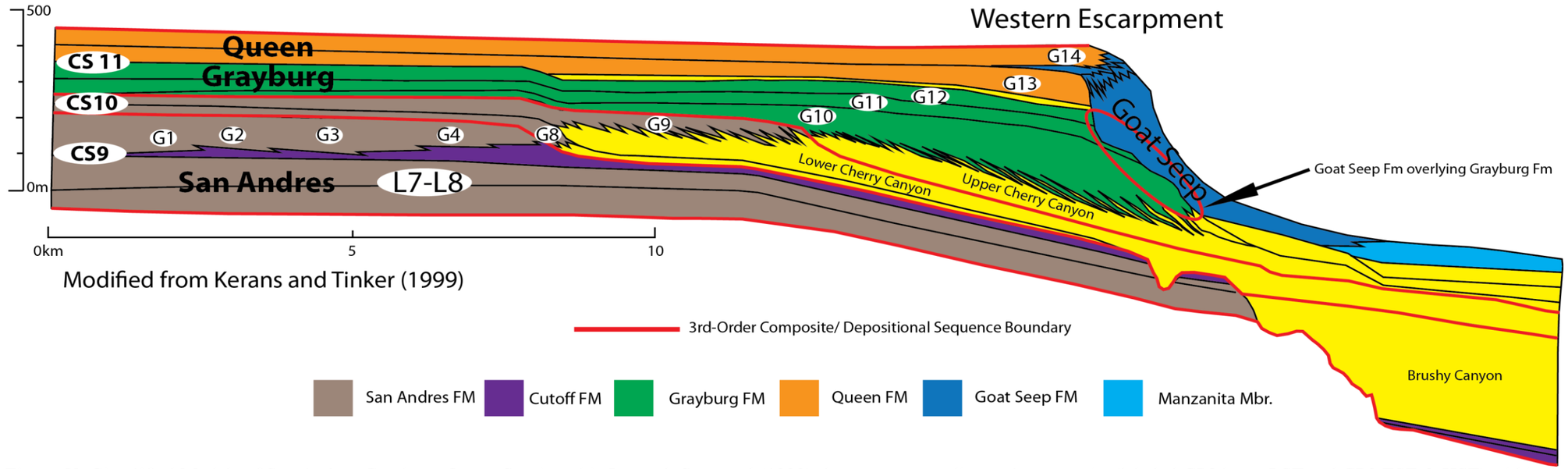

Figure 52: Simplified Models of San Andres-Grayburg-Queen Stratigraphic Interval: Sarg et al (1999) show two prograding carbonate units (labeled GP2 latest LST and GP2 TST & HST) within the San Andres GP2 depositional sequence. The upper carbonate unit labeled GP2 TST and HST within the San Andres GP2 interval of Sarg et al (1999) should be changed to the Grayburg Fm. With this change both Kerans and Tinker (1999) and Sarg et al (1999) show Goat Seep Fm overlying San Andres at the Western Escarpment.

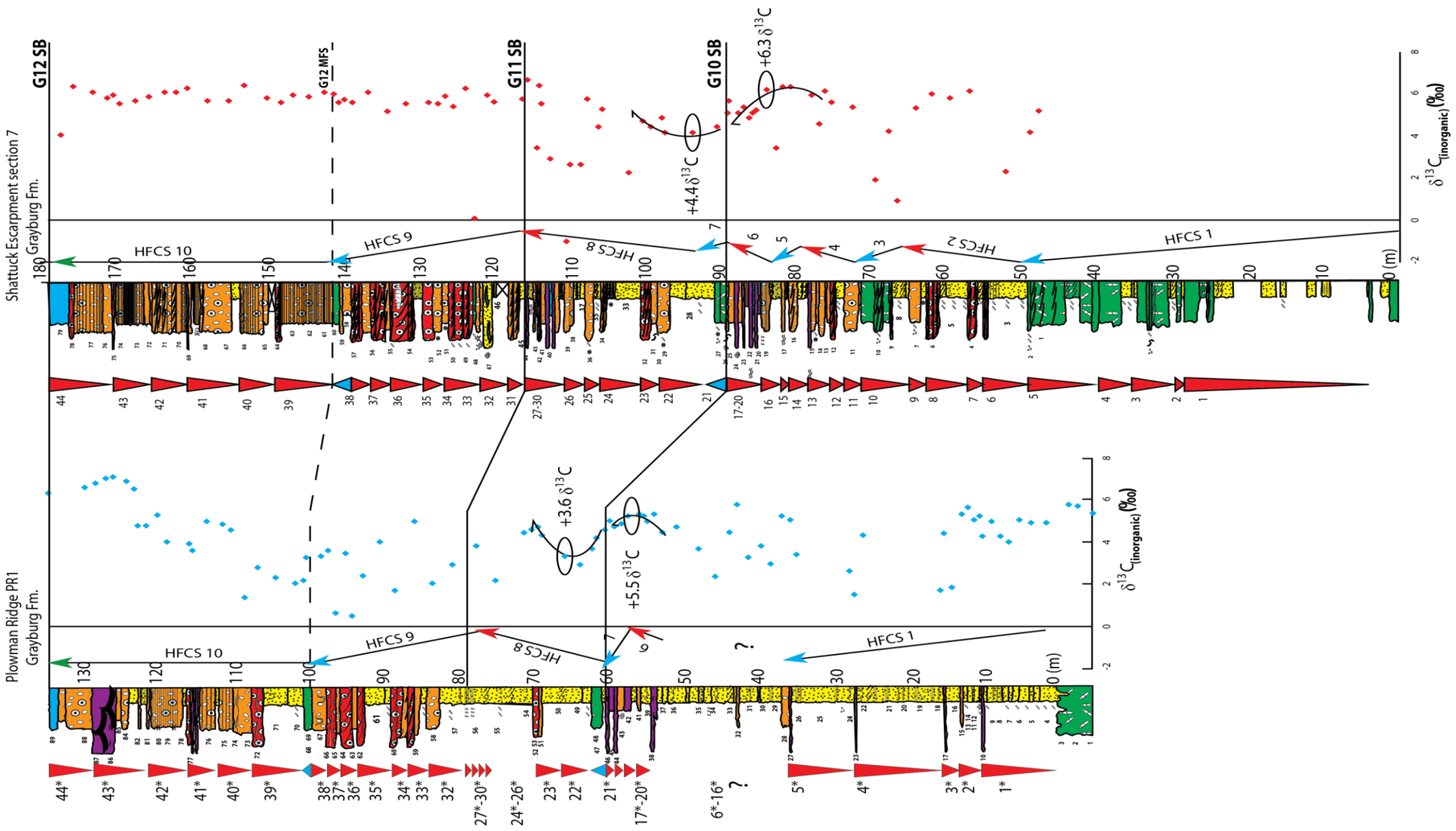

Figure 53: Inorganic $\delta^{13}C$ Profile for Shattuck Section S7 and Plowman Section PR1: A 2 per mil $\delta^{13}C$ shift across the Grayburg G10 HFS boundary is documented at both Shattuck section S7 in the Guadalupe Mountains and Plowman section PR1 in the Brokeoff Mountains

CONCLUSIONS

The San Andres and Grayburg Formations are important units for making shelf-to-basin correlation frameworks of the Guadalupe Mountains. This thesis provides the first high-confidence correlation of mixed carbonate-siliciclastic Grayburg strata between the southern Guadalupe Mountains and the Brokeoff Mountains. One- and two-dimensional cycle stacking analysis was used to construct the Grayburg Formation high-resolution sequence stratigraphic framework at the Shattuck Escarpment in the Guadalupe Mountains. The Grayburg was divided into the G10, G11, and G12 high-frequency sequences. The Grayburg G10 HFS is composed of 20 high-frequency cycles that are divided into 6 high-frequency cycle sets. The Grayburg G11HFS is composed of 9 high-frequency cycles divided into 2 high-frequency cycle sets, and the Grayburg G12 HFS is composed of 14 cycles divided into 2 cycle sets. Correlation of Grayburg strata between section S7 in the Guadalupe Mountains and section PR1 in the Brokeoff Mountains is made at high-frequency sequence, high-frequency cycle set, and when feasible, high-frequency cycle scales.

The Grayburg G10 high-frequency sequence at Shattuck section S7 in the Guadalupe Mountains interpreted here to correlate to the G10 high-frequency sequence at Plowman section PR1 in the Brokeoff Mountains in terms of overall thickness and vertical facies succession. Grayburg G10 HFS fenestral laminite-capped inner-middle shelf tract cycles 17-20 at section S7 are an excellent match to laminite-capped cycles 17*-20* at section PR1. The Grayburg G10 HFS boundary is correlated between the top of cycle 20 at section S7 and cycle 20* at section PR1.

The Grayburg G11 high-frequency sequence at Shattuck section S7 interpreted here to correlate to the G11 high-frequency sequence at PR1 in terms of overall thickness and vertical facies succession. The Grayburg G11 maximum flooding surface is correlated between sections within fusulinid-dominated outer shelf tract cycle 21 at section S7 and the fusulinid-dominated outer shelf cycle 21* at section PR1. The Grayburg G11 HFS boundary is correlated between sections at the top of fenestral

laminite capped inner-middle shelf tract cycle 30 at section S7 and algal laminated sandstone capped inner-middle shelf tract cycle 30* at section PR1.

The Grayburg G12 high-frequency sequence at Shattuck section S7 is an excellent match to the G12 high-frequency sequence at PR1 in terms of overall thickness, high-frequency cycle number, cycle thickness, vertical facies succession, and facies proportion. G12 HFS cycle set 9 shelf-crest cycles 32-38 at section S7 are correlated to shelf-crest cycles 32*-38* at section PR1 on a one-to-one cycle scale. The G12 HFS maximum flooding surface is correlated between sections within the fusulinid-dominated base of cycle 39 at section S7 to the fusulinid-dominated base of cycle 39* at section PR1. The Grayburg-Queen contact is the G12 HFS boundary. The G12 HFS boundary is correlated between sections at the karsted top of cycle 44 at section S7 and at the top of cycle 44* at section PR1. Cycle 44 at section S7 is overlain by 6 m of recessive, slope-forming Queen Formation sandstones. Cycle 44* at section PR1 is overlain by 3 m of recessive, slope-forming Queen Formation sandstones.

Correlation of Grayburg G10-G12 high-frequency sequences between the Shattuck Escarpment and Plowman Ridge was used to address discrepancies within the San Andres-Grayburg interval of the shelf-to-basin correlation frameworks of Sarg et al (1999) and Kerans and Tinker (1999). Sarg et al (1999) considered the upper two-thirds of Plowman Ridge to be San Andres Formation and depicted the interval in a shelf-to-basin correlation framework as an upper prograding carbonate unit within the San Andres GP2 depositional sequence. This unit should be changed to the Grayburg Formation. If the change is made, the stratigraphic relationship of Goat Seep Formation overlying Grayburg Formation at the Bush Mountain collapse scarp on the Western Escarpment is shown in the shelf-to-basin frameworks of Kerans and Tinker (1999) and Sarg et al (1999).

APPENDIX

Included in the appendix CD-ROM are: (1) measured sections from the Shattuck Escarpment and Plowman Ridge with corresponding GPS points, (2) spreadsheets of $\delta^{13}C_{(inorganic)}$, $\delta^{18}O$, and total inorganic carbon data produced from bulk rock samples collected at sections S7 and PR1, and (3) high-resolution Grayburg Fm cross section constructed at the Shattuck Escarpment in the Guadalupe Mountains..

REFERENCES

Allan, J. R., and W. D. Wiggins, 1993, Dolomite reservoirs: Geochemical techniques for evaluating origin and distribution: AAPG Continuing Education Course Notes 36, 129 p.

Barnaby, R.J., and Ward, W.B., 2007. Outcrop analog for mixed siliciclastic-carbonate ramp reservoirs – stratigraphic hierarchy, facies architecture, and geologic heterogeneity: Grayburg Formation, Permian Basin, USA. Journal of Sedimentary Research, v. 77, no. 1, p. 34–58.

Batt, L.S., Pope, M.C., Isaacson, P.E., Montanez, I.M., and Abplanalp, J., 2007. Multi-carbonate component reconstruction of mid-carboniferous (Chesterian) seawater $d^{13}C$. Paleogeography, Paleoclimatology, Paleoecology 256, 298-318.

Bebout, D. G., and P. M. Harris, eds., 1986, Hydrocarbon reservoir studies, San Andres/Grayburg formations, Permian Basin: Permian Basin Section, Society of Economic Paleontologists and Mineralogists, Publication 86-26, 143 p.

Bebout, D. G. and P. M. Harris, eds., 1990, Geologic and engineering approaches in evaluation of San Andres/Grayburg hydrocarbon reservoirs—Permian Basin: University of Texas at Austin, Bureau of Economic Geology, 297 p.

Boyd, D.W., 1958, Permian Sedimentary Facies, Central Guadalupe Mountains, New Mexico: New Mexico Bureau of Mines and Mineral Resources, Bulletin 49, 100 p.

Buggisch, W., Wang, X., Alekseev, A.S., and Joachimski, M.M., 2011. Carboniferous-Permian carbon isotope stratigraphy of successions from China (Yangtze platform), USA (Kansas) and Russia (Moscow Basin and Urals). Paleogeography, Paleoclimatology, Paleoecology 301, 18-38.

Coffin, M., Gahagan, L., Lawver, L., Lee, T.-Y., and Rosencrantz, E., 1992, Atlas of Mesozoic/Cenozoic reconstructions (200 Ma to present day) plates: University of Texas Institute for Geophysics, Technical Report 122, 49 p.

Corsetti, F.A., Awramik, S.M., and Pierce, D. 2000. Using chemostratigraphy to correlate and calibrate unconformities in Neoproterozoic strata from the southern Great Basin of the United States. International Geology Review, v. 42, p. 516-533.

Dutton, S.P., Kim, E.M., Broadhead, R.F., Raatz, W.D., Breton, C.L., Ruppel, S.C. and Kerans, C. (2005) Play analysis and leading-edge oil-reservoir development methods in the Permian Basin; increased recovery through advanced technologies. AAPG Bulletin, v. 89, p.553–576.

Fekete, T.E., Franseen, E.K., and Pray, L.C., 1986, Deposition and erosion of the Grayburg Formation (Guadalupian, Permian) at the shelf-to-basin margin, western escarpment, Guadalupe Mountains, Texas, in Moore, G.E., and Wilde, G.L., eds., Lower and Middle Guadalupian Facies, Stratigraphy, and Reservoir Geometries, San Andres–Grayburg Formations, Guadalupe Mountains, New Mexico and Texas: SEPM, Permian Basin Section, Special Publication 25, p. 69–81.

Fischer, A.G., and Sarnthein, M., 1988, Airborne silts and dune-derived sands in the Permian of the Delaware Basin: Journal of Sedimentary Petrology, v. 58, p. 637–643.

Fitchen, W.M., 1993, Sequence stratigraphic framework of the Upper San Andres Formation and equivalent basinal strata in the Brokeoff Mountains, Otero County, New Mexico: New Mexico Geological Society, 44th Field Conference, Guidebook, Carlsbad Region, New Mexico and West Texas, p. 185–193.

Franseen, E.K., Fekete, T. E., and Pray, L.C., 1989, Evolution and destruction of a carbonate bank at the shelf margin: Grayburg Formation (Permian) western escarpment, Guadalupe Mountains, Texas, in Crevello, P.D., Wilson, J.L., Sarg, J.F., and read, J.F., eds., Controls on Carbonate Platform and Basin Development: Society of Economic Paleontologists and Mineralogists, Special Publication No. 44, p. 289-304.

Gardner M. H., and Sonnenfeld, M. D., 1996, Stratigraphic changes in facies architecture of the Permian Brushy Canyon Formation in Guadalupe Mountains National Park, West Texas, in DeMis, W. D., and Cole,A. G., eds., The Brushy Canyon Play in Outcrop and Subsurface: Concepts and Examples: Midland, Permian Basin Section SEPM, Society for Sedimentary Geology Publication 9638, p. 140.

Given, R.K., and Lohmann, K.C., 1985. Isotopic evidence for early meteoric diagenesis of the reef facies, Permian reef complex of west Texas and New Mexico. Journal of Sedimentary Petrology, v. 56, no. 2, p. 183-193.

Grotzinger, J.P., 1986, Cyclicity and paleoenvironmental dynamics, Rocknest platform, northwest Canada: Geological Society of America, Bulletin, v. 97, p. 1208–1231.

Harris, P.M., Kerans, C., and Bebout, D.G., 1993, Ancient outcrop and modern examples of platform carbonate cycles-implications for subsurface correlation and understanding reservoir heterogeneity, in Loucks, R.G., and Sarg, J.F., eds., Carbonate Sequence Stratigraphy: American Association of Petroleum Geologists, Memoir 57, p. 475-492.

Hayes, P.T. ,1964.Geology of the Guadalupe Mountains, New Mexico. U.S. Geological Survey Professional Paper, U.S. Geological Survey, Reston, VA, 69 pp.

Kendall, C. G. St. C, 1969, An environmental re-interpretation of the Permian evaporite/ carbonate shelf sediments of the Guadalupe Mountains: GSA Bulletin, v. 80, p. 2503-2525.

Kerans, C., and Nance, H.S., 1991, High-frequency cyclicity and regional depositional patterns of the Grayburg Formation, Guadalupe Mountains, New Mexico, in Meader-Roberts, S., Candelaria, M.P., and Moore, G.E., eds., Sequence Stratigraphy, Facies and Reservoir Geometries of the San Andres, Grayburg and Queen Formations, Guadalupe Mountains, New Mexico and Texas: SEPM, Permian Basin Section Publication 32, p. 53–96.

Kerans, C., Lucia, F.J., and Senger, R.K., 1994, Integrated characterization of carbonate ramp reservoirs using Permian San Andres Formation outcrop analog: American Association of Petroleum Geologists, Bulletin, v. 78 p. 181-216.

Kerans, C., and Tinker, S.W., 1999, Extrinsic stratigraphic controls on development of the Capitan Reef complex, in Saller, A.H., Harris, P.M., Kirkland, B.L., and Mazzullo, S.J., eds., Geologic Framework of the Capitan Reef: SEPM, Special Publication 65, p. 15–36.

Kerans, C., and Fitchen, W.M., 1995, Sequence hierarchy and facies architecture of a carbonate-ramp system: San Andres Formation of Algerita Escarpment and Western Guadalupe Mountains, West Texas and New Mexico: The University of Texas at Austin, Bureau of Economic Geology, Report of Investigations 235, 86 p.

Kerans, C, and Kempter, K, 2002, Hierarchical stratigraphic analysis of a carbonate platform, Permian of the Guadalupe Mountains: The University of Texas at Austin, Bureau of Economic Geology (American Association of Petroleum Geologists/Datapages Discovery Series No. 5), CD-ROM.

King, P. B., 1948. Geology of the Southern Guadalupe Mountains, Texas. Washington D.C., U.S. Geological Survey Professional Paper 215, 183 p.

Kocurek, G., and Kirkland, B.L., 1998, Getting to the source: aeolian influx to the Permian Delaware Basin region: Sedimentary Geology, v. 117, p. 143–149.

Kump, L.R., and Arthur, M.A., 1999. Interpreting carbon-isotope excursions: Carbonates and organic matter. Chemical Geology 161, p. 181-198.

Lang, W.B., 1937. The Permian Formations of the Pecos Valley of New Mexico and Texas: American Association of Petroleum Geologists Bulletin, v. 21, p. 833-898.

Lehrmann, D.J., Goldhammer, R.K., 1999. Secular variations in facies and parasequence stacking patterns of platform carbonates: a guide to application of the stacking patterns technique in strata of diverse ages and settings. Recent Advances in Carbonate Sequence Stratigraphy; Applications to Reservoirs, Outcrops and Models, Harris, P.M., Saller, A.H., Simo, J.A. (Eds.), Soc. Econ. Paleontol. Mineral., Spec. Publ. 62, 187-226.

Lindsay, R. F., D. L. Hendrix, R. H. Jones, C. M. Keefer, D. L. Lindsey, S. P. McDonald, and D. J. Rittersbacher, 1992, Role of sequence stratigraphy in reservoir characterization: an example from the Grayburg Formation, Permian basin, in D. H. Mruk and B. C. Curran, eds., Permian basin exploration and production strategies: applications of sequence stratigraphic and reservoir characterization concepts: West Texas Geological Society Symposium, p. 19–26.

Lottes, A.L., and Rowley, D.B., 1990, Early and Late Permian reconstructions of Pangaea, in McKerrow, W.S., and Scotese, C.R., eds., Paleogeography and Biogeography: Geological Society of London, Memoir 12, p. 383–395.

Meissner, F.F., 1972, Cyclic sedimentation in Middle Permian strata of the Permian Basin, West Texas and New Mexico: West Texas Geological Society, Publication 60, p. 118–142.

Mitchum , R. M., 1977, Seismic stratigraphy and global changes of sea level, Part 1: Glossary of terms used in seismic stratigraphy, in Payton, C. E., ed., Seismic Stratigraphy—Applications to Hydrocarbon Exploration: *American Association of Petroleum Geologists Memoir 26, p. 205*-212.

Oehlert, A.M., Wozniak, A.K., Sevlin, Q.B., Mackenzie, G.J., Reijmer, J.J., and Swart, P.K., 2012. The stable carbon isotopic composition of organic material in platform derived sediments: implication for reconstructing the global carbon cycle. Sedimentology, v. 59, p. 319-335.

Phelps, R.M., Kerans, C., Loucks, R.G., Da-Gama, R., Jeremiah, J., and Hull, D. 2013. Oceanographic and eustatic control of carbonate platform evolution and sequence stratigraphy on the Cretaceous (Valanginian-Campanian) passive margin, northern Gulf of Mexico. Sedimentology, Accepted Article; doi: 10.1111/sed.12062.

Rankey, E.C., Riegl, B., and Steffen, K., 2006, Form, function and feedbacks in a tidally dominated ooid shoal, Bahamas: Sedimentology, v. 53, p. 1191-1210.

Ruppel, S. C., and Lucia, F. J., 1996, Diagenetic control of permeability development in a highly cyclic, shallow water carbonate reservoir: South Cowden Grayburg field, Ector County, Texas, in Martin, R. L., ed., Permian Basin oil and gas fields: keys to success that unlock future reserves: West Texas Geological Society, Publication 96-101, p. 7–24.

Ruppel, S. C., and Bebout, D. G., 2001, Competing effects of depositional architecture and diagenesis on carbonate reservoir development: Grayburg Formation, South Cowden field, West Texas: The University of Texas at Austin, Bureau of Economic Geology Report of Investigations No. 263, 62 p.

Ruppel, S. C., and Rowe, H., 2013. Stable carbon isotopes for constraining sequence stratigraphic and Paleogeographic interpretations of carbonate successions: fact or fantasy? AAPG Search and Discovery #90163. May 19-22, 2013.

Saltzman, M.R., 2003. The Late Paleozoic Ice Age: Oceanic gateway or PCO2? Geology 31, 151–154.

Saltzman, M.R., and Thomas, E., 2012. Carbon Isotope Stratigraphy p 207-232.

Sarg, J. F. and Lehmann, P. J., 1986b, Facies and stratigraphy of lower-upper San Andres shelf-crest and outer shelf and lower Grayburg inner shelf; in Moore, G. E. and Wilde, G. L., eds., Lower and middle Guadalupian facies, stratigraphy and reservoir geometries, San Andres/Grayburg Formations, Guadalupe Mountains, New Mexico and Texas: Permian Basin Section/Society of Economic Paleontologists and Mineralogists Publication 86-25, p. 9-35.

Sarg, J. E. ,Markello, J. R. ,Bloch, R. B. ,and Clarke, R T., 1997, Stratigraphic architecture of the transgressive and turnaround phases Guadalupian Supersequence Cherry Canyon and San Andres Formations Brokeoff and Guadalupe Mountains, New Mexico: Tulsa, American Association of Petroleum Geologists 1997 Annual Convention, Dallas Guidebook Field Trip No. 16, 213 p.

Sarg, J.F., Markello, J.R. , and Weber, L.J., 1999, The second-order cycle, carbonate-platform growth, and reservoir, source, and trap prediction, Advances in carbonate sequence stratigraphy: Application to reservoirs, outcrops and models: SEPM Special Publication, v. 63, p. 11-34.

Shackleton, N.J., and Hall, M.A., 1984. Carbon isotope data from Leg 74 sediments. Initial Reports of the Deep Sea Drilling Project 74, 613–619.

Scholle, P A., and Halley, R. B., 1980, Upper Paleozoic depositional and diagenetic facies in a mature petroleum province (a field guide to the Guadalupe and Sacramento Mountains): USGS Open-File Report 80-383, 191 p.

Scotese, C.R., and McKerrow, W.S., 1990, Revised world maps and introduction, in McKerrow, W.S., and Scotese, C.R., eds., Palaeogeography and Biogeography: Geological Society of London, Memoir 12, p. 1–21.

Silver, B.A., and Todd, R.G., 1969, Permian cyclic strata, northern Midland and Delaware basins, West Texas and southeastern New Mexico: American Association of Petroleum Geologists, Bulletin, v. 53, p. 2223–2351.

Sonnenfeld, M.D., 1991, High-frequency cyclicity within shelf-margin and slope strata of the upper San Andres sequence, Last Chance Canyon, in Meader-Roberts, S., Candelaria, M.P., and Moore, G.E., eds., Sequence Stratigraphy, Facies and Reservoir Geometries of the San Andres, Grayburg, and Queen Formations, Guadalupe Mountains, New Mexico and Texas: SEPM, Permian Basin Section, Special Publication 32, p. 11–51.

Sonnenfeld, M.D., 1993, Anatomy of offlap: Upper San Andres Formation (Permian, Guadalupian), Last Chance Canyon, Guadalupe Mountains, New Mexico: NewMexico Geological Society, 44th Field Conference, Guidebook, p. 195–203.

Sonnenfeld M. D., and Cross, T. A., 1993, Volumetric partitioning and facies differentiation within the Permian upper San Andres Formation of Last Chance Canyon Guadalupe Mountains New Mexico in Loucks R G and Sarg J E eds Carbonate Sequence Stratigraphy Recent Developments and Applications Tulsa American Association of Petroleum Geologists Memoir 57 p. 437-445.

Sundquist, E.T., and Visser, K., 2004. The Geologic History of the Carbon Cycle. Treatise on Geochemistry 8, p. 425-472.

Tierney, K., 2010. Permian carbon and strontium isotope stratigraphy in Nevada and China: Implications for a greenhouse-icehouse transition. Unpublished PhD. Dissertation, The Ohio State University.

Tye, E.N., 1986, Stratigraphy and formation of tepee structures in the Guadalupian Grayburg Formation, southeast New Mexico, in Moore, G.E., and Wilde, G.L., eds., Lower and Middle Guadalupian Facies, Stratigraphy, and Reservoir Geometries, San Andres–Grayburg Formations, Guadalupe Mountains, New Mexico and Texas: SEPM, Permian Basin Section, Special Publication 25, p. 95–105.

Van Wagoner, J.C., Posamentier, H.W., Mitchum, R.M., Vail, P.R., Sarg, J.F., Loutit, T.S., and Hardenbol, J., 1988, An overview of the fundamentals of sequence stratigraphy and key definitions, in Wilgus, C.K., Hastings, B.S., Kendall, C.G.ST.C., Posamentier, H.W., Ross, C.A., and Van Wagoner, J.C., eds., Sea-Level Changes: An Integrated Approach: SEPM, Special Publication 42, p. 39–45.

Van Wagoner, J. C., 1985, Reservoir facies distribution as controlled by sea-level change: Abstract and Poster Session, Society of Economic Mineralogists Mid-Year Meeting, Golden, Colorado, p. 91-92.

Ward, R.F., Kendall, C.G.ST.C., and Harris, P.M., 1986, Upper Permian (Guadalupian) facies and their association with hydrocarbons—Permian Basin, West Texas and New Mexico: American Association of Petroleum Geologists, Bulletin, v. 70, p. 239–262.

VITA

Samuel Franz Hiebert received a Bachelor of Arts in Geological Sciences with honors from the Jackson School of Geosciences, University of Texas at Austin. As an undergraduate Sam worked with Professor Charlie Kerans on a departmental honors project in Sonora Mexico. The work in Sonora culminated in the publication of *Stratigraphic Hierarchy and Shelf-to-Basin Architecture of Aptian-Albian Mural Shelf, Cerro Caloso Range, Sonora, Mexico* in 2012 v.10 of The Sedimentary Record. Prior to starting his Masters work at the University of Texas at Austin, Sam spent 1 year working with the Reservoir Characterization Research Laboratory at the Bureau of Economic Geology. As a graduate student Sam served as President of the student chapter of the American Association of Petroleum Geologists, was the recipient of a Chevron Fellowship, was an assistant instructor for the graduate level sequence stratigraphy course taught by Professors William Fisher and Charlie Kerans, was a teaching assistant twice for the undergraduate summer field camp course directed by Mark Helper, and was a research assistant in the Reservoir Characterization Research Laboratory at the Bureau of Economic Geology.

Permanent address: samuelhiebert@utexas.edu
This thesis report was typed by the author.